Ruthenium-Ligand Complexes as Bioanalytical Luminescent Probes for Polarization and Energy Transfer Systems

DISSERTATION ZUR ERLANGUNG DES
DOKTORGRADES DER NATURWISSENSCHAFTEN
(DR. RER. NAT.)

DER FAKULTÄT CHEMIE UND PHARMAZIE
DER UNIVERSITÄT REGENSBURG

vorgelegt von

Christine Augustin

aus Burglengenfeld / Oberpfalz

im Mai 2001

Promotionsgesuch eingereicht am: 29.05.2001

Die Arbeit wurde angeleitet von Prof. Dr. Wolfbeis

Kolloquiumstermin: 05.07.2001

Prüfungsausschuss: Vorsitzender: Prof. Dr. Manfred Liefländer
                          Erstgutachter: Prof. Dr. Otto S. Wolfbeis
                          Zweitgutachter: Prof. Dr. Werner Kunz
                          Drittprüfer: Prof. Dr. Jörg Daub

Danksagung

Diese Arbeit entstand in der Zeit vom März 1998 bis Mai 2001 am Institut für Analytische Chemie, Chemo- und Biosensorik der Universität Regensburg.

Mein besonderer Dank gilt Herrn Professor Otto S. Wolfbeis für die Bereitstellung des interessanten Themas, die Förderung und die Unterstützung während der Arbeit.

Dem BMBF und der Firma Roche, Penzberg, danke ich für die finanzielle Unterstützung.

Weiterhin danke ich Dr. Frank Lehmann und Dr. Ewald Terpetschnig für die Unterstützung und die zahlreichen wissenschaftlichen Diskussionen.

Meinen Laborkolleginnen und –kollegen Michala Arbter, Axel Dürkop, Bernhard Oswald, Erika Pringsheim, Mario Probst, Erika Simo und Bernhard Weidgans für das angenehme Arbeitsklima.

Ein spezielles Dankeschön gilt Nadia Wrobel, Thomas Hirsch und Gerhard Neurauter für die Freundschaft und für die Unterstützung in wissenschaftlichen und privaten Dingen.

Sowie allen Mitarbeiterinnen und Mitarbeiter des Lehrstuhls, die zum Gelingen dieser Arbeit beigetragen haben.

Ganz besonders möchte ich mich bei meinen Eltern bedanken, die mich während meines gesamten Studiums unterstützten.

Contents

IV

Abbreviations and Symbols

Ab	Antibody
Ag	Antigen
anti-HSA	polyclonal anti-human serum albumin
bipy	2,2'-bipyridine
CE	Capillary electrophoesis
D/P	Dye-to-protein ratio
DCC	Dicyclohexylcarbodiimide
dm	Demodulation
DMAP	Dimethylaminopropionnitrile
DMF	N,N-Dimethylformamide
DPH	1,6-Diphenyl-1,3,5-hexatriene
DPPC	1,2-dipalmitoyl-sn-glycero-3-phosphatidylcholine
EB	Ethidium bromide
EDC	1-Ethyl-(3-(3-dimethylaminopropyl)-carbodiimide
Eq.	Equation
ET	Energy transfer
f	Modulation frequency
FITC	Fluorescein isothiocyanate
FRET	Fluorescence resonance energy transfer
HSA	Human serum albumin
I	Luminescence intensity
k_T	Non-radiative energy transfer
LED	Light emitting diode
Lit.	Literature
MeOH	Methanol
MLC	Metal-ligand complex
MLCT	Metal to ligand charge transfer
MPLC	Middle pressure liquid chromatography
NEt_3	Triethylamine

NHS	N-Hydroxysuccinimide
NMR	Nuclear magnetic resonance
PBS	Phosphate buffered saline
PDA	Pyrene decanoic acid
PE	1,2-dipalmitoyl-sn-glycero-3-phosphoethanolamine
phen	Phenanthroline
PMT	Photomultiplier
Q.Y.	Quantum Yield
R_0	Förster radius
Ref.	Reference
RET	Resonance energy transfer
RT	Room temperature
Ru-1	[Ru(2,2'-bipyridine)$_2$(4-carboxy-2,2'-bipyridine)](PF$_6^-$)$_2$
Ru-2	[Ru(2,2'-bipyridine)$_2$(4,4'-dicarboxy-2,2'-bipyridine)](PF$_6^-$)$_2$
T_m	Phase transition temperature
UV	Ultra-violet
λ	Wavelength
τ	Fluorescence lifetime
τ_0	Fluorescence lifetime in absence of quenchers

1. Introduction

1.1. Fluorescence spectroscopy in life science

Luminescent techniques are among the fastest-growing analytical tools in life science and analytical chemistry. The potential of this techniques are the easy automated luminescence monitoring in accordance with their high sensitivity and selectivity. This, in turn, has increased the commercial availability of fluorescent probes during the last decade[1].

Fluorescence spectroscopy allows the measurement of numerous parameters. These include fluorescence intensity, quantum yield, fluorescence polarization, quenching efficiency, radiative and non-radiative energy transfer as well as combinations of these techniques. Measurements can be performed in solid, liquid or gaseous phases. Beside the traditional acquisition of convential spectra of samples in cuvettes, fluorescence is applied to microscopy and imaging, fluorescence energy transfer (FRET) and single molecule detection. New dyes are steadily developed for labeling biomolecules. Most biomolecules are non-fluorescent or show fluorescence in the UV region. The new probes are fluorescent in the visible or NIR region, can be attached to, or intercalate in, biomolecules and are excitable by affordable lasers.

1.2. Labels and probes

Dyes for bioanalytical applications can be classified into labels and probes. *Labels* are dyes covalently attached to a non-fluorescent biomolecule rendering them fluorescent. Recent advances in gene technology have led to a great interest in labels for DNA and RNA, respectively. Nucleic acids are non-fluorescent in the visible region and therefore labels are needed to visualize the nucleic acid. To achieve this goal, nucleic acids have to be modified with

amino or thiol groups for the attachment of the label, which carries reactive groups such as an isothiocyanate or an NHS ester. An other approach is the use of a phosphoramidite dye as label, offering the opportunity to attach the phosphoramidite dyes directly to a nucleic acid without any modification of the DNA/RNA. A brief description of the mechanism is presented in figure 1-1.

Labeled DNA can be employed for separation techniques like liquid chromatography or electrophoresis. In numerous applications the dyes are also attached to proteins for fluorescence immunoassays.
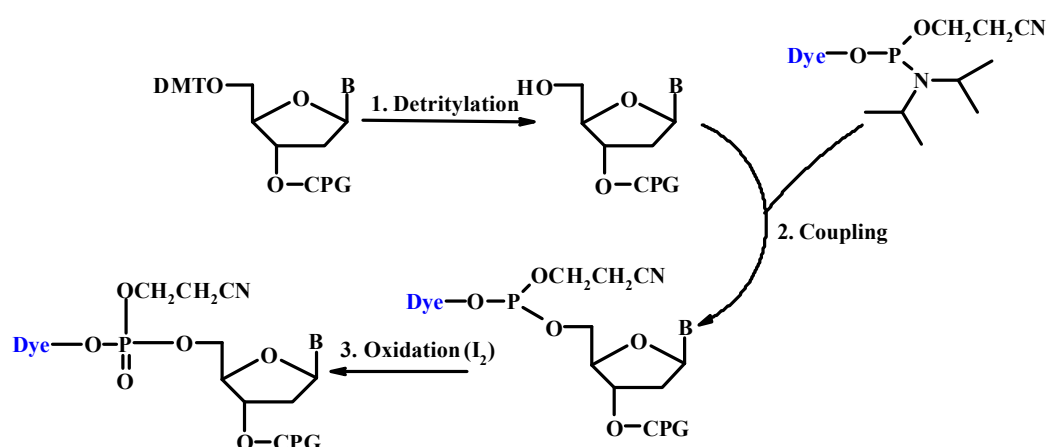
Fig. 1-1. *Coupling of a phophoramidite dye to an oligonucleotide.*

Probes in contrast to labels are used to report the micro-environment of a chemical species or structural unit. Usually, the micro-environment of membranes or living cells are investigated in terms of viscosity, ion strength, pH or cell dynamics. Therefore, fluorescent probes are needed enabling to convert the respective information of a cell into dye specific behaviors like fluorescence intensity, life time or changes in its potential sensitivity. In contrast to labels, probes do not possess a reactive group. Furthermore, membrane probes contain side chains or tails rendering the fluorophore soluble in living cells or membranes.

1.3. Methods and applications using luminescent dyes in life science

1.3.1. Electrophoresis in DNA sequencing

Capillary electrophoresis has become the most valuable tool for the high speed and efficient separation of such analytes as pharmaceuticals [2], oligonucleotides [3] and proteins [4]. The popularity of CE results preliminarily from the high speed at which separation can be carried out as well as the high efficiency in separation of even minute quantities. The speed of separation is produced by using high electric fields. In many CE application one would potentially like to detect several types of labeling dyes, with each dye targeted for a specific analyte (multiplex assays). For example in DNA sequencing, one generates a series of fragments, which differ in the number of bases and are terminated by a common nucleotide base. These are then fractionated in a capillary gel column according to size. Since the DNA is composed of four bases, it becomes advantageous to identify the four bases in a single CE run to improve throughput. This is commonly done using spectral discrimination in which each dye has a unique emission maximum and the color is sorted using filter systems onto the appropriate read-out channel.

The fluorophores first developed for CE as labeled primer sequence did not have high molar absorbances at a single common excitation wavelength [5]. To compensate this deficiency, many CE sequencing detection systems used either two excitation wavelengths [6] or alternative base-coding strategies [7]. The most powerful solution to overcome this problem was provided by improved fluorescent labels. Energy transfer (ET) primers have been developed that overcome this limitation in a simple and elegant manner [8]. These primers contain a common donor dye at the 5´ end and an acceptor dye approximately 8-10 nucleotides away. The presence of the common donor fluorophore allows the use of a single laser at 488 nm to efficiently excite the donor. The excitation is non-radiatively transferred by

resonance ET to the acceptor dye, and therefore the observed emission is that of the acceptor. In commercially available ET primers, a fluorescein derivative is used as the donor and a rhodamine derivative as the acceptor (see figure 1-2). Recently, the advantage of cyanine dyes in ET primers has been demonstrated. The advantage of cyanine dyes [9] compared to fluorescein dyes is the high molar absorbance along with absorption and emission maxima in the near-infrared. As a result a lowered detection limit is obtained and therefore spectral cross talks are reduced.
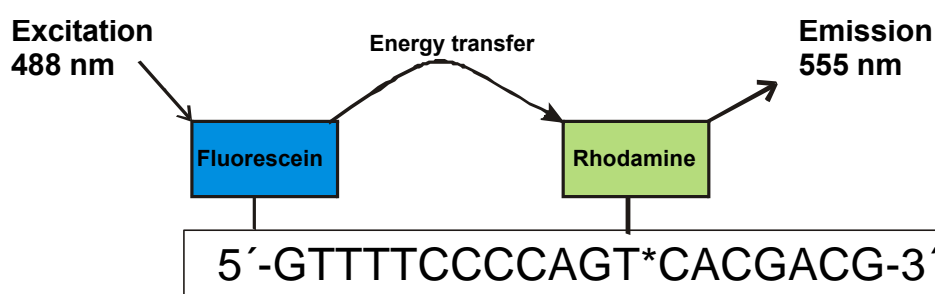
Fig. 1-2. *Schematic of energy transfer primers for capillary electrophoresis.*

1.3.2. Flow cytometry

Flow cytometry is a technique for carrying out rapid measurements on particles or cells as they flow one by one in a fluid stream through the detector. Flow cytometers enable multiparameter measurements of individual cells. They allow the quantitative measurement of up to 16 parameters of each cell at rates of several thousand cells per second. These measurements are made separately for each particle within a suspension. This is a main advantage of that technique with respect to other methods. Nowadays, flow cytometers are available with laser- and arc-lamps enabling the measurement of multiple cellular parameters based on light scatter and fluorescence. This makes flow cytometry a routine technique in immunology to evaluate, for example, three immuno-fluorescence parameters and two light scattering effects for each cell [10].

The evaluation of single cells plus sensitive analysis of a large variety of cellular molecules are possible with the fluorescence technique, accomplished with specific fluorescent labels and probes. Multi parametric measurements require a wide range of fluorescent dyes with individual emission characteristics. A broad range of probes and labels are commercially available. Parameters such as nucleic acid content, enzyme activity, membrane potential or pH can be estimated directly [11].

1.3.3. Fluoroimmunoassays

Immunoassays are indispensable tools in clinical and analytical biochemistry. The relevance is still increasing due to their outstanding specificity and sensitivity. Possibility of extending them to a nearly unlimited number of analytes and their adaptability to automation make them to an ideal tool for routine assays. Hence, immunoassays became centrally important in the analysis of drugs, pesticides, hormones and proteins. Immunological methods are based on the competitive binding of labeled and unlabeled antigens to highly specific antibody receptor sites. Fluorescent labels may be bound to antigens or antibodies. Specific determination of the signal corresponding to either labeled or unlabeled analyte can be achieved in two ways, the heterogeneous and the homogeneous immunoassay.

Heterogeneous and homogeneous immunoassays

The heterogeneous immunoassay requires physical separation of labeled analyte from label-free analyte. This separation avoids endogenous background interference and achieves low detection limits. Therefore, analyte or antibody are attached to a solid surface. The reactant distribution of the liquid phase and the solid phase are followed by physical separation of these phases [12, 13]. Homogeneous fluorescent immunoassays do not require any separation of labeled antigens from free-labeled antigens. In fact, the number of procedural steps is reduced decreasing time requirements and avoiding sample loss through transfer processes [14].

Labels for immunoassays

To minimize the effect of non-specific background, labels should have high fluorescence quantum yields along with an excitation and emission maximum at longer wavelengths. The absorption mamima are expected to be longer than those typically shown by proteins (280 and 340 nm). The most widely used fluorescent labels in immunoassays are derivatives of fluorescein isothiocyanate (FITC). Their advantages are highly molar absorbencies and quantum yields. However, the Stokes' shift of FITC is small. Alternative probes show specific advantages compared to FITC. For example, rhodamine B isothiocyanate conjugates have excitation and emission maxima at 550 / 585 nm and an increased quantum yield. To overcome limitations caused by autofluorescence of biological samples, new red and near infra-red dyes (NIR) were introduced [15, 16] providing emission maxima between 600 and 800 nm.

1.4. Applications of metal-ligand complexes in life science

During the last years metal-ligand complexes (MLCs) have become important in biophysics and clinical chemistry, because they display a wide range of absorption and emission wavelengths and their decay times range from 100 ns to 100 μs. Optimally tailored MLCs can be obtained by careful selection of the metal and the ligand. For instance, lifetimes as long as 100 μs can be obtained using rhenium as the metal ion in such complexes. Rhenium complexes display also good quantum yields and high initial polarizations in aqueous solutions. Absorption wavelengths of 460 nm and 700 nm can be obtained using osmium and ruthenium in MLCs, respectively. In clinical routine analysis the excitation with a 488 nm argon ion laser is a common tool, which offers many applications for ruthenium complexes in clinical chemistry.

Recently, these complexes have been developed as luminescent probes for immunoassays [17-20]. The polarized emission combined with a lifetime in

the microsecond range offers the possibility to study processes like the rotation of proteins or other macromolecules. MLC labels are often used in fluorescence microscopy [21-24]. The combination of temporal and spectral resolution in fluorescence microscopy based on MLC labels offers also an increase in resolution and probe selectivity. This effect is based on the suppression of scattered light and short-lived autofluorescence of the sample. The use of ruthenium complexes instead of the most commonly used ethidium bromide in DNA analysis was reprted [25]. The complex luminescence is increasing when intercalating the probe into the double strand of a DNA. The oxygen sensitivity of ruthenium complexes with 4,7-diphenyl-1,10-phenanthroline as ligand is used for measuring oxygen routinely [26, 27]. Also, lifetime-based optical sensors for pH [28, 29], chloride [30], carbon dioxide [31] and potassium [32] were presented recently using ruthenium complexes.

1.5. Objective of the work

The aim of this work was to synthesize new dyes useful for labeling proteins and DNA oligomers. The work also focused on the development of dyes for membrane characterization. In contrast to available luminophores, these dyes should fulfill the criterion of being excitable with an 488 nm argon ion laser used in clinical routine analysis. In a further approach, unsymmetrical MLC luminophores, which exhibit lifetimes in the hundred nanosecond range, were designed.

In this thesis, ruthenium MLC and fluorescein membrane probes were also synthesized and characterized for measuring membrane dynamics. The optimal membrane probe was evaluated using the method of steady-state polarization. Varying luminophore, ligand and lipid systems were tested in DPPC liposomes for its temperature and cholesterol sensitivity to polarization.

Furthermore, this thesis presents the development of an assay for HSA/anti-HSA using the principle of energy transfer. A ruthenium MLC was

used as donor and a squarine dye as acceptor. The energy transfer assay was developed in terms of emission intensity and lifetime. Additionally, a DNA hybridization system was evaluated with the same donor and acceptor pair used for the protein assay.

4.7. References

[1]   R.P. Haugland, *Handbook of Fluorescent Probes and Research Chemicals*, Molecular Probes, Sixth Edition.

[2]   Swartz M. E., *J. Chrom. A* **1993**, 441.

[3]   Soper S. A., *Anal. Chem* **1995**, *67*, 3427.

[4]   Mattuch J., Dittrich K. J., *J. Chrom. A* **1994**, *680*, 279.

[5]   Smith L.M. et al., *Nature* **1986**, *321*, 674.

[6]   Takahashi S., Murakami K., Anazawa T., Kambara H., *Anal. Chem.* **1994**, *66*, 1021.

[7]   Li Q., Yeung E. S., *Appl. Spectrosc.* **1995**, *49*, 1528.

[8]   Ju J., Glazer A. N., Mathies R. A., *Nature Medicine* **1996**, *2*, 246.

[9]   Hung S-C., Mathies R. A., Glazer A. N., *Anal. Biochem.* **1997**, *252*, 78.

[10]   Darzynskiewith Z., **1994**, Flow *Cytometry, Methods in Enzymology* 41/42, Academic Press, London.

[11]   Ormerod M. G., **1994**, *Flow Cytometry: A practical approach*, 2nd edition, IRL Press.

[12]   Sidk A. M., Al-Abdullah I. H., Powell F. J., *Clin. Chem.* **1987**, *33*, 463.

[13]   Nargessi R. D., Landon J., Poufarzaneh M., Smith D. S., *Clin. Chim. Acta* **1978**, *89*, 455.

[14]   Dandliker W. B., 1977, *Immunochemistry of Proteins*, Plenum, New York.

[15]   Oswald B., *Dissertation* **1999**, Universität Regensburg.

[16] Mank A. J. G., Yeung E. S., *J. Chromatogr.* **1995**, *708*, 309.

[17] Terpetschnig E., Szmacinski H., Malak H. Lakowicz J. R., *Biophys. J.* **1995**, *68*, 342.

[18] Terpetschnig E., Dattelbaum J. D., Szamcinski H., Lakowicz J. R., *Anal. Biochem.* **1997**, *254*, 179.

[19] Szmacinski H., Terptschnig E., Lakowicz J. R., *Biophys. Chem* **1995**, *62*, 109.

[20] Castellano F., Dattelbaum J. D., Lakowicz J. R., *Anal. Biochem.* **1998**, *255*, 165.

[21] Vereb G., Jares-Erijman E., Selvin P. R., Jovin T. M., *Biophys. J.* **1998**, *74(59),* 2210.

[22] Beverloo H. B., van Schadewijk A., Bonnet J., van der Gest R., Runia R., Verwoerd N. P., Vrolijk J., Ploem J. S., Tanke H. J., *Cytometry* **1992**, *13*, 561.

[23] Hennink E. J., de Haas R., Verwoerd N. P., Tanke H. J., *Cytometry* **1996**, *24*, 312.

[24] Marriott G., Heidecker M., Diamandis E. P., Yan-Marriott Y., *Biophys. J.* **1994**, *67*, 957.

[25] Friedmann A., Egenbrib H.-C., Sauvage J.-P., Turro N. J., Barton J. K., *J. Am. Chem. Soc.* **1990**, *112*, 4960.

[26] Wolfbeis O. S., *Fiber Optic Chemical Sensors and Biosensors*, Vol. II, CRC Press, Boca Raton, Florida, **1991**, 19.

[27] Lippitsch M. E., Pusterhofer J., Leiner M. J. P., Wolfbeis O. S., *Anal. Chim. Acta* **1988**, *205*, 1.

[28] Kosch U., Klimant I., Werner T., Wolfbeis O. S., *Anal. Chem.* **1998**, *70*, 3892.

[29] Murtaza Z., Chang Q., Rao G., Lin H., Lakowicz J. R., *Anal. Biochem.* **1997**, *247,* 216.

[30] Huber Ch., Werner T., Krause Ch., Klimant I., Wolbeis O. S., *Anal.*

Chim. Acta **1998**, *364*, 143.

[31]   Neurauter G., Klimant I., Wolfbeis O. S., *Anal. Chim. Acta* 1999, *382*, 67.

[32]   Krause Ch., Werner T., Huber Ch., Klimant I., Wolfbeis O. S., *Anal. Chem.* **1998**, *70*, 3983.

2. Background

In this chapter an introduction is given to the methods used in this thesis. The theories of lifetime, fluorescence resonance energy transfer and steady-state fluorescence polarization are explained. Additionally, a briefly description of the way of measurement for each method is presented.

2.1. Lifetime

2.1.1. Theory

The fluorescence lifetime of a substance indicates the average time a molecule remains in the excited state before it returns into the ground state [1, 2]. In case of a single-exponential decay, the lifetime (decay time) τ is defined as the time after which the fraction of 1/e of the excited molecules still exists in the excited state.

Lifetime measurements are frequently necessary in fluorescence spectroscopy. The measurement of the fluorescence lifetime rather than fluorescence intensities allows the elimination of several drawbacks known from intensity measurements. The lifetime is independent of signal fluctuations of the light source and the photo detector. In contrast to other methods there are no drifts occurring from photobleaching, photodecomposition or leaching. The concentration of the indicator dye has also no effect on the lifetime provided that the signal to noise ratio is sufficiently high. Especially in case of dynamic quenching from oxygen, the measurement of the luminescence lifetime is a well established technique [3-5].

There are two widely used methods for the measurement of fluorescence lifetime: The pulse (or time domain) method and the phase modulation (or frequency domain) method [1]. In the pulse method the luminophore is excited with a short pulse of light and the time dependent decay of fluorescence intensity is measured. In the phase-modulation method the luminophore is excited with sinusoidally modulated light. The lifetime of the fluorophore causes a time lag between absorption and emission, expressed by the phase shift ϕ and a decrease in emission intensity relative to the incident light, called demodulation (dm) (figure 2-1).
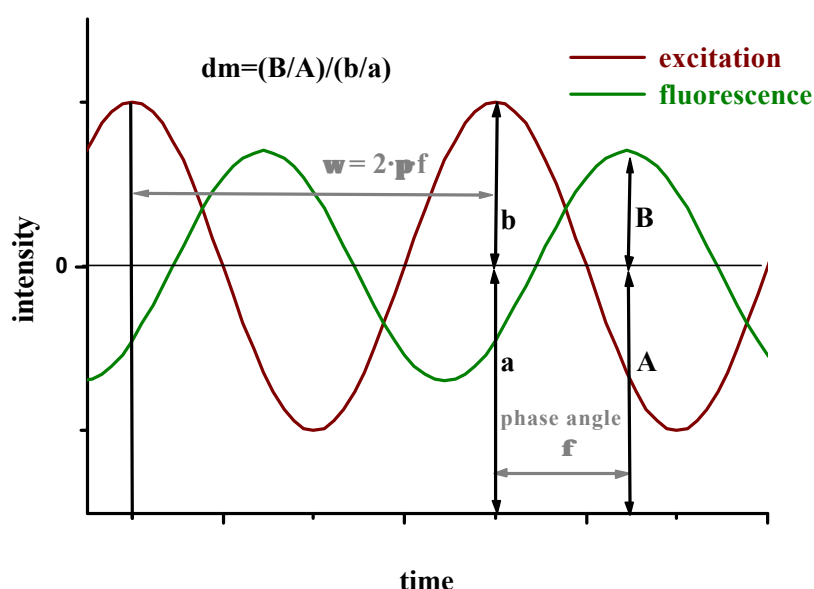
Fig. 2-1. *Schematic description of the frequency domain method. The sinusoidally modulation light is shifted (ϕ) and demodulated (dm).*

The loss of intensity in the emission relative to the excitation is described by the demodulation. The amplitude (B/A) of the emission is smaller than the amplitude of the excitation. The phase delay ϕ and the demodulation dm can be separately used to calculate the lifetime (eq. 2-1 and 2-2) of the fluorophore [1].

$$\boldsymbol{t}_p = \boldsymbol{w}^{-1} \cdot \tan \boldsymbol{f} \tag{2-1}$$

$$\boldsymbol{t}_{dm} = \boldsymbol{w}^{-1} \cdot [(1/dm^2) - 1]^{\frac{1}{2}} \tag{2-2}$$

with $\omega = 2 \cdot \pi \cdot f$.

However, the assumption that $\tau_p = \tau_{dm} = \tau$ is only valid for a single exponential decay. Otherwise, the calculated lifetimes are apparent values only, and the lifetime measurement is more complicated.

In practice, the phase modulation technique is a very attractive analytical tool. In contrast to other detection methods (i.e. absorptiometry, fluorimetry) it shows increased accuracy. The instrumentation used is rather simple that light emitting diodes (LED) can serve as excitation light source, photodiodes or photomultiplier tubes (PMT) for detection of the emitted light, suitable excitation and emission filters and a lock-in amplifier. Moreover, electronical cross talks and ambient light have little effect on the signal obtained.

Frequency domain decay time measurements can be performed in the ns and ps range. For short lifetimes, modulation frequencies in the upper MHz range are required and therefore the equipment is rather expensive.

2.1.2. Method of measurement

Lifetime measurements were carried out on a ISS K2 multifrequency phase modulation fluorometer using an argon ion laser as the excitation source and two signal generators. The light was passed through a Pockels cell which provides modulated light. Emission was detected perpendicular to the excitation through a 610-nm filter. Lifetimes were referenced against a dilute suspension of glycogen. Each measurement was carried out at ten modulation frequencies (logarithmically spread from 50 to 1500 kHz). The lifetime was calculated with the respective software of the instrument.

2.2. Fluorescence resonance energy transfer (FRET)

FRET is a distance-dependent non-radiant energy transfer of excited state energy from a donor to an acceptor and arising from dipole-dipole interactions between the donor and acceptor molecule. Non-radiative energy transfer does non involve the emission and re-absorption of photons. A transfer, where the acceptor dye reabsorbs photons emitted by the donor is called radiative transfer or inner filter effect [1]. The rate of non-radiative energy transfer (k_T) depends on the fluorescence quantum yield of the donor, the overlap of the emission spectrum of the donor with the absorption spectrum of the acceptor, and their relative orientation and distance. The theory was developed by Förster [6], who derived the quantitative expression of k_T between a donor and acceptor pair at a fixed separation distance r (eq. 2-3).

$$k_T = \frac{8.71 \cdot 10^{23} \cdot \boldsymbol{k}^2 \cdot \boldsymbol{f}_d}{r^6 \cdot n^4 \cdot \boldsymbol{t}_d} \cdot J = \frac{1}{\boldsymbol{t}_d} \left(\frac{R_0}{r} \right)^6 \tag{2-3}$$

with

$$J = \int_0^\infty F_D(\boldsymbol{l}) \cdot \boldsymbol{e}_A(\boldsymbol{l}) \cdot \boldsymbol{l}^4 \cdot d\boldsymbol{l} \tag{2-4}$$

where κ^2 is a factor describing the relative orientation in space of the transition dipoles of the donor and acceptor, ϕ_d and τ_d are the quantum yield and lifetime of the donor in absence of the acceptor, r is the distance between donor and acceptor and n is the refractive index. J is the overlap integral (eq. 2-4), which expresses the degree of spectral overlap between the donor emission and the acceptor absorption. J depends on $F_D(\lambda)$, the corrected fluorescence intensity of the donor in the wavelength range $\lambda + d\lambda$, with the total intensity normalized to unity, and $\varepsilon_A(\lambda)$ the acceptor extinction coefficient at the wavelength λ. Eq. 2-3 shows that k_T is dependent on the sixth power of the intermolecular distance, thus making FRET an interesting tool for monitoring distances between donor and acceptor labeled targets like biological macromolecules [7, 8].

Energy transfer measurements were carried out by using the measurement methods of fluorescence intensity and lifetime. Energy transfer from the donor to the acceptor will quench the fluorescence and alter both the fluorescence intensity and lifetime. The advantage of an energy transfer system based on lifetime measurement is the conversion of an emission based signal into an intensity independent decay time signal.

A ruthenium metal ligand complex with 2, 2´-bipyridine as ligand was used as the donor. This ligand is less susceptible to oxygen quenching than for example the phenanthroline ligands. Additionally, the lifetime in the hundreds of nanoseconds region simplifies the instrumentation needed for lifetime measurements.

2.3. Steady-state fluorescence polarization

2.3.1. Theory [1]

Since the absorption and the emission of light depend on the orientation of the transition dipole moments, the introduction of vertically polarized excitation light can provide information on the rotational motion of the fluorophore. After distribution of excited fluorophores, the excited fluorophores are able to relax to an uniform random set. This process can be traced in order to determine the rotational motion of fluorophores by measuring the state of emission anisotropy with time. This can generally be described as a multiexponential decay given by

$$r(t) = \frac{I_{II}(t) - I_{\perp}(t)}{I_{II}(t) + 2I_{\perp}(t)} = r_0 \sum_i f_i e^{-t/q_i} \qquad (2\text{-}5)$$

where r(t) is the anisotropy at the time t after excitation and r_0 is the limiting anisotropy in the absence of rotational diffusion. Maximum values for r_0 are observed when the absorption and emission dipol moments are collinear ($r_{max,0}$=0.4). The subscripts of I(t) indicate the relative orientation, parallel (II)

and perpendicular ($\perp$), of the polarizers, respectively (see figure 2-2). q_i are the individual rotational correlation times, and f_i are the associated fractional amplitudes ($\sum_i f_i = 1$). The extend of depolarization of the emission of the fluorophore in a biomolecule reflects the degree to which a population of photoselected excited fluorophores loses its initial selective orientation and becomes randomized.

Anisotropy (r) and polarization (P) are related by

$$P = \frac{I_{II} - I_\perp}{I_{II} + I_\perp} \qquad (2\text{-}6)$$

$$r = \frac{I_{II} - I_\perp}{I_{II} + 2I_\perp} \qquad (2\text{-}7)$$

where I_{II} and $I_\perp$ are the vertically and horizontally polarized components of the emission.
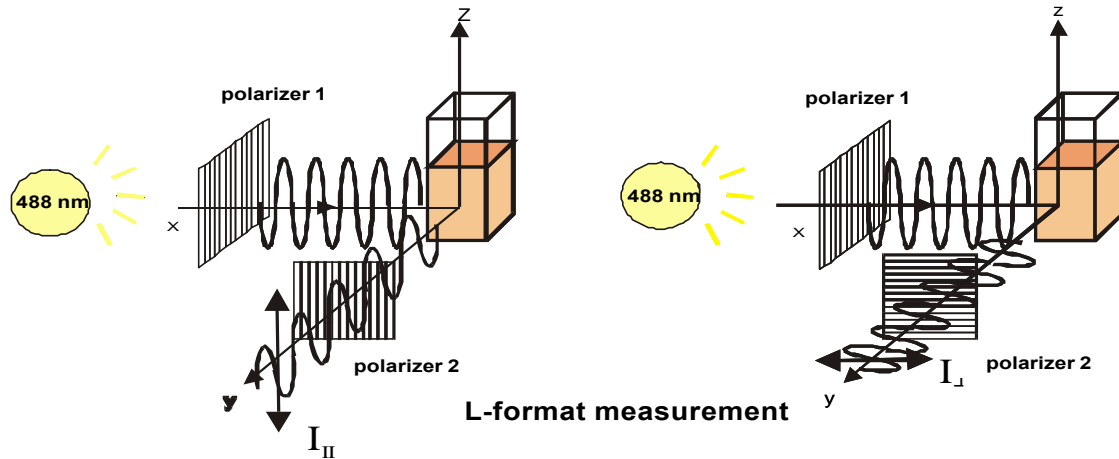
Fig. 2-2. *Schematic description of the L-format measurement of the I_{II} and $I_\wedge$ component for polarization and anisotropy determination.*

The values of P and r can be converted into each other according to eq. 2-8 and eq. 2-9

$$r = \frac{2P}{3 - P} \qquad (2\text{-}8)$$

$$P = \frac{3r}{2 - r}$$ (2-9)

2.3.2. Method of measurement

Steady-state polarization measurements were carried out with an ISS K2 multi-frequency phase modulation fluorometer. The instrument was aligned to the L-format light path and equipped with polarizers, and a xenon lamp as the excitation light source. The excitation wavelength was adjusted to 488 nm and a 610 nm long-pass filter was placed in the emission light path to separate stray light. The steady-state polarization P was calculated [8] according to:

$$P = \frac{I_{VV} - GI_{VH}}{I_{VV} + GI_{VH}}$$ (2-10)

where G is the instrumental correction factor ($G = I_{HV}/I_{HH}$), I_{VV} the emission intensity at vertically polarized excitation and emission filters, and I_{VH} the emission intensity at vertically polarized excitation and horizontally polarized emission filters. The temperature was controlled at a constant temperature of 25 °C by a circulating thermostated water bath connected to the sample cell. The ISS instrument used for steady-state polarization measurement is illustrated in figure 2-3.
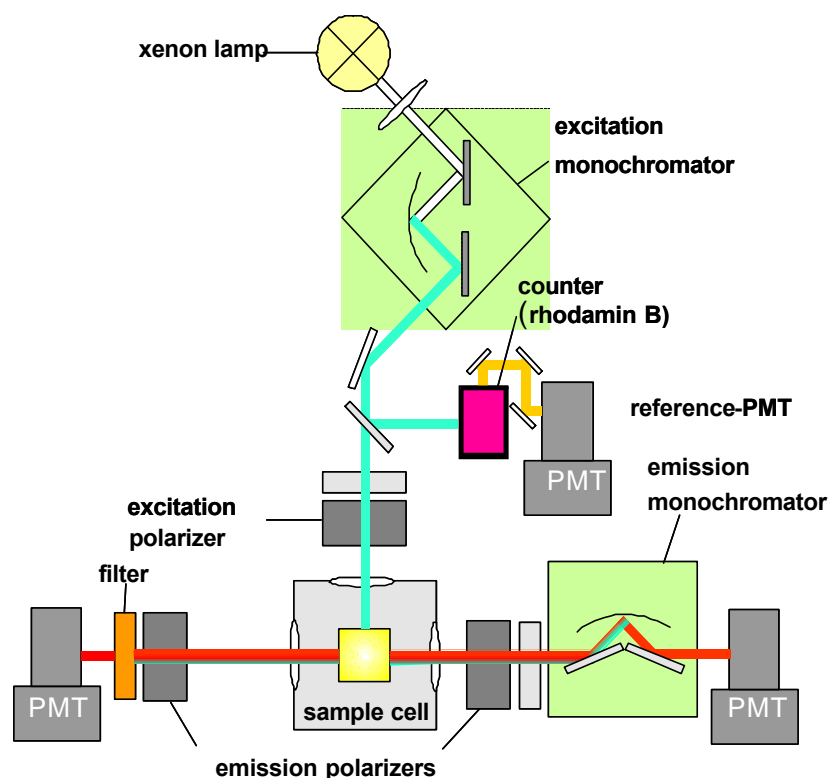
Fig. 2-3. *Schematic illustration of the ISS K2 multifrequency phase modulation fluorimeter aligned for polarization measurements.*

2.4. References

[1]   Lakowicz J. R., *Principles of Fluorescence Spectroscopy, Plenum Press* 2nd Edn., New York / London, **1999**.

[2]   Wolfbeis O. S., *Fiber Optic Chemical Sensors and Biosensors*, in Wolfbeis O. S. (ed.), Vol. 1, CRC Press, Boca Raton, Fl. **1991**, 32 ff.

[3]   Papkovsky D. B., *Sensors Actuat. B* **1995**, *29*, 213.

[4]   Bacon J. R., Demas J. N., *Anal. Chem.* **1987**, *59*, 2780.

[5]   Klimant I., Beiser P., Wolfbeis O. S., *Talanta* 1**994**, *41*, 985.

[6]   Förster, T., *Ann. Phys.* **1948**, *2*, 55.

[7]   Gösele, U., Hauser M., Klein U. K. A., *Z. Phys. Chem.* **1976**, *99*, 81.

[8]   Selvin, P. R., *Methods Enzymol.* **1995**, *246*, 300.

3. Syntheses and Spectral Characterization

In this chapter, the synthesis and characterization of two labels are presented. They can be both covalently conjugated to HSA, anti-HSA and DNA. Furthermore, the syntheses of ruthenium MLC and fluorescein membrane probes is introduced.

3.1. Labels

3.1.1. The mono-reactive ruthenium metal-ligand complex Ru-1

Synthesis

Luminescent probes covalently linked to biological macromolecules are of widespread interest for basic studies such as characterizing biologically relevant energy- and electron-transfer reactions and for clinical applications such as detecting proteins and deoxyribonucleic acids (DNA) [1-4]. Probes like metal-ligand complexes known for a number of favorable properties for these puposes including (a) reversible electrochemical behavior, (b) photochemical stability, (c) energetic excited states and (d) long lifetimes in solution (see figure 3-1). Furthermore, such chromophores are widely used to study a number of photophysical processes including energy-transfer and electron-transfer reactions in supramolecular inorganic assemblies [5, 6] and biological systems [7]. For investigating protein and DNA systems, the mono-reactive ruthenium MLC Ru-(bipy)$_2$-(mcbpy) **Ru-1** was synthesized and activated to the corresponding NHS ester.
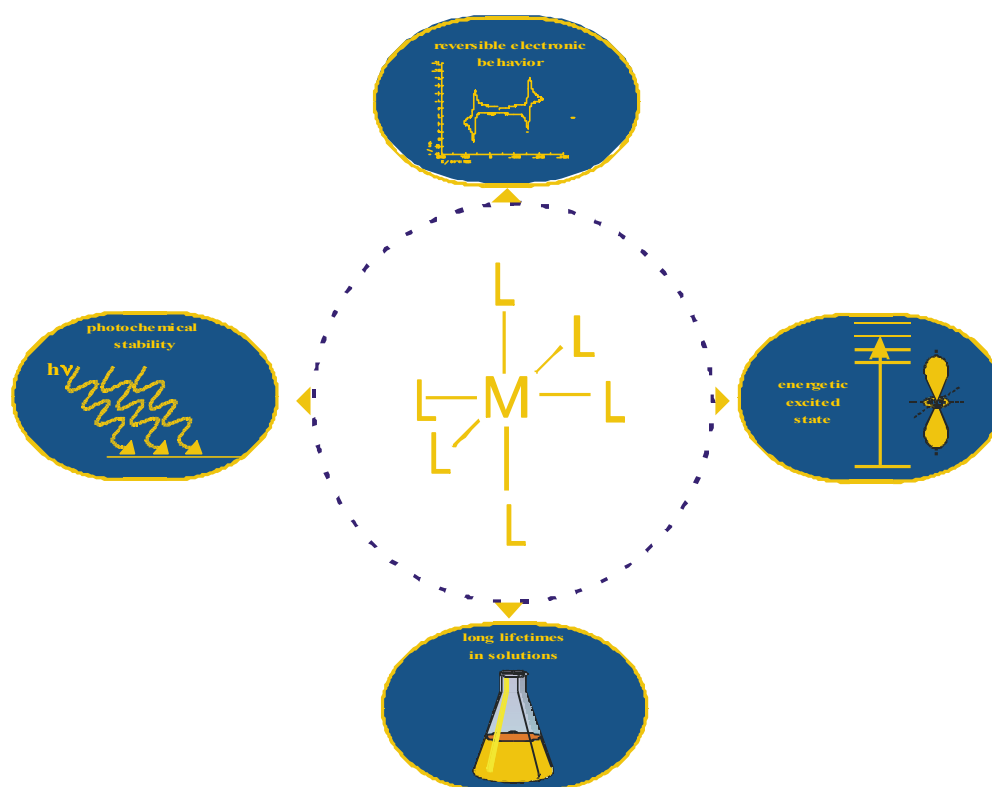
Fig. 3-1. *Properties of metal ligand complexes.*

The synthetic pathway of the activated NHS ester of **Ru-1** is shown in figure 3-2. The corresponding methyl derivatives are potentially useful precursors for carboxy compounds. Therefore, the mono-reactive ligand 4,4´-dimethyl-2,2´-bipyridine (**1**) was selectively oxidized to afford the 4´-mono-carbaldehyde derivative (**2**), using selenium dioxide as oxidizing reagent [8]. The carbaldehyde obtained was oxidized with $AgNO_3$ to the carboxylic acid **3**) in a yield of 75% [9]. The coupling of the third ligand (**3**) to $Ru(bipy)_2 \cdot 2H_2O$ was performed in an ethanol:water mixture (7:3, v/v) saturated with $NaHCO_3$. The reaction was carried out under reflux heating and the reaction time was set to 12 h. The active NHS ester of **Ru-1-NHS** was prepared by reacting N-hydroxysuccinimide/DCC with the carboxylic acid **Ru-1**.
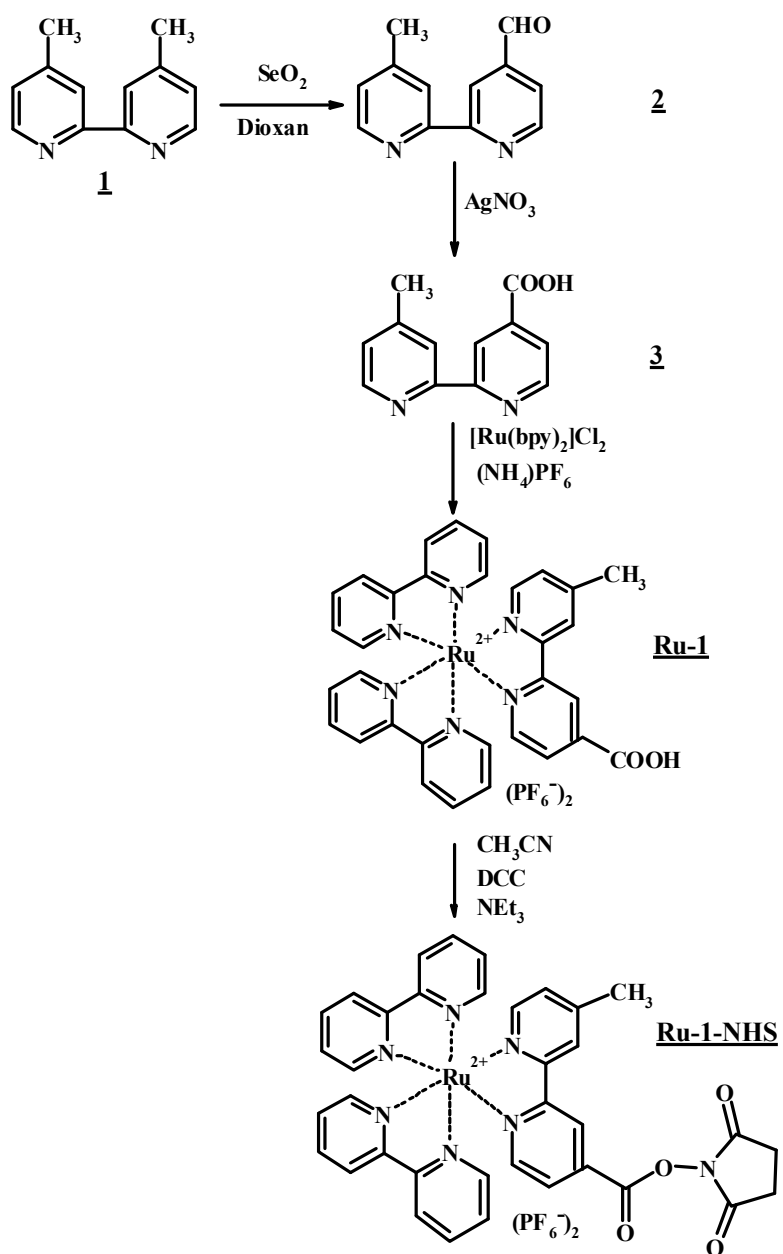
Fig. 3-2. *Synthetic pathway to the **Ru-1**-NHS ester.*

Characterization of **Ru-1**

The spectroscopic properties of **Ru-1** are presented in figure 3-3. **Ru-1** exhibits the characteristic metal-to-ligand charge-transfer band (MLCT), centered at 456 nm in the absorption spectrum. The same is found for $Ru(bipy)_3^{2+}$. The π-π^* transition of bipyridine is present at 280 nm. Excitation of the MLCT band at 450 nm results in an emission with a maximum at 612 nm in (phosphate buffer). Under these conditions the emission lifetime of **Ru-1** is 329 ns.
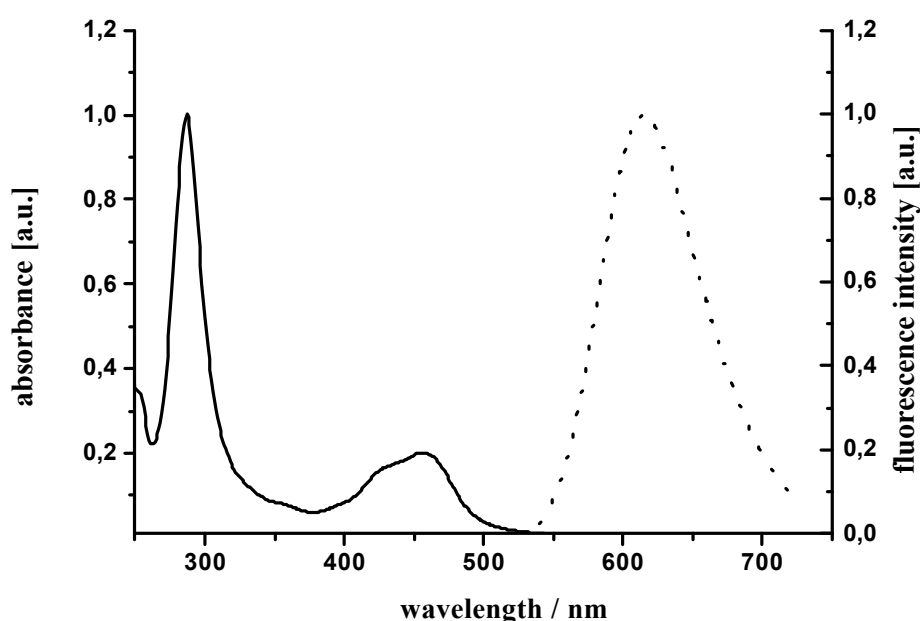
Fig. 3-3. *Absorption (straight line) and emission spectra (dotted line) of **Ru-1** in PBS.*

Sensitivity to oxygen

An investigation on the effect of oxygen on the fluorescence intensity and lifetime of the free and protein bound form was performed, when measuring the behavior of **Ru-1** and **Ru-1**/HSA either in air-equilibrated solutions or saturated with argon. The results are depicted in table 3-1. As compared to the deoxygenated solutions, the relative fluorescence intensities of **Ru-1** and **Ru-1**/HSA in air-equilibrated buffer solutions are 0.79 and 0.91, respectively.

The intensity of the free ruthenium complex is more sensitive to dissolved oxygen than the protein bound species. The lifetime measurements are in accordance with the obtained fluorescence intensity data. The results show that the sensitivity of the protein bound form is modest and do not require elimination of oxygen.

Table 3-1. Sensitivity of **Ru-1** (in PBS and when covalently bound to HSA) to oxygen in terms of emission intensity and lifetime.

| | **Ru-1** | | **Ru-1/HSA** | |
	air	argon	air	argon
rel. emission intensity	0,79	1	0,91	1
lifetime (ns)	395	517	488	512

3.1.2. The mono-reactive dye RB-631

Choice of label

The synthesis of unsymmetrical squarylium dyes has been demonstrated by Oswald et al. [10]. The advantage of these unsymmetrical dyes are their single reactive site, thus enabling the substance to be labeled only in a molar ratio of 1:1. Moreover, the bis-reactive dye can also react in a ratio of 1:2, leading to undesired dimers, or conjugates with decreased biological activity.

*Synthesis of **RB-631**-NHS*

RB-631 was synthesized by analogy to a procedure of Oswald [11]. The synthetic pathway is illustrated in figure 3-4. The unsymmetrical squarylium dye **RB-631** was synthesized in a 4-step reaction (**I-IV**). A carboxypentyl quaternized indole was reacted with the equamolar amount of squaric acid dibutyl ester (**I**). The dibutyl ester instead of the respective free acid has the advantage of a lowered reactivity. Thus, a direct synthesis to the symmetrical squarylium dye can mostly be avoided. This squaric acid derivative was reacted with a second indole, an ethyl quaternized one (**II**). The substitution of

hydrogen by an ethyl group at the indole nitrogen makes the dye pH insensitive to optical properties, which might appear at dyes having a free proton at this position. The long reaction time of 15 h results in the formation of the butyl ester, which is purified by MPLC. The butyl ester is hydrolyzed with 0.1 N HCl (**III**). The yield of this reaction is almost quantitative. Thus no further purification was necessary at this step. The last step of the synthesis is the activation to the NHS ester (**IV**). The NHS/DCC method was found to be the best due to the higher yield of NHS ester, compared to the N,N,N´,N´-tetramethyl(succinimido)uranium method [11].
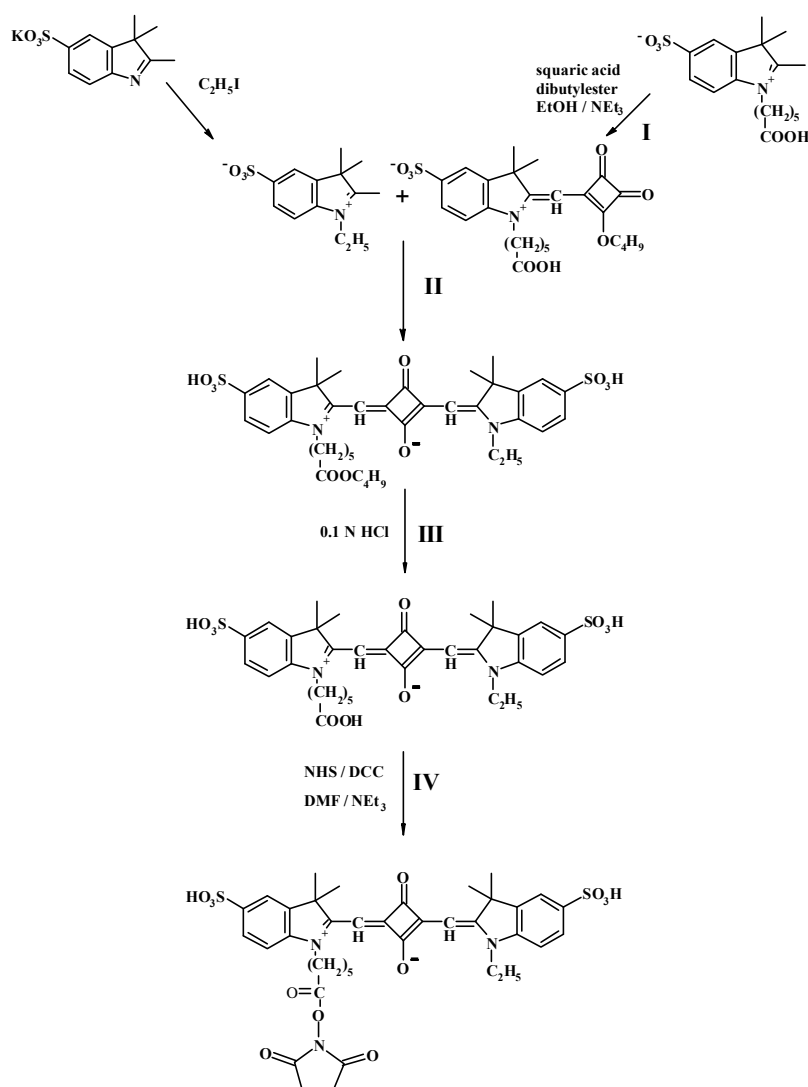
Fig. 3-4. Synthetic pathway to the **RB-631-NHS** ester.

*Characterization of **RB-631***

In figure 3-5, the spectroscopic properties of **RB-631** in PBS are shown. **RB-631** has an absorption maximum at 631 nm and an emission maximum at 645 nm. The molar absorbance is 95,000 L/(mol· cm) and the quantum yield is 0.04, using Cy5 as reference standard (QY_{CY5} = 0.25).
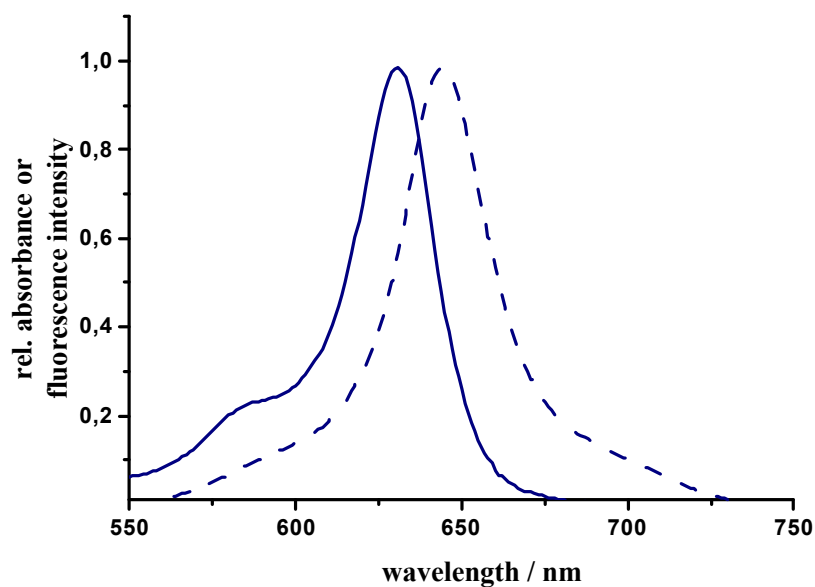
Fig. 3-5. *Absorption (straight line) and emission spectra (dotted line) of **RB-631** in PBS.*

3.2. Membrane probes

Fluorescent analogues of naturally occurring lipids are already applied primarily as probes of biological membrane structures and as tracer of lipid metabolism and transport. These membrane probes are frequently covalently attached to fatty acids or phospholipids. Most phospholipids are esters of glycerol comprising two fatty acyl residues (nonpolar tails) and a single phosphate ester substituent (polar head group). Fluorescent phospholipids analogues can be further classified according to the location of the attached fluorophore. A fluorophore can be bound either to one of the fatty acyl chains or to the polar head group and is situated either in the nonpolar interior or at the water/lipid interface. The fluorescent analog is incorporated into a lipid bilayer membrane. Fluorescent fatty acids can be substituted by the corresponding phospholipids as membrane probe [12]. The fluorescent sterols and cholsteryl esters are widely used as structural probes and transport markers for these important lipid constituents of membrane and lipid proteins.

In this work, phospholipids and fatty acids analogues of the luminescent ruthenium metal ligand complexes and the fluorescent fluorescein were synthesized and investigated for membrane characterization. All phospholipid analogues were covalently attached to the polar head group of the phospholipid. Therefore, the amphiphilic membrane probes are located at the water lipid interface when incorporated into a lipid bilayer.

3.2.1. Fluorescein membrane probes

The reactive NHS-fluorescein was used to link the lipophilic fatty acids and PE to the fluorophore. This fluorescein derivative was also used to label proteins and other macromolecules containing primary amine groups.

NHS-fluorescein is an amine-reactive fluorescent probe that contains a carboxysuccinimidyl ester group at position 5 or 6 carbons on fluorescein´s lower ring structure [13, 14]. The 5- and 6- isomers are identical in their

reactivity and fluorescence characteristics. The spectral properties of NHS-fluorescein are similar to those of the carboxy compound. The wavelength of the absorbance and emission maxima are 491 nm and 518 nm, respectively. The molar extinction coefficient is 66 000 mol $\cdot$ L^{-1} $\cdot$ cm^{-1}.

The reaction of the membrane probe (figure 3-6) was performed in chloroform, due to good solubility of the lipid and the membrane probe produced. However, the low solubility of the dye in chloroform required a reaction time of 24 h. The crude product was further purified by MPLC.
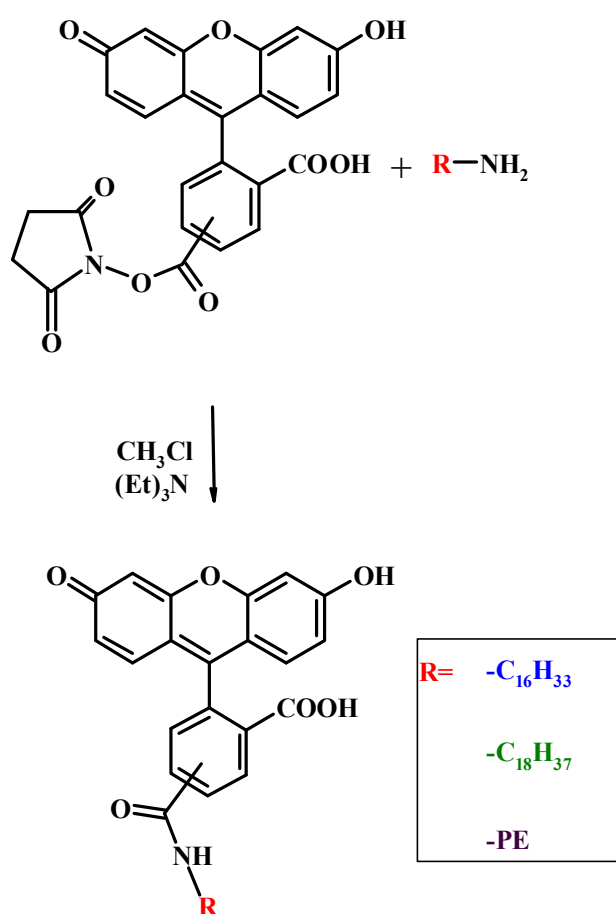
Fig. 3-6. *Synthesis of the fluorescein membrane probes (PE: 1,2-dipalmitoyl-sn-glycero-3-phosphoethanolamine).*

3.2.2. Ruthenium MLC membrane probes

*Membrane probes of the type **Ru-1-R***

Ru-1 was used as initial product for the synthesis of the membrane probes of the type **Ru-1-R** via the NHS/DCC method. The reaction was also carried out in chlorofom, because of the good solubility of the membrane probes and the lipid. The required analytical grade of the membrane probes was achieved by further purification with MPLC.
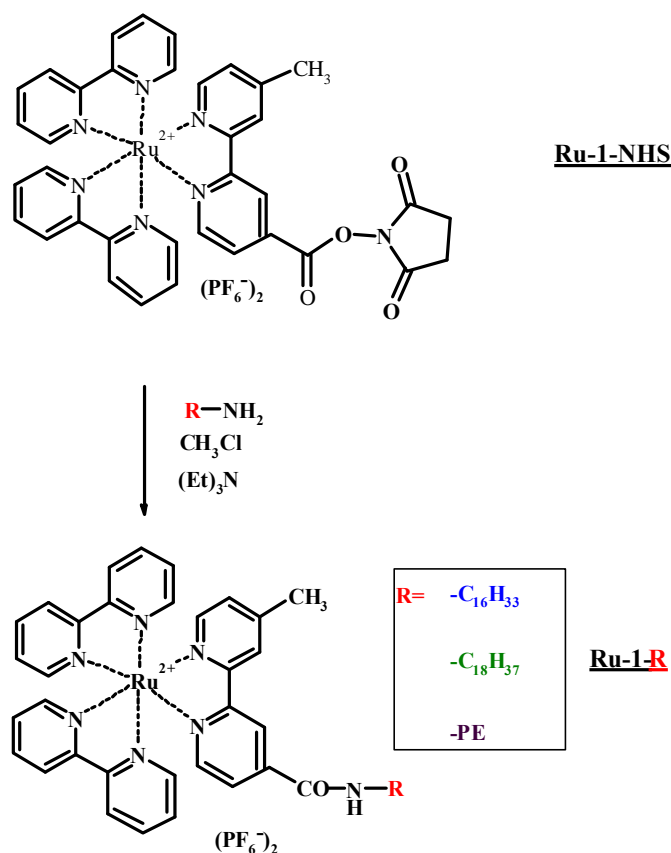
Fig. 3-7. *Synthesis of the membrane probes of the type* **Ru-1-R** *(PE: 1,2-dipalmitoyl-sn-glycero-3-phosphoethanolamine).*

Membrane probes of the type Ru-2-R₂

The membrane probes of the type **Ru-2-R₂** were synthesized in a 4-step reaction, starting from 4,4´-dimethyl-2,2´-bipyridine. The oxidation of 4,4´-dimethyl-2,2´-bipyridine to the respective carboxypyridine (**4**) was performed

by a simple oxidation step using aqueous chromium(VI)oxide. The yield of 90% was surprisingly good for the oxidation with CrO_3.

The coupling of the third ligand (**4**) to Ru(bipy)$_2$Cl$_2 \cdot$ 2H$_2$O was performed in a methanol:water mixture (4:1, v/v), saturated with NaHCO$_3$. The reaction was carried out by reflux heating for 12 h.

First, for the conversion of **Ru-2** to the respective membrane probe the NHS/DCC method was used with only a 5% yield. To increase the yield of the membrane probe an alternative method was found. The activation of the dicarboxy compound **Ru-2** was carried out by using the carbodiimide EDC and DMAP as catalyst. The reaction mixture was stirred at room temperature in chloroform. The enhanced reaction time of 15 h results in the formation of the specific membrane probe, which was purified by MPLC.
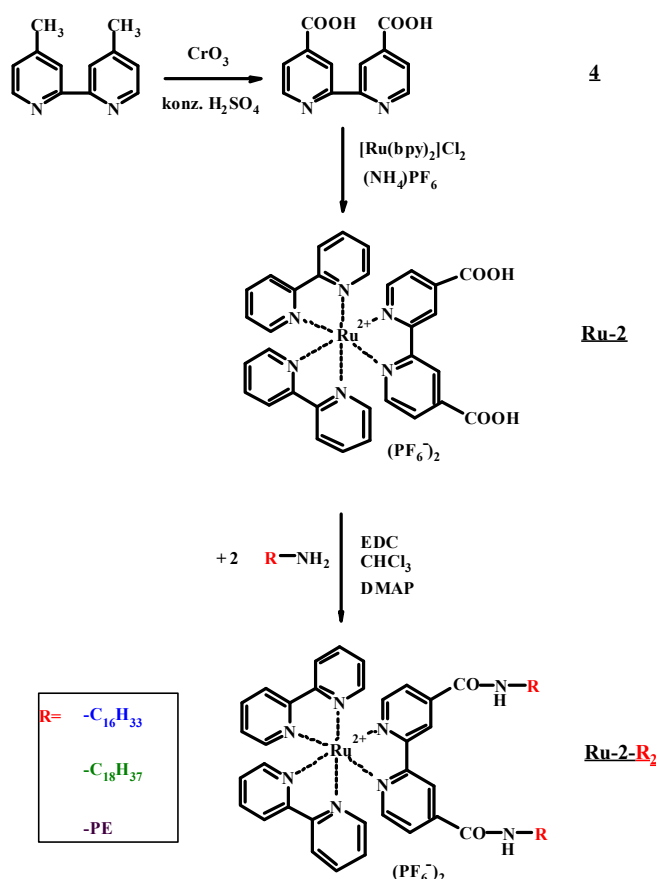
Fig. 3-8. *Synthetic pathway to the membrane probes of the type **Ru-2-R₂** (PE: 1,2-dipalmitoyl-sn-glycero-3-phosphoethanolamine).*

3.2.3. Spectral characterization of the membrane probes

In table 3-2, the absorption and emission maxima as well as the lifetime of fluorescein membrane probes are faced with the ruthenium MLC membrane probes. The data were recorded in methanol at 25 °C. All fluorescein derivatives exhibit the same spectral properties and are similar to those of the carboxy compound. The absorption and emission maxima were found at 497 nm and 520 nm, respectively. The average lifetime of the fluorescein membrane probes are about 4 ns.

Table 3-2. Absorption, emission and lifetime properties of the fluorescein and ruthenium MLC membrane probes.

membrane probe	λ_{max} (abs)	λ_{max} (em)	t (ns)
Fl-PE	497	520	4
Fl-C$_{16}$	497	520	4
Fl-C$_{18}$	497	520	4
Ru-1-C$_{16}$H$_{33}$	456	635	274
Ru-1-C$_{18}$H$_{37}$	456	635	279
Ru-1-PE	456	650	345
Ru-2-PE$_2$	456	665	398
Ru-2-(C$_{16}$H$_{33}$)$_2$	456	655	307
Ru-2-(C$_{18}$H$_{38}$)$_2$	456	655	305

The major absorption peak of all ruthenium MLC membrane probes is at 456 nm due to the metal-to-ligand charge transfer (MLCT). The results are similar to **Ru-1**. In contrast to the respective carboxy compound **Ru-1**, the emission maxima of all MLC membrane probes are shifted to higher wavelengths (see table 3-2).
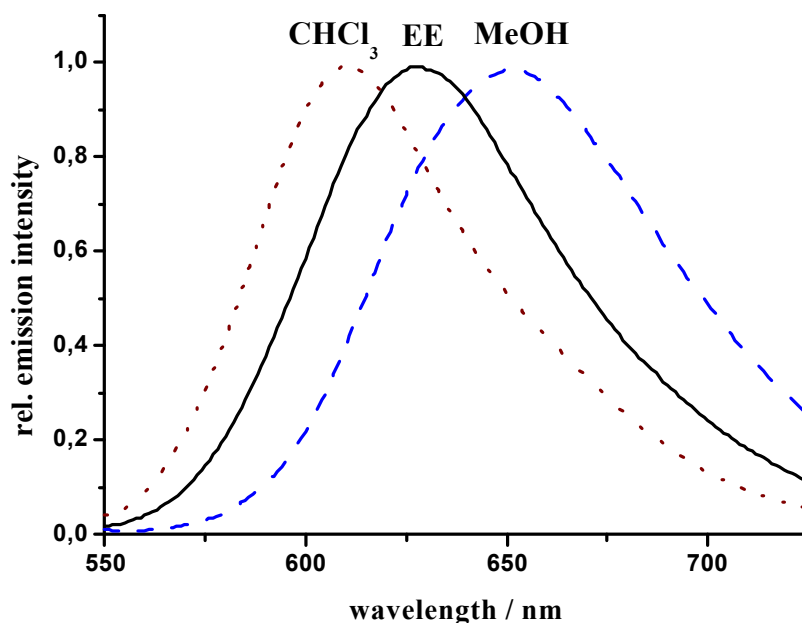
Fig. 3-9. *Emission behavior of the membrane probe* **Ru-2-(C₁₆H₃₃)₂**
for different solvents.

To investigate this effect, the emission maxima of the membrane probe **Ru-2-(C₁₆H₃₃)₂** was measured under different polar conditions (see figure 3-9). The emission maximum in methanol was found at 655 nm, while in chloroform the emission maxima is at 610 nm. A larger bathochromic shift was observed when a higher extend of alkylation of the membrane probe is used. The membrane probes with only one lipid anchor like **Ru-1-C₁₆** are smaller red-shifted than the probes of the type **Ru-2-R₂**. This effect is also concerned to the different behavior of the membrane probes in different solvent environments.

3.3. References

[1]   Kelley S. O., Barton J. K., *Science* **1999**, *283*, 375.

[2]   Clarke M. J., *Adv. Chem. Ser.* **1997**, *253*, 249.

[3]   Grinstaff M. W., *Angew. Chem., Int. Ed. Engl.* **1999**, *38*, 3629.

[4]   Holmlin R. E., Dandliker P. J., Barton J. K., *Angew. Chem., Int. Ed. Engl.* **1997**, *36*, 2713-3730.

[5]   Hurley D. J., Tor Y., *J. Am. Chem. Soc.* **1998**, *120,* 2194.

[6]   Dupray L. M., Devenney M., Striplin D. R., Meyer T. J., *J. Am. Chem. Soc.* **1997**, *119*, 10243.

[7]   Holmlin R. E., Dandliker P. J., Barton J.K., *Angew. Chem, Int. Ed. Engl.* **1997**, *36*, 2714.

[8]   Kus P., Knerr G., Czuchajowski L., *J. Heterocyclic Chem.* **1990**, *27*, 1161.

[9]   Peck B. M., Ross G. T., Edwards S. W., Meyer G. I., Meyer T. J., Erickson B. W., *Int. J. Peptide Protein Res.* **1991**, *38*, 113.

[10]   Oswald B., Patsenker L., Duschl J., Szmacinski H., Wolfbeis O. S., Terptschnig E., *Bioconj. Chem.* **1999**, *10*, 925.

[11]   Oswald B., *Dissertation* **1999**, Universität Regensburg.

[12]   Miller J., Thompson R., *Biochem* **1986**, *25*, 1717.

[13]   Brinkley M., *Bioconj. Chem.* **1992**, *3*, 2.

[14]   Vigers G. P. A., Coue J. R., Mcintosh J., *J. Cell biol.* **1988**, *107*, 1011.

4. Membrane Probes

Two types of lipophilic analogues of ruthenium metal-ligand complexes (MLC) and fluorescein derivatives were synthesized. These probes display polarized emission, thus making them viable probes for studying membrane dynamics and molecular orientational order. The probes were incorporated into lipid bilayers. The temperature-dependent properties of this lipid bilayers were investigated in terms of emission intensity, lifetime and steady-state fluorescence polarization.

4.1. Introduction

4.1.1. Membrane viscosity

Membrane viscosity, a parameter known to be affected by the structural and dynamic properties of cell membranes, is a key parameter in arteriosclerosis research. Cholesterol is the main sterol in animal organisms and plays a central role in modulating chemical and physical properties [1]. It is present in membranes of liver cells and erythrocytes in equimolar concentrations of phospholipids. Alterations in the cholesterol content in natural membranes are responsible for the membrane viscosity due to significant changes in the conformation and amplitude of the motions of the bilayer components [2-3].

4.1.2. Measuring membrane viscosity

Hydrophobic fluorescent molecules have proven to be suitable as probes for the characterization of various membrane properties including surface charge,

fluidity, lateral diffusion and metabolism of the lipid [4-6]. In studies of model and biological membranes, most of the useful probes are derivatives of pyrene and 1,6-diphenylhexatriene (DPH) [7]. So far, two methods were used to measure membrane viscosity. On the one hand, the excimer formation of pyrene decanoic acid (PDA) and on the other hand the fluorescence polarization of DPH is used. For both methods, the fluorophore is embedded in the membrane of interest.

Excimer formation of PDA

It is well known that an excited pyrene molecule in close proximity to a molecule remaining in its ground state may form a dimer in an excited singlet state ("excimer") [8]. The fluorescence emitted by the excimer is broad, unstructured, and red-shifted with respect to the monomer emission and is therefore readily distinguishable and well resolved from it. Since an excimer can form only if the excited pyrene molecule becomes a nearest neighbor to one in its ground state in a time comparable to the excited state lifetime, the relative yields of excimeric and monomeric fluorescence from a pyrene containing lipid analogue is a measure of the probes lateral mobility within the membrane [9, 10].
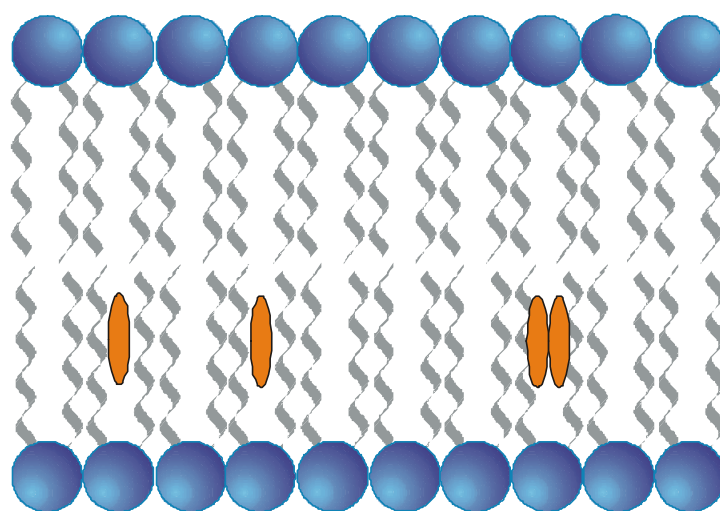
Fig. 4-1. *Schematic description of the excimer formation in membranes.*

Fluorescence polarization of DPH

Diphenylhexatriene and its derivatives are the probes of choice for structure and dynamic membrane studies [11, 12]. There, DPH has been used rather often to estimate membrane fluidity [13, 14]. DPH and its derivatives are well suited for such experiments because they exhibit a strongly increased fluorescence when bound to lipids. Additionally, their fluorescence polarization is sensitive to phospholipid orientational order, a parameter used to measure membrane viscosity. DPH is incorporated in the lipophilic part of the lipid bilayer. The membrane viscosity is measured by fluorescence polarization depending on the motion of DPH in the lipid bilayer, which corresponds itself to the membrane viscosity.

However, the use of PDA and DPH as membrane probes are limited due to their need for excitation in the UV, where fluorescence background is rather strong in "real" samples, and due to their lifetimes, which is in the nanosecond region.

4.1.3. Phase transition of DPPC liposomes

Phase transition in liposomes is a characteristic parameter to measure the properties and the composition of certain membrane. For our investigation we used the phospholipid di-palmitoyl-glycero-phosphatidylcholine (DPPC) for liposome preparation. The characteristic phase transition of DPPC occurs at 41 °C, which is presented in figure 4-2. The steady state fluorescence polarization of DPPC in the liquid crystalline phase is significantly lower than that in the gel phase, because greater static and dynamic molecular disorder is present in the liquid crystalline phase of the bilayer [15-17].
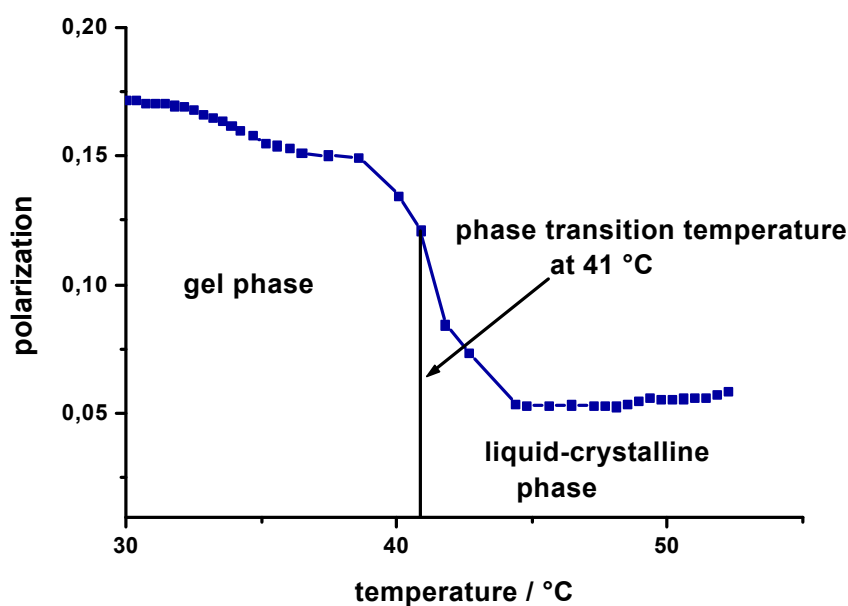
Fig. 4-2. *Temperature-dependent polarization of an incorporated dye in DPPC liposomes.*

4.2. New Membrane Probes

Probes with absorption and emission at wavelengths in the visible and near-infrared region are highly desirable, because background luminescence decreases strongly with wavelength (as does light scatter). We searched for probes excitable by the argon ion laser line (488 nm) and compatible with respective instrumentation in clinical research. Therefore, we considered two classes of luminophores being preferable for measuring membrane dynamics, namely amphiphilic fluorescein and ruthenium metal-ligand complexes, because both dye classes exhibit high fluorescence polarization.

4.2.1. Fluorescein membrane probes
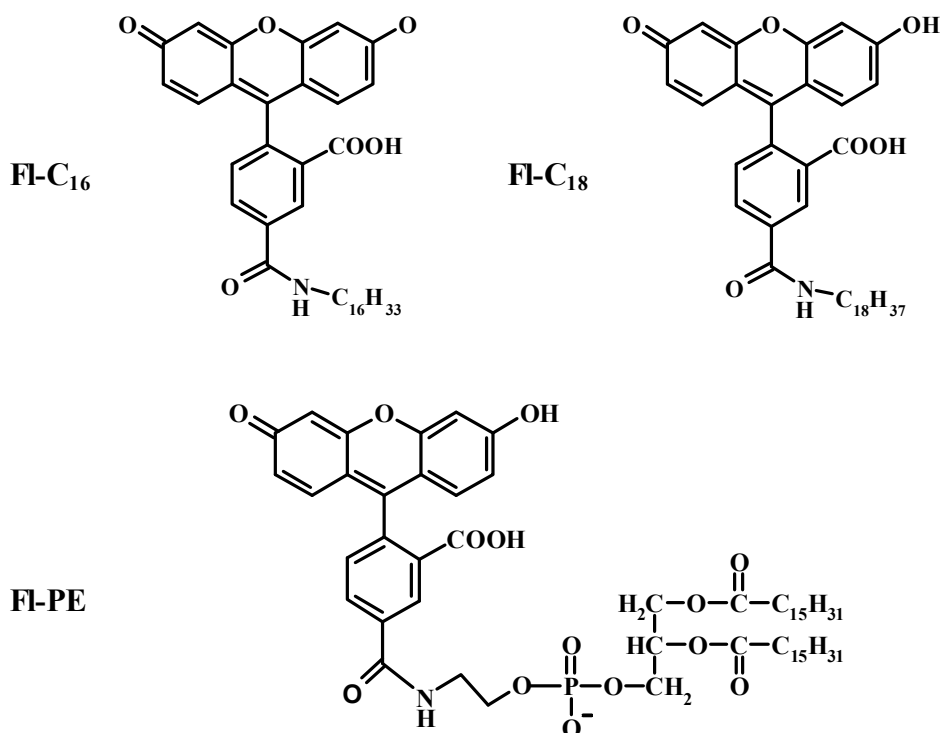
Fig. 4-3. *Amphiphilic fluorescein dyes synthesized for membrane probes.*

Fluorescein derivatives are the probes of choice for measuring membrane dynamics, because they exhibit a high fluorescence polarization of about 0.4. However, by employing amphiphilic fluorescein derivatives as membrane probe, the small Stokes' shift of 20 nm arises the problem of separating excitation to stray light and emitted light. The lifetimes of these fluorescein derivatives are in the nanosecond region similar to that which can be found for DPH.

To make the probe amphiphilic, dicarboxyfluorescein was covalently bound to hexadecylamine (**Fl-C₁₆**), octadecylamine (**Fl-C₁₈**) and 1,2-dipalmitoyl-sn-glycero-3-phosphoethanolamine (**Fl-PE**). The chemical structures of the synthesized fluorescein membrane probes are illustrated in figure 4-3.

4.2.2. Ruthenium MLC membrane probes

The ruthenium complexes comprise a class of metal-ligand complexes (MLCs) that are known to display luminescence if excited with light of 440 to 490 nm. Their luminescence exhibits a large Stokes' shift with a maximum at 610 nm. However, all conventional ruthenium MLCs are rather hydrophilic and do not incorporate into lipids or lipid membranes. They have to be rendered lipophilic by introduction of lipophilic side groups [18].

Ruthenium complexes show a certain advantages in terms of varying the characteristics of the membrane probes. Ruthenium membrane probes are comprised of three parts, which can affect the properties of the membrane probes (figure 4-4). The *preliminary compound of the metal-ligand complex* consists of two ligands, which can be varied. That can be hydrophilic, lipophilic and charged ligands influencing the incorporation of the membrane probe in the bilayers. The *reactive ligand* can be chosen as mono- or bisreactive ligand, which dispose to the degree of rotational freedom of the dye when incorporated in the membrane. Finally, the *lipophilic part* of the dye can be varied. Adherence of tails with varying chain length of phospholipids or lipids influences the depth of incorporation of the dye in the membrane [19].
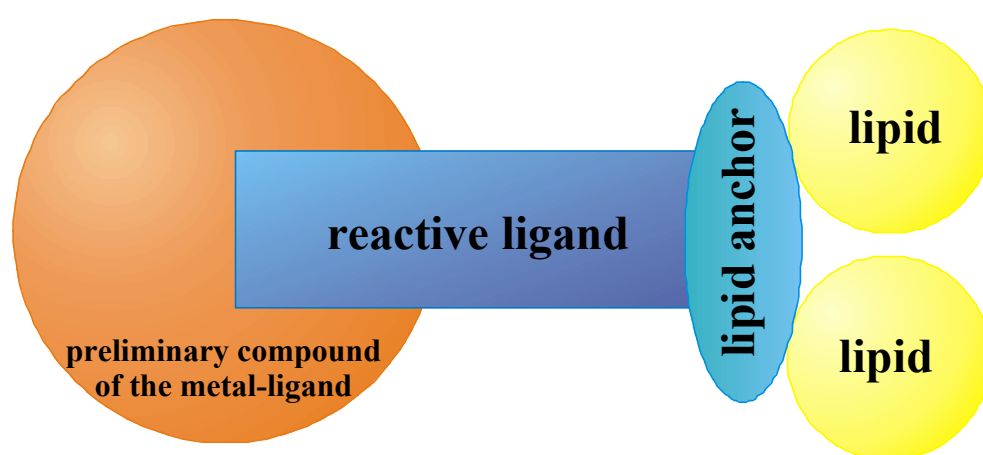
Fig. 4-4. *Schematic picture of a ruthenium metal-ligand complex membrane probe.*

The synthesis of new membrane probes based on a Ru-MLC fluorophore covalently bound to lipids and phospholipids is reported here. These amphiphilic probes incorporate their non-fluorescent tail into the bilayer, while the fluorescent moiety remains partly in the lipid-water interface (figure 4-5).
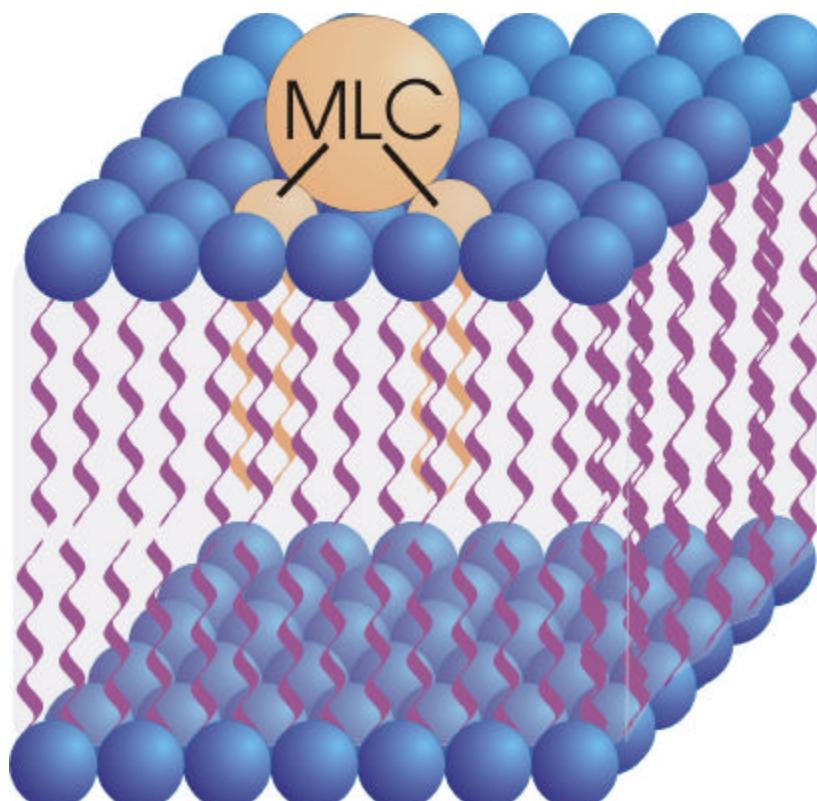
Fig. 4-5. *Schematic of the MLC probes incorporated into liposomes of DPPC.*

When designing the MLC membrane probes, we considered the pseudoglyceryl backbone and the C_{16} and C_{18} alkyl chains as a suitable structural anchor enabling incorporation into bilayers. These types of building blocks are ubiquitously present in naturally occurring phospholipids. Especially, two kinds of this MLC lipid probes were synthesized. In the first (**Ru-1-R**), the mono-carboxy derivative Ru(bpy)$_2$(mcbpy) is linked to a single lipid moiety. In

the second type (**Ru-2-R₂**), the dicarboxy MLC Ru(bpy)₂(dcbpy) was linked to two lipids. Probes of the kind **Ru-1-R** were expected to undergo free rotation on the membrane surface. For **Ru-2-R₂**, the MLC is linked to two lipid moieties and it was expected that this may retard or even prevent free rotation of the MLC and thus improves the resolution at comparatively long rotational correlation times. The excitation and emission maxima of these complexes are at approximately 460 and 640 nm, thus making them compatible with commonly used flow cytometers based on a 488-nm excitation source. The chemical structures of the ruthenium MLC membrane probes are displayed in figure 4-6.
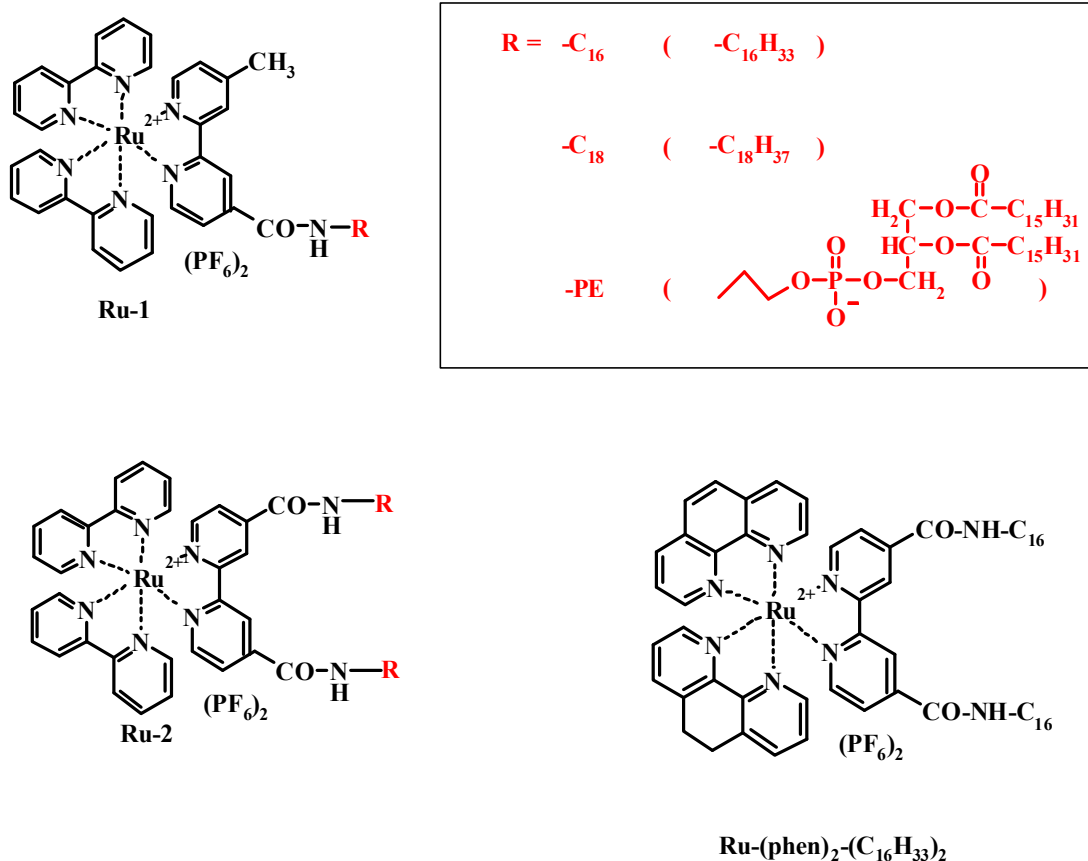
Fig. 4-6. Chemical structures of the ruthenium metal-ligand complex membrane probes.

4.3. Methods and Materials

4.3.1. Materials

DPPC (1,2-dipalmitoyl-sn-glycero-3-phosphatidylcholine), PE (1,2-dipalmitoyl-sn-glycero-3-phosphoethanolamine) and cholesterol were purchased from Sigma. All other chemicals were supplied from Fluka and used as received. Solvents were from Merck. The water used was double distilled.

4.3.2. Preparation of Liposomes

For liposome preparation, aliquots (typically 1 mg of DPPC and an aliquot quantity of the lipid probes in a dye to lipid ratio of 1:100) were dissolved in 2 mL of chloroform and placed in a test tube. This solution was kept in a water bath at 55 °C and the solvent was removed by a stream of nitrogen. Liposomes were prepared by sonication in a buffer (10 mM Tris and 50 mM KCl, pH 7.5) at a final lipid concentration of 1 mg/mL. After vortex-mixing, the sample was passed through a polycarbonate filter (100 nm pore size) with an extruder (Avestin Lipofast, Avestin, Ottawa, Canada). For visualization the colloid liposomes in the lipid mixture were digitalized with a fluorescence microscope shortly before the extruding step (figure 4-7). After extruding solely a homogeneous red fluorescence was observed when verified with the fluorescence microscope. This indicates a liposome size < 100 nm.
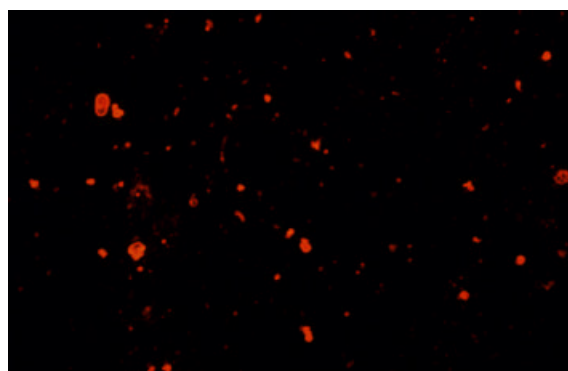
Fig. 4-7. *Ruthenium membrane probes shortly before the extruding step.*

4.4. Results

There are certain requirements for membrane probes to be suitable for measuring membrane dynamics. The amphiphilic dyes have to display polarization in such a way that membrane dynamics can be measured according to the DPH method. The polarized emission has to be sensitive to the characteristic phase transition temperature of the liposomes, where the dye is embedded. After all, the membrane probes has to show cholesterol-dependent polarization.

The suitable fluorescein and ruthenium MLC membrane probes have to accomplish

  (a) a temperature-dependent polarization in glycerol,

  (b) a sensitivity to the phase transition of DPPC at 41 °C when embedded in DPPC liposomes, and

  (c) a cholesterol sensitivity when embedded in DPPC liposomes with variable cholesterol content.

4.4.1. Temperature-dependent steady-state polarization

Membrane probes in glycerol

Due to its high viscosity, glycerol was used as the solvent instead of aqueous solutions to dissolve the membrane probes. An increased viscosity reduces the rotational freedom of the membrane probe enabling polarization measurements. The fluorescence polarization was quantified as a function of the temperature or rather the viscosity of the solvent. Both the fluorescein (figure 4-8) and the ruthenium MLC membrane probes (figure 4-9) indicate a change in polarization by varying the temperature. The membrane probe **Ru-2-PE$_2$** could not be specified directly due to the low solubility in a glycerol/water mixture.
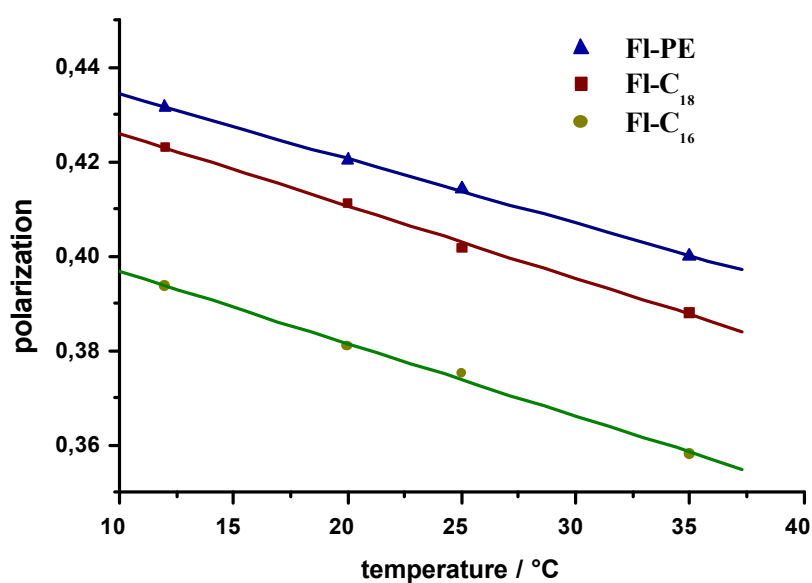
Fig. 4-8. *Temperature-dependent polarization of the fluorescein membrane probes in glycerol.*
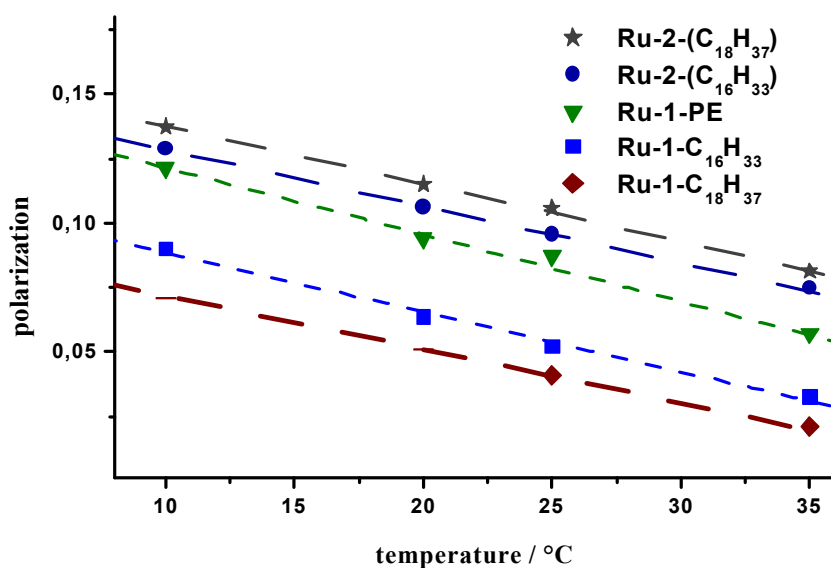
Fig. 4-9. *Temperature-dependent polarization of the ruthenium MLC membrane probes in glycerol.*

It is found that the fluorescein membrane probes **Fl-PE, Fl-C$_{18}$** and **Fl-C$_{16}$** have polarization values higher than 0.4. This is attributed to the low lifetime (4 ns) of the fluorescein derivatives, since the polarization is inversely

proportional to the lifetime of the respective dyes (see chapter 2). As expected, the polarization values of the ruthenium MLC membrane probes were found to be about 0.1 owing to their lifetime which is in the range of hundred nanoseconds.

All membrane probes have two fatty acyl residues (non-polar tail). The fluorescein as well as the ruthenium MLC membrane probes tend to have an increased polarization in contrast to the membrane probes with only one lipid anchor. This effect can be directed to the reduced rotational freedom caused by the two anchors attached to the fluorophore. In comparison to the fluorescein membrane probes in glycerol, the ruthenium MLC probes show an enhanced change in polarization with temperature (see table 4-1). This effect may be a first hint for preferring the ruthenium MLC membrane probes.

Table 4-1. Temperature-dependent polarization (P) of the fluorescein and ruthenium MLC membrane probes in glycerol.

membrane probe	P (12 °C)	P (35 °C)	D P
Fl- PE	0.431	0.400	**0.031**
Fl- C_{18}	0.423	0.393	**0.030**
Fl- C_{16}	0.389	0.358	**0.031**
Ru-2-$(C_{18}H_{37})_2$	0.137	0.081	**0.056**
Ru-2-$(C_{16}H_{33})_2$	0.128	0.074	**0.054**
Ru-1-PE	0.121	0.057	**0.064**
Ru-1-$C_{16}H_{33}$	0.090	0.030	**0.060**
Ru-1-$C_{18}H_{37}$	0.080	0.024	**0.056**

Fluorescein and ruthenium MLC membrane probes in DPPC

The polarization behavior of the membrane probes at the phase transition temperature of DPPC liposomes (i.e. 41 °C) was investigated. The membrane probes **Fl-PE** and **Ru-2-PE$_2$** were first studied in terms of their polarization sensitivity to phase transition. The probes were incorporated in DPPC

liposomes as described in chapter 4.2.1. The results are depicted in figure 4-10. **Fl-PE** has an increased polarization, but there was no change in polarization at the phase transition temperature of DPPC. The same results were obtained for the dyes **Fl-C$_{16}$** and **Fl-C$_{18}$**. Obviously, the low lifetimes of the fluorescein membrane probes are the reason for no lateral diffusion in the DPPC liposomes. In contrast, **Ru-2-PE$_2$** displays the typical phase tranisition at 41 °C. Its significant change in polarization of 0.13 at the phase transition temperature of DPPC makes the group of the amphiphilic ruthenium metal-ligand complexes to a promising luminophore for studying membrane dynamics. Therefore, the ruthenium MLC membrane probes were used for further investigations.
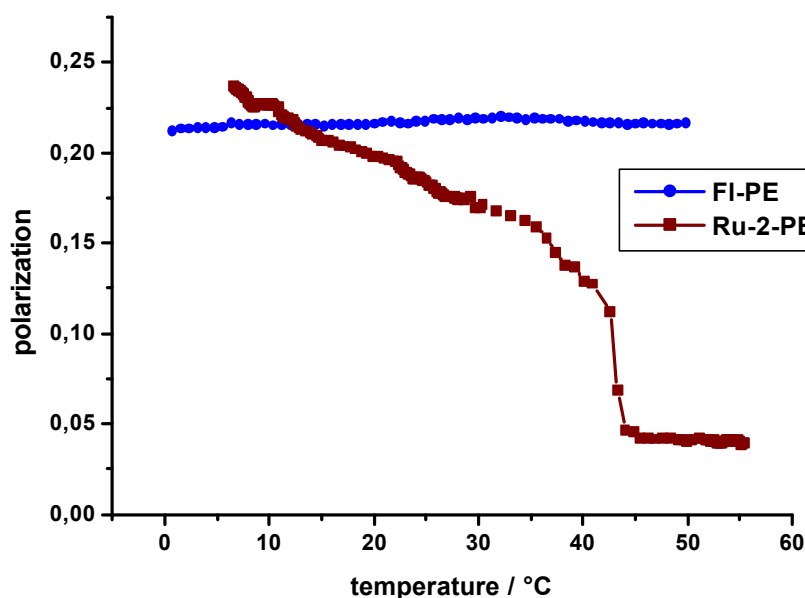
Fig. 4-10. *Temperature-dependent polarization of the ruthenium MLC membrane probes in glycerol. Faced with **Fl-PE**, **Ru-2-PE$_2$** displays a slope at the phase transition temperature of 41 °C of DPPC.*

Varying chain length and ligand

The effect of the chain length of membrane probes with the same anchor type on polarization was investigated for the pair **Ru-2-(C$_{16}$H$_{33}$)$_2$** and **Ru-2-(C$_{18}$H$_{37}$)$_2$**. It was found that the two membrane probes display similar polarized emission at 35 °C. Additionally, the sensitivity in polarization to phase transition (ΔP) was identical (table 4-2). A similar result was obtained for the pair **Ru-1-C$_{16}$H$_{33}$** and **Ru-1-C$_{18}$H$_{37}$**.

Table 4-2. Temperature-dependent polarization of ruthenium MLC membrane probes incorporated in DPPC liposomes.

membrane probe	P (35 °C)	P (45 °C)	Ð P
Ru-2-(C$_{16}$H$_{33}$)$_2$	0.126	0.029	**0.097**
Ru-2-(C$_{18}$ H$_{37}$)$_2$	0.128	0.036	**0.092**
Ru-phen$_2$-(C$_{16}$ H$_{33}$)$_2$	0.127	0.035	**0.092**
Ru-1- C$_{16}$H$_{33}$	0.112	0.053	**0.059**
Ru-1- C$_{18}$ H$_{37}$	0.114	0.053	**0.061**

At last, the effect of the ligands on the properties of the membrane probes in liposomes were quantified with the ligands bipyridyl (**Ru-2-(C$_{16}$)$_2$**) and phenanthroline (**Ru-phen$_2$-(C$_{16}$)$_2$**). As one can see in table 4-2, no significant difference in temperature-dependent polarization was observed.

The results demonstrate that the membrane probes of the type **Ru-1-R**, **Ru-1-C$_{16}$H$_{33}$** and **Ru-1-C$_{18}$H$_{37}$** exhibit a reduced polarization effect in terms of phase transition. As a result, these two probes were excluded from further measurements. For the membrane probes with two anchors, **Ru-2-(C$_{16}$)$_2$** acts as representative for the probes **Ru-2-(C$_{18}$H$_{37}$)$_2$** and **Ru-phen$_2$-(C$_{16}$)$_2$**, because the same polarization behavior was found at phase transition in DPPC liposomes. In the following chapter, the investigation were restricted to the three most promising membrane probes **Ru-2-(C$_{16}$)$_2$,** **Ru-1-PE** and **Ru-2-PE$_2$**. The dye derivatives were evaluated for the use as

membrane probes in terms of emission intensity, temperature-dependent polarization and cholesterol-dependent polarization.

4.4.2. Characterization of the membrane probes Ru-2-(C$_{16}$)$_2$, Ru-1-PE and Ru-2-PE$_2$

Spectral characterization

The absorption and emission spectra of probe **Ru-2-(C$_{16}$)$_2$** in DPPC liposomes with and without cholesterol are shown in figure 4-11.
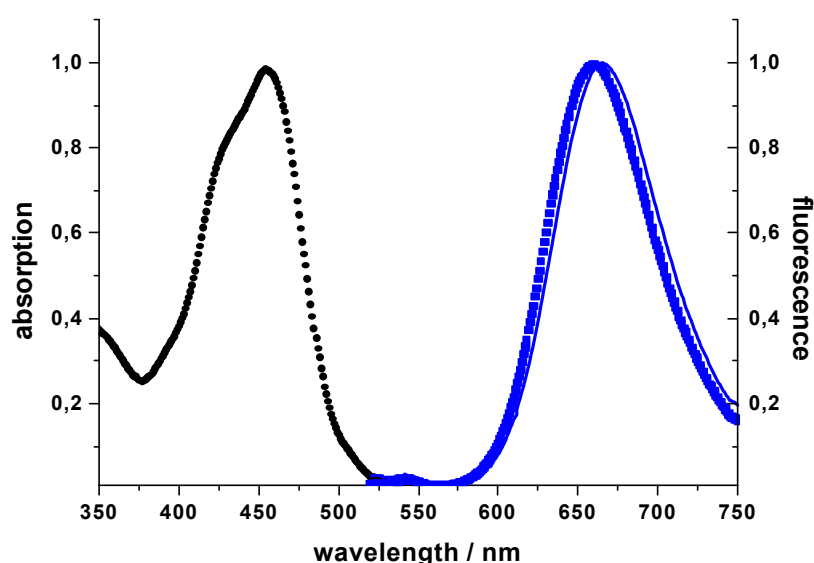
Fig. 4-11. *Absorption and emission spectra of* **Ru-2-(C$_{16}$)$_2$** *in DPPC (----) and DPPC /cholesterol (1:1) (——) liposomes at 20 °C.*

The maximum of the low energy absorption band at about 450 nm is the characteristic metal-to-ligand charge transfer transition of an MLC of the Ru(bipy) type. This band is hardly affected by the environment. In comparison to the emission maxima of the respective carboxy compounds (without lipid side chain), which are at 610 nm, the emission maxima of the membrane probes are shifted to longer wavelengths (647 - 674 nm; see table 4-3). This effect is observed only in case of incorporation into liposomes, while in chloroform solution the emission maxima are in the range of 610 nm. The

bathochromic shift is assumed to be due to solvent effects since similar spectra are observed in methanol solution and related effects have been found elsewhere [20]. Characteristic spectroscopic data of the membrane probes **Ru-1-PE**, **Ru-2-PE$_2$**, and **Ru-2-(C$_{16}$)$_2$** are summarized in table 4-3.

Table 4-3. Absorption and emission maxima (in nm) of membrane probes **Ru-1-PE, Ru-2-PE$_2$** and **Ru-2-(C$_{16}$)$_2$** in liposomes at 22 °C.

probe	λ_{max} (abs)	λ_{max} (em) in DPPC	λ_{max} (em) in DPPC/cholesterol (1:1)
Ru-1-PE	456	647	655
Ru-2-PE$_2$	456	666	674
Ru-2-(C$_{16}$)$_2$	456	659	666

The existence of phase transitions within membranes is a characteristic feature of liposomes. The membrane probes were embedded in DPPC as described. The emission intensity of these liposomes depends on temperature. An increase in temperature showed a small shift to lower emission intensities and a sharp decrease at the phase transition temperature (T$_m$) of DPPC at 41 °C, as can be seen in figure 4-12. This behavior is typical [21] for Ru-MLC complexes due to the enhancement of nonradiative decay pathways. At temperatures below the phase transition, the probes can be assumed to be located closer to the interior of the lipid bilayer and therefore to be protected from fluorescence quenching by water. Above the transition temperature, the probes are pushed out of the bilayer and localized at the lipid-water interface. This effect is more obvious for **Ru-2-(C$_{16}$)$_2$** which can be assumed to be closer to the membrane bilayer because of the presence of two alkyl chains.
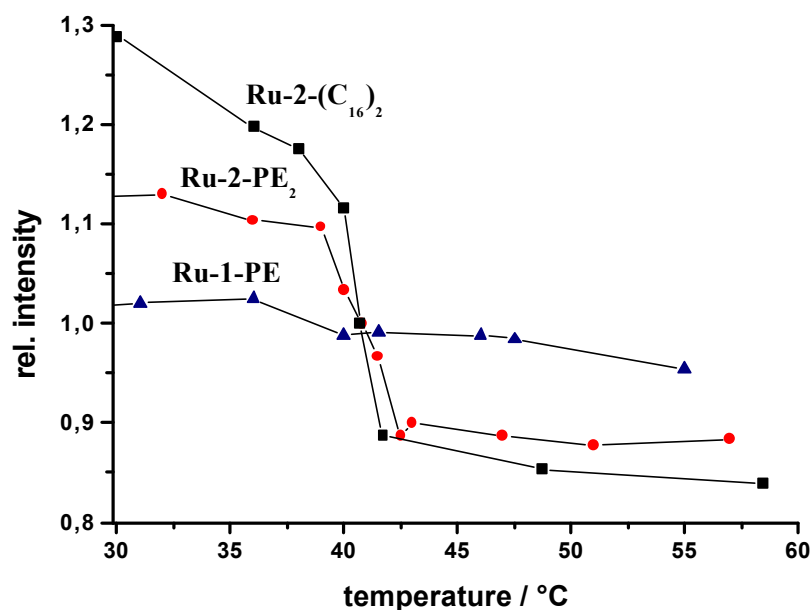
Fig. 4-12. *Temperature-dependent fluorescence of the membrane probes* **Ru-1-PE** *,* **Ru-2-PE₂** *and* **Ru-2-(C₁₆)₂** *incorporated into DPPC liposomes.*

Lifetime Measurements

Time-resolved fluorescence measurements of the probe **Ru-2-(C$_{16}$)$_2$** at several temperatures are presented in figure 4-13. The data were analyzed assuming a single exponential decay. The data for the probes **Ru-1-PE**, **Ru-2-PE$_2$** and **Ru-2-(C$_{16}$)$_2$** incorporated in DPPC as a function of both the temperature and the phospholipid/cholesterol ratio are compiled in table 4-4.
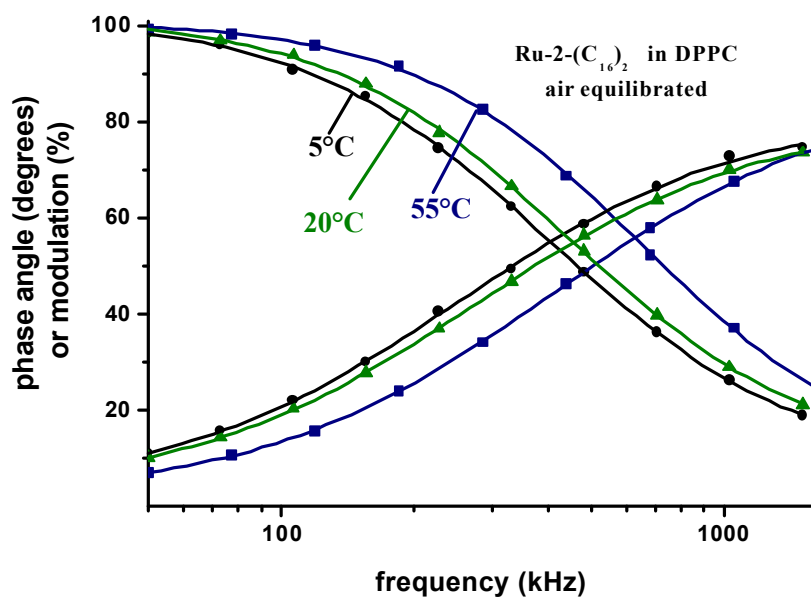
Fig. 4-13. *Frequency-domain intensity decays of Ru-2-(C₁₆)₂ in DPPC liposomes at various temperatures.*

Table 4-4. Fluorescence lifetimes τ (in ns) of probes **Ru-1-PE** , **Ru-2-PE₂**, and **Ru-2-(C₁₆)₂** in DPPC liposomes and in DPPC/cholesterol (1:1) liposomes (data in brackets).

probe	τ (5 °C)	τ (20 °C)	τ (35 °C)	τ (45 °C)	τ (55 °C)
Ru-1-PE	485	443	415	382	379
	(448)	(401)	(397)	(374)	(347)
Ru-2-PE₂	612	522	463	408	357
	(550)	(482)	(408)	(392)	(351)
Ru-2-(C₁₆)₂	624	597	509	434	385
	(551)	(494)	(423)	(416)	(389)

The mean decay times of **Ru-2-PE₂** and **Ru-2-(C₁₆)₂** drop from approximately 600 ns at 5 °C to ~ 400 ns at 55 °C. The lifetime of **Ru-1-PE** is shorter and less affected by the micro-environment. This can be reasoned by the possibility of free rotation of the probe on the membrane surface. Due to

their long decay times, the MLC membrane probes can be used to measure rotational motions in membranes up to $2\mu s$, i.e. three times the mean decay time [22]. On increasing the fraction of cholesterol in the liposomes, the decay times decrease steadily. In the liquid-crystalline phase, the lifetimes are quite similar to those in pure DPPC liposomes.

Temperature-dependent steady-state polarization

In order to be useful for lipid hydrodynamic studies, the probes need to display polarized emission. Because of the poor solubility of the membrane probes in water:glycerol, the maximal polarization of the carboxy MLCs Ru-(bpy)$_2$(mcbpy) and Ru-(bpy)$_2$(dcbpy) were measured and found to be 0.17 and 0.23, respectively (21).   The polarization spectrum of the synthesized MLC membrane probes are similar to the polarization spectra of (a) the free carboxy acids of the MLCs (10) and (b), the MLC carboxy compound covalently linked to the amino groups of proteins [23].

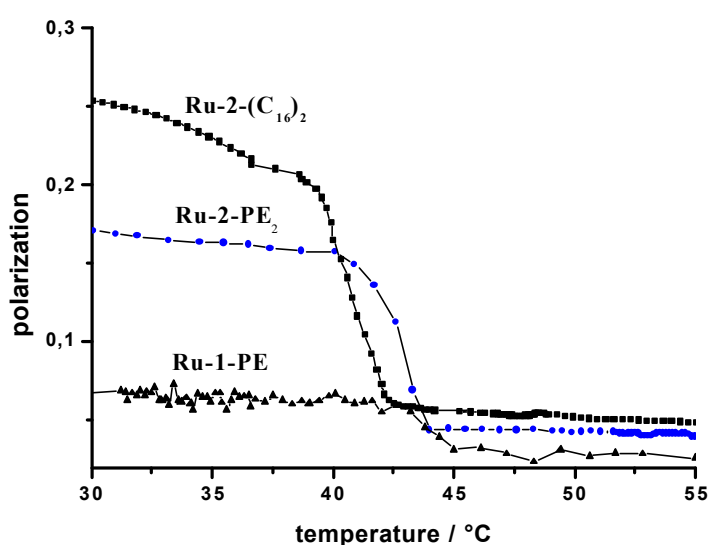**Fig. 4-14.** *Temperature-dependent fluorescence polarization of* ***Ru-1-PE*** *,* **Ru-2-PE$_2$** *and* **Ru-2-(C$_{16}$)$_2$** *incorporated into DPPC in a ratio of 1:100.*

The steady-state fluorescence polarization data were acquired between 30 and 55 °C, i.e. under conditions where DPPC is either in the gel state or the liquid-crystalline state. The steady-state fluorescence polarization data of the membrane probes are presented in figure 4-14. The polarization decreases progressively with increasing temperature as expected for a probe undergoing thermal motion. The steady-state fluorescence polarization of the membrane probes is significantly lower in the liquid-crystalline state than in the gel phase of DPPC, suggesting that greater static and dynamic molecular disorder is present in the liquid-crystalline phase of the bilayer (figure 4-14). A sharp phase transition occurs about 41 °C for all membrane probes, which is in accordance with findings obtained with DPH-labeled membranes [24]. **Ru-2-(C$_{16}$)$_2$** shows the highest sensitivity to phase transition, probably because of the presence of two lipid chains which may reduce free rotation in the membrane. A second reason for this finding may result from a closer distance between the chromophore of **Ru-2-(C$_{16}$)$_2$** and its lipid anchor located in the liposome membrane (in comparison to **Ru-1-PE** and **Ru-2-PE$_2$**).

Cholesterol-dependent steady-state polarization

Cholesterol is an integral part of melanoma cell membranes and known for non-covalent association with lipids within the cell [25]. Such interactions can affect the orientational order of lipid hydrophobic chains in membranes [26-32] which, in turn, can change the solid-fluid transition temperature of the resulting bilayers [33]. The probe **Ru-2-(C$_{16}$)$_2$**, solubilized in various vesicular assemblies, was used to measure the effect of cholesterol on the polarized emission of **Ru-2-(C$_{16}$)$_2$**. In phospholipid liposomes, cholesterol differently modifies the gel phase and the liquid-crystalline phase. The disorder of the gel phase increases on addition of cholesterol, while the liquid crystalline phase becomes more ordered on addition of cholesterol [34-35].

As expected, the incorporation of cholesterol into DPPC bilayers reduces the disorder in the liquid-crystalline state of our membrane probes, as can be deduced from the observed larger steady-state polarization (figure 4-15). In

contrast to the behavior in the liquid crystalline state, the polarization was smaller in liposomes with a higher fraction of cholesterol. It can be assumed that this is due to the enhanced rotational freedom of the dye in the gel phase.
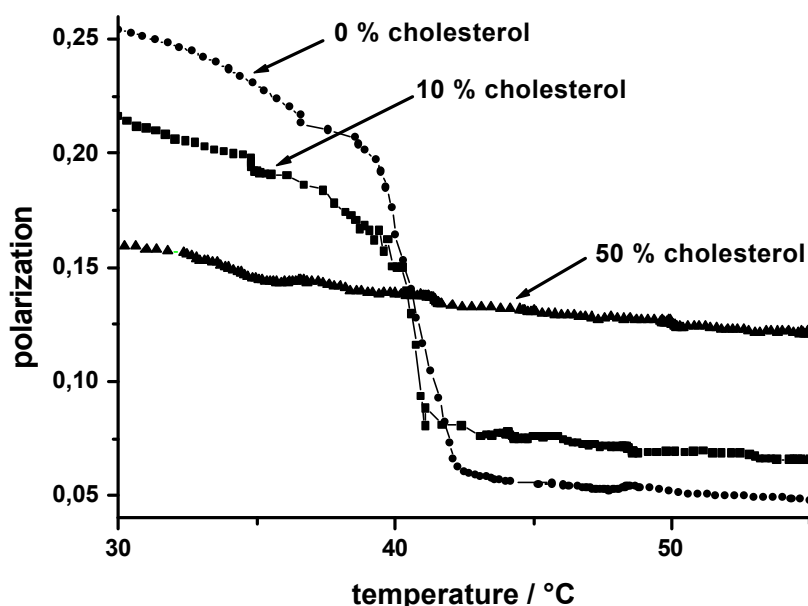
Fig. 4-15. *Temperature dependence of the steady-state fluorescence polarization of Ru-2-$(C_{16})_2$ in DPPC/cholesterol liposomes at various sterol concentration.*

To compare the membrane probes in terms of sensitivity to cholesterol, the differences in the polarization in the liquid crystalline form and in the gel phase, respectively, were plotted against the fraction of cholesterol in the DPPC liposomes. The results are shown in figure 4-16. The probe **Ru-1-PE** displays low sensitivity to cholesterol. In contrast, **Ru-2-PE$_2$** and **Ru-2-(C$_{16}$)$_2$** display sensitivity to cholesterol in the range from 0 to 30% cholesterol in the DPPC liposomes. **Ru-2-(C$_{16}$)$_2$** is more sensitive. It is important to note that the results obtained with the ruthenium MLCs are quite similar to those obtained with DPH (which was often used for cholesterol-dependent measurements in liposomes).
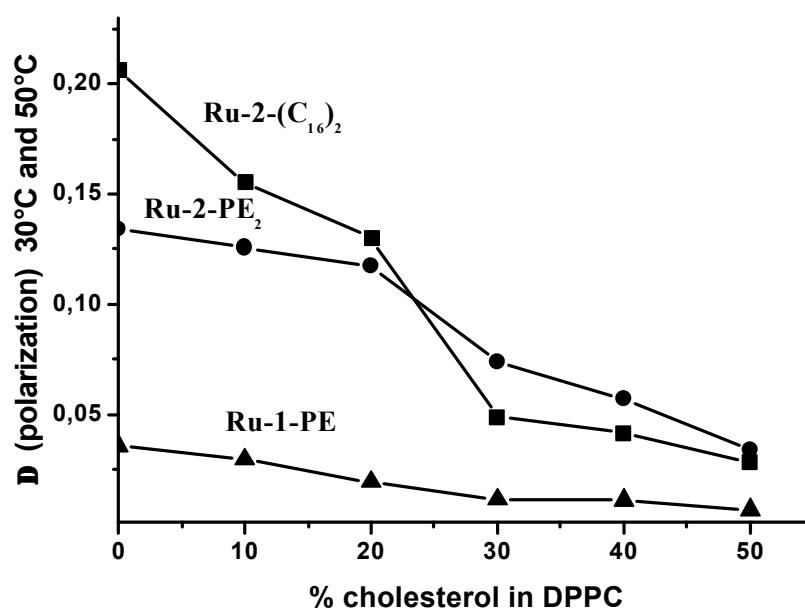
Fig. 4-16. *Comparison of membrane probes **Ru-1-PE**, **Ru-2-PE$_2$** and*
***Ru-2-(C$_{16}$)$_2$** in terms of the polarization at 30 °C and 50 °C in*
liposomes of DPPC containing different fractions of cholesterol.

4.4.3. Real sample: Ru-1-PE as membrane probe in erythrocytes[1]

The membrane probe **Ru-1-PE** was incorporated into a real sample, namely erythrocytes. The determination of the cholesterol content in erythrocytes in arteriosclerosis research is of large clinical interest. A way to quantify cholesterol is to specify the viscosity of the erythrocytes. The first step to enable such a measurement is to identify a membrane probe that can be incorporated into a living cell. For this purpose **Ru-1-PE** was incubated in erythrocytes and the temperature-dependent polarization was measured. The polarization of the probe in erythrocytes was six times higher in comparison to the probe in PBS. This effect verifies the incorporation of **Ru-1-PE** in the erythrocytes resulting in a higher polarization value due to reduced rotational

---

[1] Measurement was performed in cooperation with the Department of Clinical Chemistry (Dr. G. Rothe, Prof. G. Schmitz), University of Regensburg

freedom of the membrane probe. The clinical evaluation of the system will be performed by the Department of Clinical Chemistry, University of Regensburg.
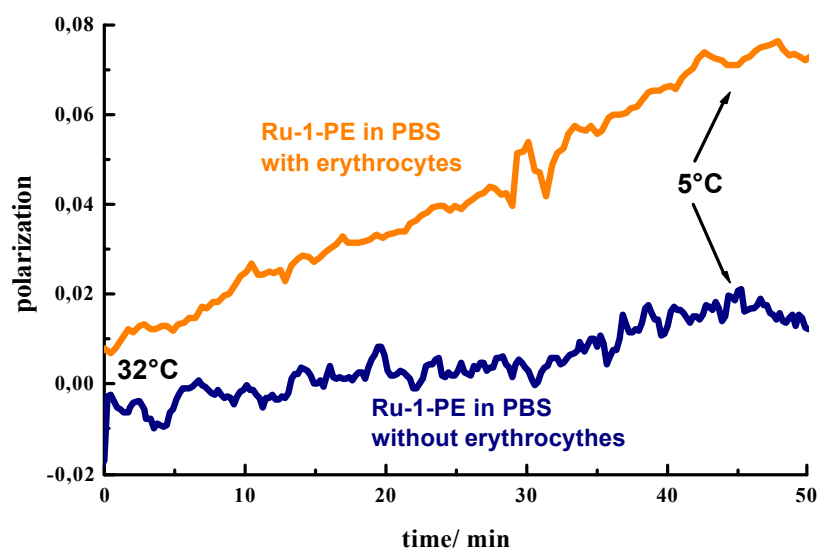
Fig. 4-16. *Temperature-dependent polarization of **Ru-1-PE** in PBS with and without erythrocytes.*

4.5. Conclusion

This work demonstrates that the new amphiphilic MLC probes are sensitive to membrane order and dynamics. However, their suitability strongly depends on: (a) the degree of the rotational freedom of the dye, (b) the lipophilicity of the probes and (c) the effect of the length of the spacer between the hydrophobic and the hydrophilic part of the probe. The results also demonstrate that the Ru-MLC probe with only one lipid anchor (**Ru-1-R**) is less sensitive to polarization and emission intensity than the two-anchor probes **Ru-2-PE$_2$** and **Ru-2-(C$_{16}$)$_2$**, both in terms of phase transitions and the fraction of cholesterol in the membranes.

Another aspect concerns the location of the Ru-MLC in the bilayer. The type of lipid covalently linked to the metal-ligand complex governs for the location of the dye in the bilayer. In fact, **Ru-2-(C$_{16}$)$_2$** shows higher sensitivity (in terms of polarization) to changes in membrane composition than the amphiphilic dye **Ru-2-PE$_2$**. Because the Ru-MLC **Ru-2-PE$_2$** is linked to two

phospholipids, one can assume that the two headgroups (which are polar) tend to partition to the hydrophobic surface of the bilayer. Membrane probe **Ru-2-(C$_{16}$)$_2$**, which is linked to two hydrophobic alkyl chains, is likely to reside deeper in the hydrophobic interior of the bilayer.

The effect of the length of the spacer between the lipid chain and the MLC needs to be considered as well. **Ru-2-PE$_2$** has a short (C$_2$) spacer between the chromophore and the phospholipid. **Ru-2-(C$_{16}$)$_2$**, in contrast, has a direct link to the alkyl chain and the MLC therefore can reside closer to the membrane surface. This seems to make **Ru-2-(C$_{16}$)$_2$** the probe of choice for biophysical membrane studies such as the effect of cholesterol on the rigidity of membranes.

In summary, we consider the MLC type probes to have particular advantages. These include (a) broad absorption bands (ranging from approximately 430 to 490 nm) which makes the probes excitable by blue LEDs and the argon ion laser; (b) emission maxima (at 640 nm) that are well separated from the excitation wavelengths and thus are hardly interfered by stray light; and (c) lifetimes in the order of 400 to 600 ns, thus enabling studies on membrane dynamics in the μs time regime (3 τ).

4.6. References

[1]   Baenziger J. E., Morris M.-L., Darsaut T. E. Ryan S. E., *J. Biol Chem.* **2000**, *275*, 777.

[2]   Yeagle P. L., *Biochim. Biophys. Acta* **1985**, *822*, 267.

[3]   Chen, J.-W., Liu, F.-S., *Chem. Phys. Lipids* **1998**, *91*, 199.

[4]   Mora, M. P., Tourne-Peteilh, C., Charveron, M., Fabre, B., Milon, A., Muller, D., *Chem. Phys. Lipids* **1999**, *101(2)*, 255.

[5]   Ho, C., Slater, S. J., Stagliano, B. A. Stubbs, C. D., *Biochem. J.* **1999**, *344(2)*, 451.

[6]   Cheng, K. HSomerharju, P., *Biophys. J.* **1999**, *77(6)*, 3108.

[7]   Ravily, V., Clary, L., Santaella, C., Vierling, P., Duportail, G., *Chem. Phys. Lipids* **1997**, *90*, 75.

[8]   Förster, T., Seidel, H.-P., *Z. Phys. Chem.* **1965**, *45*, 58.

[9]   Galla, H.-J., Hartmann, W., *Chem. Phys. Lipids* **1980**, *27*, 199.

[10]   Sassaroli, M., Vauhkonen, M., Perry, D., Eisinger, J., *Biophys. J.,* **1990**, *57*, 281.

[11]   Kaiser R. D., London, E., *Biochemistry* **1998**, *37*, 8180.

[12]   Hashimoto, M., Masumura, S., *Gerentol.* **1999**, *34(5),* 687.

[13]   Bernsdorff, C., Wolf, A., Winter, R., *Z. Phys. Chem.* **1996**, *193*, 151.

[14]   Rothe G., Schäfer B., Wimmer M., Schmitz G., *Proc. SPIE - Int. Soc. Opt. Eng.* **1998**, *3260*, 255.

[15]   Shiniztky M., Barenholz Y., *Biochim. Biophys. Acta* **1978**, *515*, 367.

[16]   Florine-Casteel K., *Biophys. J.* **1990**, *57*, 1199.

[17]   Mouritsen O., Bolothroyd A., Harris N., Jan T., Lookman T., MacDonald D., Zuckermann M., *J. Chem. Phys.* **1983**, *79*, 2027.

[18]   Li L., Szmacinski H., Lakowicz J.R., *Anal. Biochem.* **1997**, *244*, 80.

[19]   Beck A., Heissler D., Duportail G., *Chem. Phys. Lipids* **1993**, *66*, 135.

[20]   Lakowicz   J.R., Principles of Fluorescence, Plenum Press, New York, **1999**, pp. 298.

[21]   Li L., Szmacinski H., Lakowicz J.R., *Anal. Biochem.* **1997**, *244*, 80.

[22]   Terpetschnig E., Szmacinski H., Malak H., Lakowicz J. R., *Biophys. J.* **1995**, *68*, 342.

[23]   Szmacinski H., Terpetschnig E.,. Lakowicz J. R. *Biophys. Chem.* **1996**, *62*, 109.

[24]   Davenport L., Dale R. F., Bisby R. H., Cundall R. B., *Biochemistry* **1985**, *24*, 4097.

[25]   Ostermeyer A. G., Beckrich B. T., Ivarson K. A., Grove K. E., Brown D.

A., *J. Biol. Chem.* **1999**, *274 (48)*, 34459.

[26]   Sankaran M. B., Thompson T. E., *Biochemistry* **1990**, *29*, 10676.

[27]   Drake C. M., Burton J. L., *Biophys. J.* **1998**, *75*, 896.

[28]   Daxin T., Van Der Meer W., Chen S., *Biophys. J.* **1995**, *68*, 1944.

[29]   Kalb E., Paltauf F., Hermetter A., *Biophys. J.* **1989**, *56*, 1245.

[30]   Demel R. A., Kruyff B., *Biochim. Biophys. Acta* **1976**, *457*, 109.

[31]   Yeagle P. L., *Biochim. Biophys. Acta* **1985**, *822*, 267.

[32]   Bloom M., Mouritsen O. G., *Can. J. Chem.* **1988**, *66*, 706.

[33]   Cheng K. H., Virtanen J., Somerharju P., *Biophys. J.* **1999**, *77*, 3108.

[34]   Vist M. R., Davis J. D., *Biochemistry* **1990**, *29*, 451.

[35]   Bagatolli L. A., Gratton E., Fidelio G.D., *Biophys. J.* **1998**, *75*, 331.

5. HSA Immunosystems

In this chapter a luminescence polarization immunoassay based on a ruthenium metal-ligand complex Ru-(bipy)$_2$-(mcbpy) (Ru-1) is described. The lifetime of Ru-1 allows the measurement of rotational motions of proteins. For this purpose, the NHS ester of Ru-1 was synthesized and conjugated to human serum albumin (HSA). The practicality of this complex for immunoassays was determined by titration of the labeled HSA with non-labeled anti-HSA. In addition, a competitive assay for HSA was developed, too. Both assays are based on the polarization method.

Furthermore, a novel immunosystem is described that exploits the effect of luminescence energy transfer from a luminescently labeled antigen to a fluorescently labeled antibody. A luminescent ruthenium-ligand complex (Ru-1) was used as the donor label, and a blue squaraine label as the fluorescent acceptor label. Specifically, HSA was labeled with Ru-1, and anti-HSA was labeled with RB-631. On formation of the antigen-antibody complex, energy transfer occurs. The radiationless energy transfer affects both the decay time of the Ru-1 and the intensities of the emissions of the Ru-1 and RB-631, respectively. The long decay time of Ru-1 (500 ns) allows frequency-domain measurements in the low kHz range and therefore can be based on the use of low-cost opto-electronics. The major difference to existing HSA immunosystems is the use of a long delayed ruthenium metal-ligand complex as donor and a squaraine dye with a high quantum yield as the acceptor.

5.1. HSA polarization immunosystem

5.1.1. Introduction

State of the art

Fluorescence based assays are widely used in analytical and clinical chemistry [1-3]. Such systems can be based on a variety of mechanism affecting the observed spectral properties like quenching, energy transfer or emission polarization. Immunoassays based on polarization or anisotropy are among the most widely used methods [4-7]. Fluorescence polarization immunoassays are based on polarization measurements of antigens labeled with fluorescent markers [8-10].

Theory

Fluorescence polarization methods are applied to study the interactions of proteins with other macromolecules. The background for such measurements are optical effects like the polarization or rather the anisotropy. The polarization can be easily converted to the anisotropy (see chapter 2) [11]. The anisotropy (r) is related directly to the rotational correlation time (θ) and to the molecular weight (MW) of a biosystem (eq. 5-1). The anisotropy of a labeled macromolecule is given by

$$r = \frac{r_0}{1 + t/\boldsymbol{q}} \qquad (5\text{-}1)$$

where r_0 is the value observed in the absence of rotational diffusion. The molecular volume of the protein is related to the molecular weight and the rotational correlation time θ

$$\boldsymbol{q} = \frac{\boldsymbol{h}V}{kT} = \frac{\boldsymbol{h}MW}{RT}(\overline{\boldsymbol{n}} + h) \qquad (5\text{-}2)$$

with R as the ideal gas constant, $\overline{\boldsymbol{n}}$ is the specific volume of the protein, and h is the hydration. In aqueous solution at 20 °C (η = 1 cP) one can expect a protein such as human serum albumin (HSA; molecular weight

~65,000 Dalton, with $\bar{n} + h = 1.9$) to display a rotational correlation time close to 50 ns [12].

In the case of binding or release of labeled HSA from the antibody/anti-HSA complex, the rotational correlation time changes, and consequently the polarization (figure 5-1). Information on the rotational motion is available over a time scale not exceeding three times the lifetime of the fluorophore. For longer rotational motions the signal is too low to affect the steady-state polarization. Since the lifetimes of typical fluorophores range from 1 to 10 ns, it is difficult to measure rotational correlation times higher than 30 ns. Therefore, polarization studies are usually limited to substances with molecular weights of less than 50 000 Daltons. The limitations imposed by the short fluorescence lifetime have been circumvented by the use of phosphorescence polarization [13, 14]. Such measurements are based almost exclusively on the triplet probe eosin, which displays a millisecond phosphorescence decay time in the absence of oxygen. However, there are few useful triplet probes. The use of phosphorescence is also inconvenient due to the need of total exclusion of molecular oxygen, and the low initial phosphorescence polarizations, typically 0.1 or lower [15].

On the opposite, ruthenium-ligand complexes display emissions from charge-transfer states with decay times ranging from 100 ns to 4 μs in solutions along with reasonable quantum yields [16].

5.1.2. Methods

Labeling Procedure

Protein labeling was carried out in a 50 mM bicarbonate buffer of pH 9.0. A stock solution of 1 mg of the NHS ester **Ru-1** (see figure 5-9) in 100 μL of anhydrous dimethylformamide was prepared and 5 mg of protein were dissolved in 1 mL of the bicarbonate buffer. Defined volumes (50 to 40 μL) of the stock solution of the respective label were added to the protein solution and the mixture was gently stirred for 5 h (HSA) or for 2 h (anti-HSA).

Unconjugated label was separated form the labeled proteins using gel permeation chromatography in a 0.5 x 20 cm column filled with Sephadex G25. A 22 mM phosphate buffer of pH 7.2 was used as the eluent. The fast-running fraction contained the dye-protein conjugate, while the fraction with an increased retention time contained the separated free dye.

Determination of the dye-to protein ratios

The labeling degree of (the "dye-to-protein ratio", D/P) is defined as the molarity of label over the molarity of the protein. The degree of labeling of the conjugates was determined by absorptiometry of the conjugates and assuming that the molar absorbance (ε) of the bound dye is the same as that of the free dye. The dye-to-protein ratio (D/P) statistically gives the number of labels covalently bound to a single protein.

5.1.3. Polarization immunoassay

To evaluate the feasibility of using **Ru-1** in a polarization immunoassay, **Ru-1**/HSA was used as an antigen. The changes in emission intensity, lifetime and polarization of **Ru-1** labeled HSA were examined in the presence of increasing amounts of anti-HSA (figure 5-1).
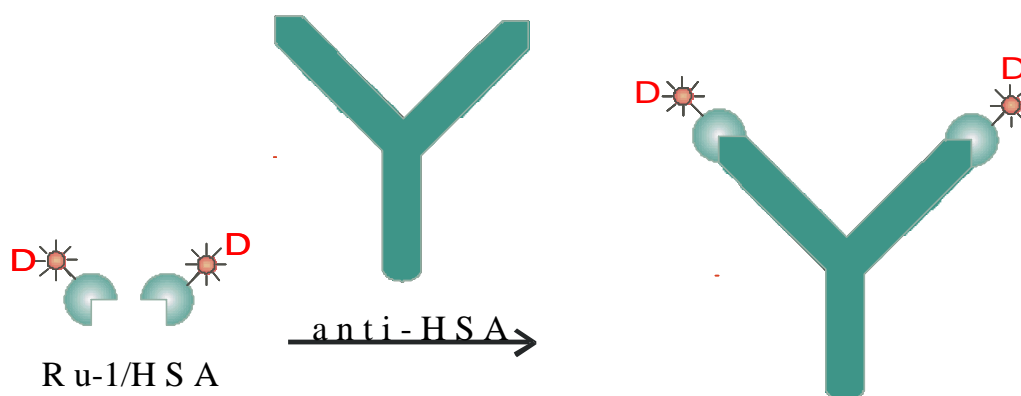

Fig. 5-1. *Scheme for the polarization assay on the system HSA/anti-HSA.*

Spectral characterization

The absorption and emission spectra of **Ru-1** unlabeled and **Ru-1** labeled to HSA are shown in figure 5-2.
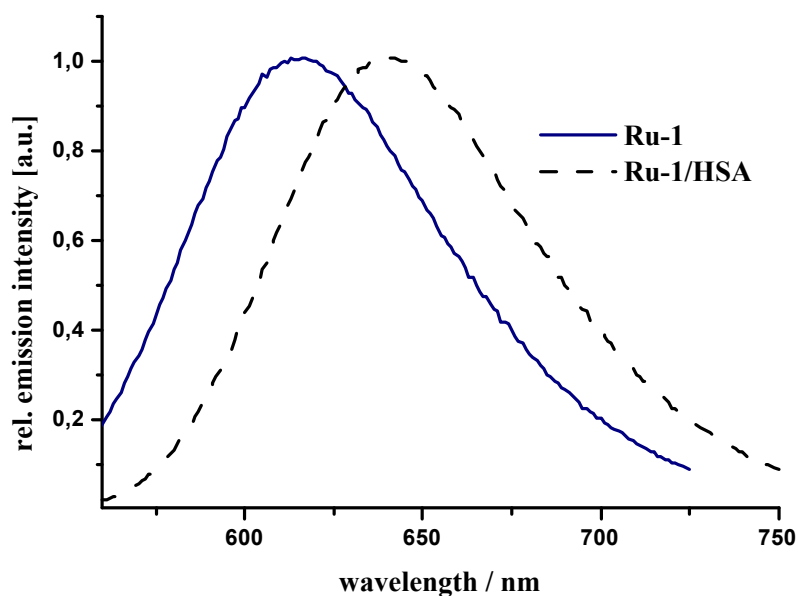
Fig. 5-2. *Emission spectra of free label and **Ru-1**-labeled HSA.*

The spectra are normalized to unity. The absorption spectra of free label and HSA labeled **Ru-1** are identical. The emission maximum of **Ru-1** at 610 nm is slightly shifted to longer wavelengths if covalently bound to HSA.

Emission intensity

Ru-1/HSA was titrated with non-labeled anti-HAS, and the results are plotted in figure 5-3. There was no change in emission intensity with increasing amount of anti-HSA observed. This experiment evaluated the assumption that the decrease of the donor fluorescence is not due to quenching of the proteins but due to energy transfer.
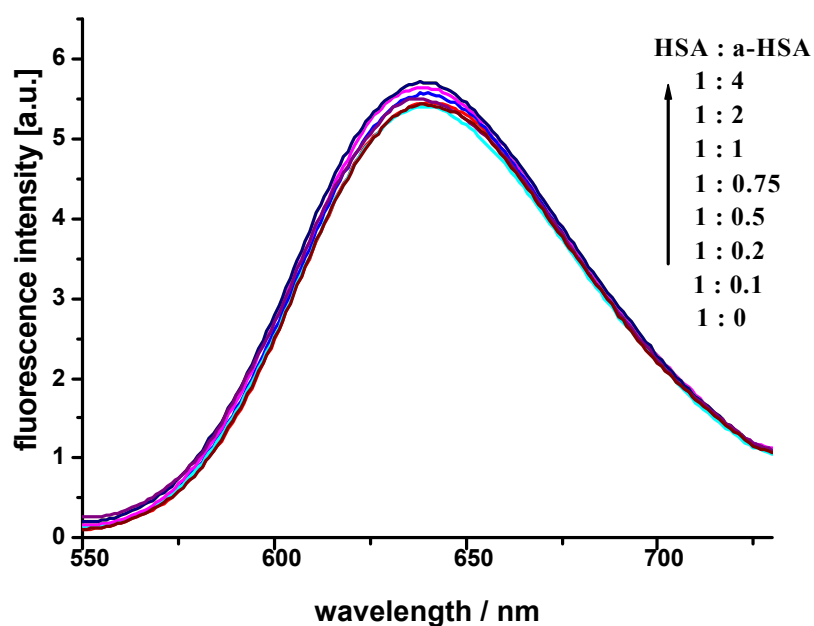
Fig. 5-3. *Emission spectra of **Ru-1**-conjugated to HSA with increasing concentration of anti-HSA.*

Lifetime measurements

The results of the decay time analysis of **Ru-1**/HSA are summarized in table-5-1. The decays fit best a second exponential decay is taken into account. The mean decay time was approximately the same for all anti-HSA concentration, with an average decay time of 485 ns.

Table 5-1. Intensity decay analysis of **Ru-1**/HSA at various concentrations of anti-HSA.

$\dfrac{anti-HSA}{\text{Ru-1}/HSA}$	**0**	**0.25**	**0.5**	**0.75**	**1**	**2**	**4**
t_l (ns)	0.488	0.480	0.481	0.486	0.487	0.490	0.496
$C_R^{2\ \mathbf{a}}$	6.7	6.4	7.1	4.1	4.3	2.1	3.5

[a] chi squared

Steady-state fluorescence polarization

The maximum polarization of the excited state lifetime of **Ru-1** in vitrified solution (glycerol, -60 °C), where rotational diffusion does not occur, was 0.17. This was already examined by Lakowicz et al.[17]. The **Ru-1** complex shows polarized emission.

To evaluate the usefulness of **Ru-1** in an immunoassay, we investigated the steady-state polarization of **Ru-1** conjugated to HSA in the presence of increasing quantities of anti-HSA. The results are shown in figure 5-4. The polarization increased by about four times at a molar ratio of **Ru-1**/HSA to anti-HSA of 1:4. Hence, the polarization of **Ru-1**/HSA is sensitive to the rate of rotational diffusion associated to the antigen/antibody complex.
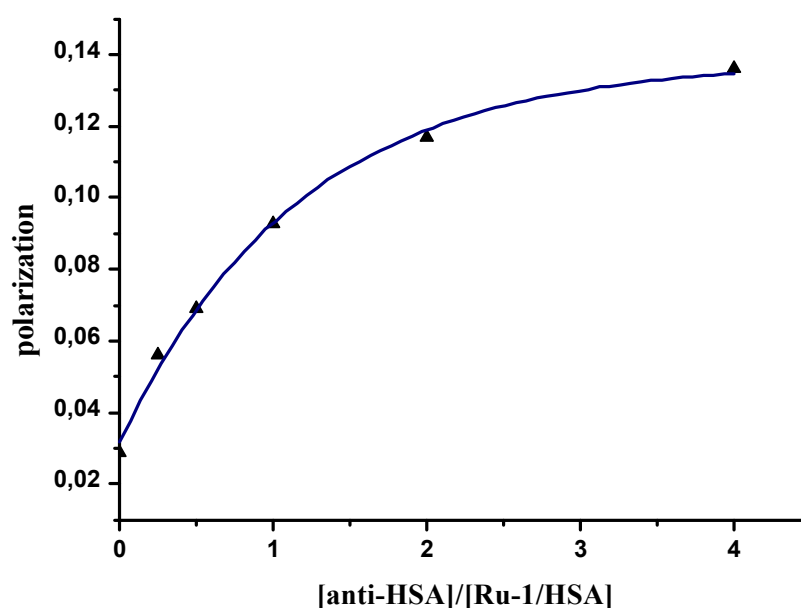

Fig. 5-4. *Steady-state polarization of* **Ru-1** *conjugated to HSA at various concentrations of anti-HSA.*

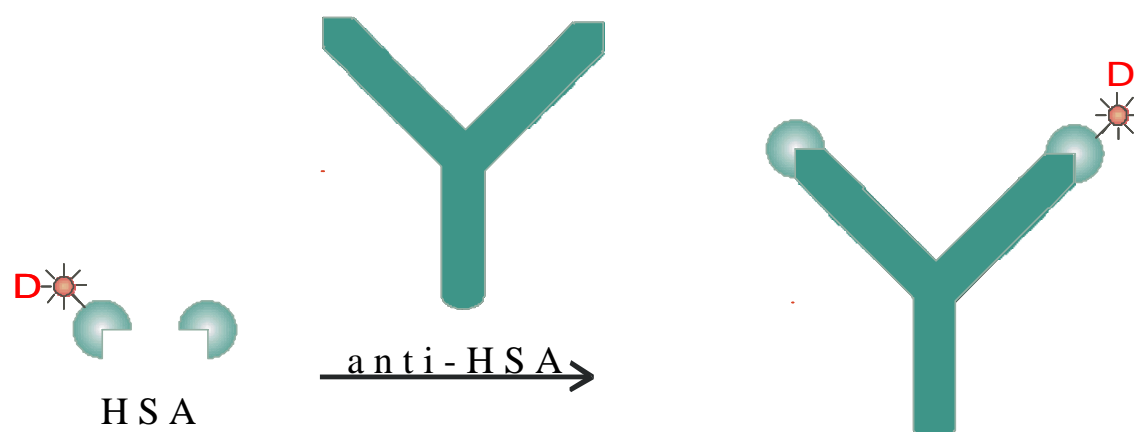### 5.1.4. **Competitive polarization immunoassay**

Fig. 5-5. *Model for the competitive polarization based immunoassay on the system HSA /anti-HSA.*

In a competitive immunoassay labeled and unlabeled antigens are allowed to simultaneously compete for the binding sites of the antibody (figure 5-5). The simultaneous exposure of labeled and unlabeled HSA to anti-HSA resulted in changes in polarization. Three titrations with increasing anti-HSA concentrations (1, 2 and 4 nmol/L) were carried out. The concentration of **Ru-1**/HSA was hold constant at 1 nmol/L for all titrations. The amount of anti-HSA was unchanged for each titrations at (1, 2 and 4 nmol/L, respectively). We found an exponential decay of the polarization with increasing fraction of unlabeled HSA for all titrations (figure 5-6). At high concentration of unlabeled HSA, the polarization could not be reversed to the value for unbound **Ru-1**/HSA with a polarization value of 0.33, which should be observed on total replacement of **Ru-1**/HSA with unlabeled HSA. This effect can be attributed to nonspecific binding of **Ru-1**/HSA to other proteins present in solution. Another reason for this behavior may result from a stronger binding affinity for **Ru-1**/HSA than for free HSA.
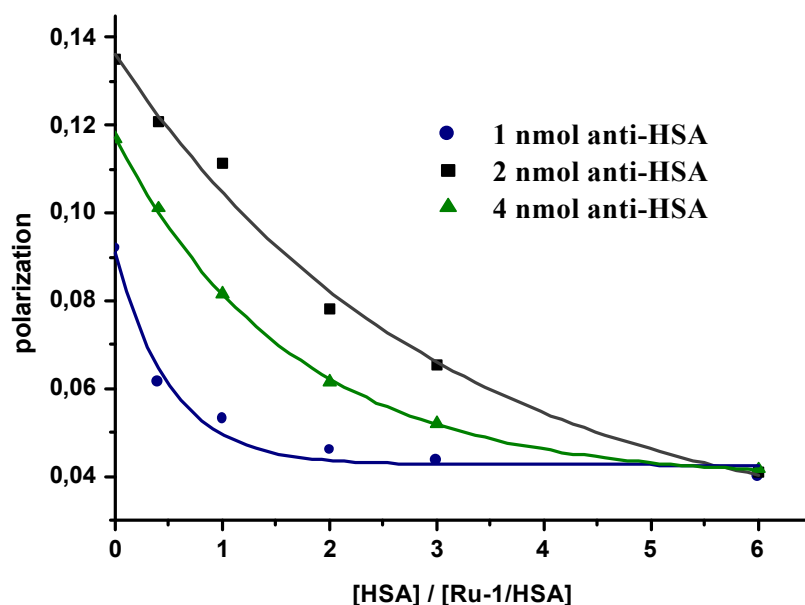
Fig. 5-6. *Steady-state polarization of **Ru-1** conjugated to HSA at rising concentrations of unlabeled HSA competing for anti-HSA.*

5.1.5. Conclusion

The label **Ru-1** turned out to be a very useful probe for performing immunoassays for high-molecular weight antigens. The favorably properties of **Ru-1** allow the use of simple instrumentation: The advantage of **Ru-1** is due to a Stokes' shift of more than 150 nm, which makes the separation of excitation and emission light easy, and an excitation maximum of 456 nm, which allows excitation with an argon ion laser or a blue LED. The emission maximum is at 641 nm when bound to HSA. At this wavelength the interference from the autofluorescence of biological samples is reduced.

5.2. HSA fluorescence energy transfer immunosystem

5.2.1. Introduction

State of the art

The quantitative determination of human serum albumin (HSA) in biological liquids has gained importance in diagnosis and preventive medicine [18]. Except for blood serum, albumin concentrations in body fluids such as urine are usually low and therefore require sensitive methods for their precise determination.

Numerous protocols for determination of HSA are reported in the past decade [19-22]. Among those, immunoassays based on fluorescence detection have been preferred in practice. These include immunoassays based on fluorescence polarization [23] and fluorescence resonance energy transfer (FRET) [24].

This detection scheme exploits the fact that electronic (photonic) energy of a first fluorophore can be transferred to a second fluorophore, if the second is in sufficient and spatial proximity. As a result, the fluorescence intensity (and decay time) of the first fluorophore decreases, while the intensity of the second increases [11].

FRET occurs over distances between typically 1-7 nm, and it is a fortunate incidence that this is the average distance of an antigen (Ag) and an antibody (Ab) once they are bound to each other. Hence, the fact that FRET does occur is indication that a (labeled) antibody has recognized its (labeled) antigen. The efficiency of energy transfer between Ag and Ab depends on the sixth power of the distance between the donor and acceptor.

Assay
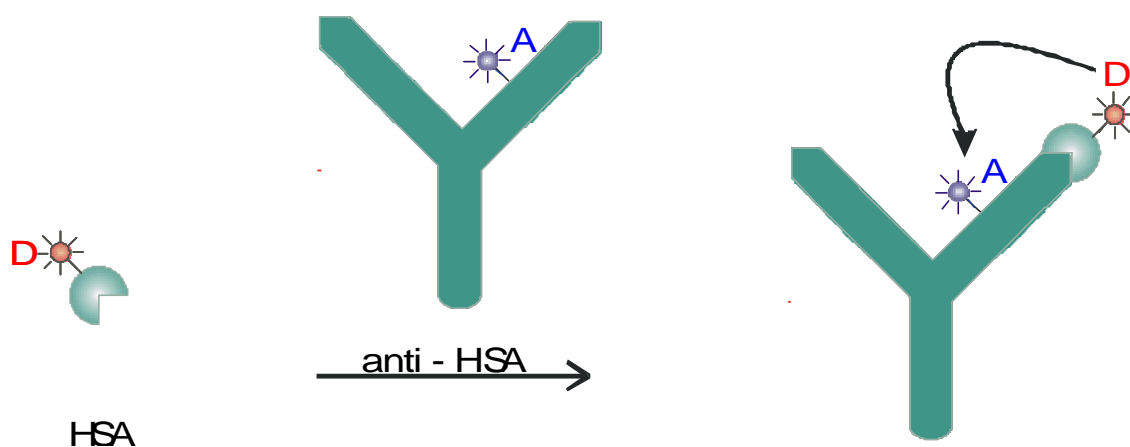
Fig. 5-7. *Scheme for the luminescence energy transfer in the system HSA (donor-labeled) and anti-HSA (acceptor labeled).*

This energy transfer system is illustrated in figure 5-7. We used HSA as an antigen covalently labeled with the donor Ru(bpy)$_2$-(mcbpy) (**Ru-1**). The antibody (anti-human serum albumin, anti-HSA) was labeled with the acceptor **RB-631**. We found that the emission intensity of the acceptor increased, while the lifetime of the ruthenium labeled antigen decreased upon binding to acceptor-labeled antibody.

5.2.2. Labeling procedures

General protein-labeling procedures and determination of dye-to protein ratios

The same labeling procedure was used as described in chapter 5.1.3.

Fig. 5-8. *Separation of the unconjugated label from the protein labeled using gel permeation chromatography (left: **RB-631**/anti-HSA; right: **Ru-1**/HSA).*

Procedure for studying energy transfer efficiency

100 μL of the donor solution (**Ru-1**/HSA) in phosphate-buffered saline (PBS; 22 mM, pH 7.2) was mixed with **RB-631**/anti-HSA acceptor solution, typically 5 to 400 μL. The mixtures were diluted with PBS to a final volume of 600 μL and incubated for 15 min at room temperature. Then, the fluorescence intensity or decay time was measured.

5.2.3. Results

Choice of labels

The choice of dyes is a key issue in designing resonance energy transfer systems. The decay times of commonly used donor fluorophores typically are in the nanosecond region and this makes measurement of decay times more tedious. One solution is to apply long-decaying labels such as europium chelates [25]. These, however, require short wavelength excitation [26]. Other labels that have been proposed may be oxidized by oxygen, have poor quantum yields, or be susceptible to quenching by proteins [27]. Ru-MLCs can overcome some of these limitations since they have lifetimes in the order of several hundred nanoseconds, can be excited with a 488 nm argon ion laser and exhibit a strongly red-shifted emission maximum at 610 nm. Therefore, we decided to use the ruthenium label **Ru-1** as the donor dye. Furthermore, its synthesis is fairly easy.

The acceptor dye was chosen such that is an absorption maximum close to the emission maximum of the ruthenium label. Both dyes have the additional advantage that their emission is in the optical window of blood and biological tissue, i.e. between 630 and 670 nm, thus minimizing re-absorption of light.

Spectral characterization of labels

Ru-1 exhibits a large Stokes' shift (approx. 150 nm) with no overlap of the excitation and emission spectra. Therefore, excitation light can be easily separated from emitted light. Decay times in the order of 500 ns allow decay time measurements to be made, which are independent of the concentration of the donor label.

RB-631 (the acceptor) also has a rather high molar absorbance of 95,000 L/(mol· cm) and a quantum yield of 0.32 when bound to proteins. The

chemical structures of the activated **Ru-1** and **RB-631** are shown in figure 5-9, the photophysical data are summarized in table 5-2.
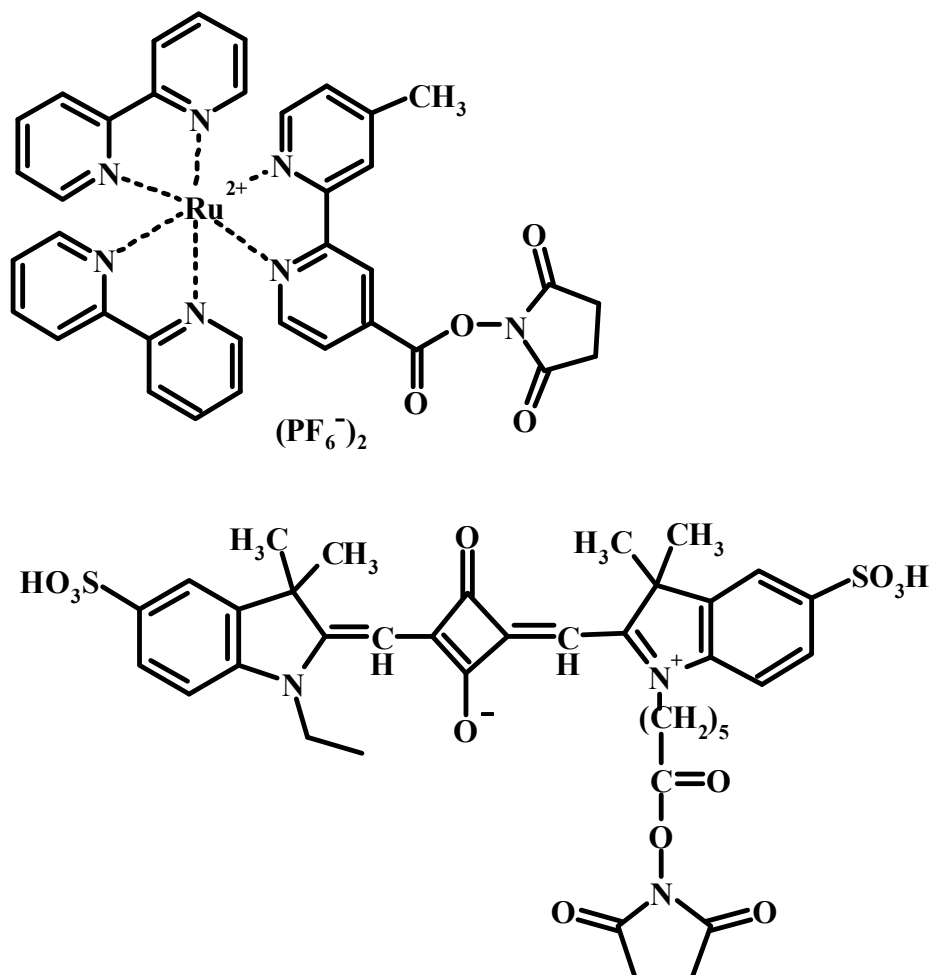
Fig. 5-9. *Chemical structeres of the N-hydroxy succinimide esters of the donor dye **Ru-1** and the acceptor dye **RB-631**.*

Spectral characterization of the protein conjugates

The absorption and emission spectra of the **Ru-1**/HSA conjugate and the **RB-631**-labeled antibody (**RB-631**/anti-HSA) are depicted in figure 5-10. The emission maximum of **Ru-1** at 610 nm is slightly shifted to longer wavelengths when covalently bound to HSA. The absorption and emission maxima of

RB-631/anti-HSA can be found at 636 nm and at 655 nm, respectively. Like **Ru-1**, **RB-631** shows a bathochromic shift in its absorption and emission maximum in the protein-bound form. There is sufficient spectral overlap between the emission of the donor and the long wavelength absorption of the acceptor.
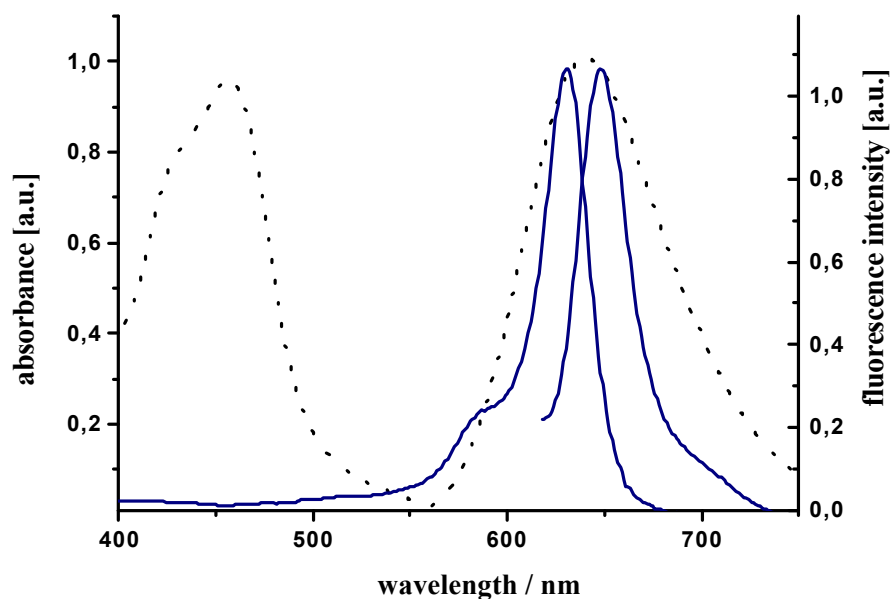
Fig. 5-10. *Absorption and emission spectra of Ru-1 (----) and* **RB-631** *(——). For l_{max} values, absorbances and quantum yields see table 5-2.*

Quantum Yields

The following equation [29] was used for the determination of the quantum yield (QY):

$$QY = QY_{\mathrm{Re}f}\left(F / F_{\mathrm{Re}f}\right).$$ (5-4)

where

$$F = \int I(\boldsymbol{l})d\boldsymbol{l}$$ (5-5)

The QY of the donor was estimated by comparing the dye $[Ru(bpy)_3]_2^+$ whose QY is reported to be 0.042 [30]. The QY of RB-631 was determined relative to that of the dye Cy5, whose QY is reported to be 0.25 [31].

The luminescence of ruthenium metal ligand complexes, especially the phenanthroline complexes, is known to be quenched by oxygen. Therefore, we have investigated the effect of oxygen on the QY of both the free and the protein-bound form of **Ru-1** by measuring luminescence intensity in air-equilibrated solution and in argon-equilibrated solution, respectively. Compared to deoxygenated solutions, the relative QYs for **Ru-1** and **Ru-1**/HSA in air-equilibrated buffer solutions were 0.79 and 0.91, respectively. Hence, the free ruthenium label is more sensitive to oxygen than the protein conjugate. However, the cross-sensitivity to oxygen is not large enough to cause serious interference.

Table 5-2. Spectral properties and quantum yields of dyes and dye-protein conjugates in PBS of pH 7.2.

Dye	Abs.max. [nm]	Em. max. [nm]	ε [L/(mol· cm)]	Q.Y.	D/P [mol/mol]
Ru-1	456	610	18,000	0,051	---
Ru-1/HSA	456	639	a	0,055	4,0
$[Ru(bipy)_3]^{2+}$	456	610	15000	0,042	---
RB-631	631	645	95,000	0,04	---
RB-631/anti-HSA	636	655	a	0,32	4,9
Cy5	647	664	250,000	0,25	---

[a] Not determined

Energy transfer studies based on measurement of luminescence intensity

The results of a representative energy transfer experiment are shown in figure 5-11. **Ru-1** labeled HSA (DPR = 4.0; [HSA] = 3.2 μM) was mixed with **RB-631**/anti-HSA (DPR = 4.8) in molar ratios of 1:4, 1:2, 1:1, 1:0.75, 1:0.5, 1:0.25, 1:0 and 0:1. As expected, the luminescence intensity of **Ru-1**/HSA decreases with increasing quantities of **RB-631**/anti-HSA, while the fluorescence of the **RB-631**/anti-HSA conjugate increases because of

resonance energy transfer. The luminescence of plain **RB-631**/anti-HSA in a concentration of 3.2 μM is only 25% of the emission intensity of the pair **Ru-1**/HSA / **RB-631**/anti-HSA at the same concentration. The excitation wavelength was 450 nm in both cases. The detection limits of **Ru-1**/HSA and of **RB-631**/anti-HSA, respectively, are at about 0.5 μM and 0.1 μM using a 150 Watt xenon lamp.

The donor/HSA conjugate was also titrated with unlabeled anti-HSA. The emission intensity of **Ru-1**/HSA does not change with increasing concentration of anti-HSA. This demonstrates that the decrease in the donor fluorescence shown in figure 5-11 is not due to fluorescence quenching by the protein but due to energy transfer.

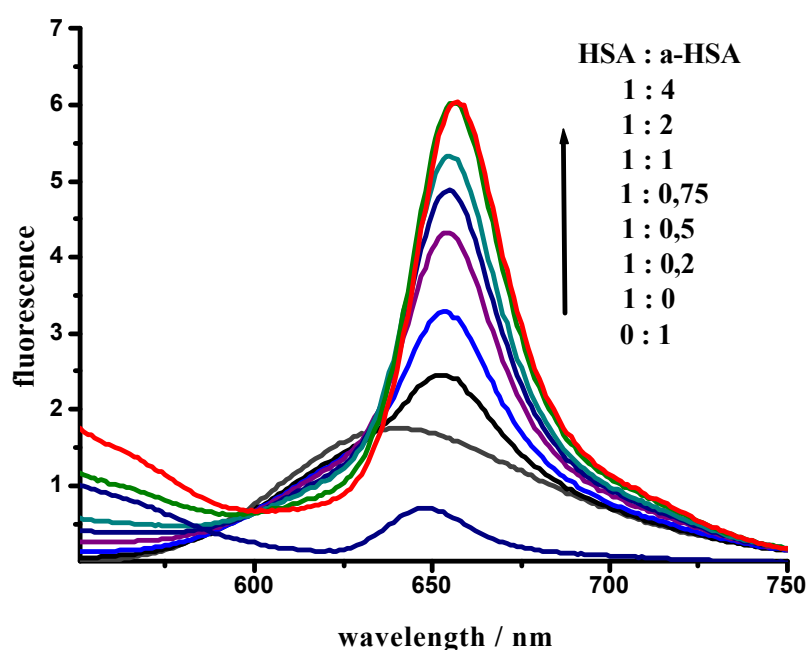*Fig. 5-11. Luminescence energy transfer study in the system HSA/anti-HSA. **Ru-1**/HSA (D/P= 4.0) of constant concentration (3.2 µM) was titrated with **RB-631**/anti-HSA (D/P= 4.8) and emission spectra were recorded at l_{exc}= 460 nm.*

All spectra shown in the following were normalized to unity for comparison purposes. Figure 5-12 shows the effect of increasing fractions of

RB-631/anti-HSA on the emission intensity of **Ru-1**/HSA. The signal drops until the molar ratio between **RB-631**/anti-HSA and **Ru-1**/HSA is 4:1, where the signal has decreased by 34%. If the titration is performed with unlabeled anti-HSA, no decrease in intensity is observed since energy transfer cannot occur.
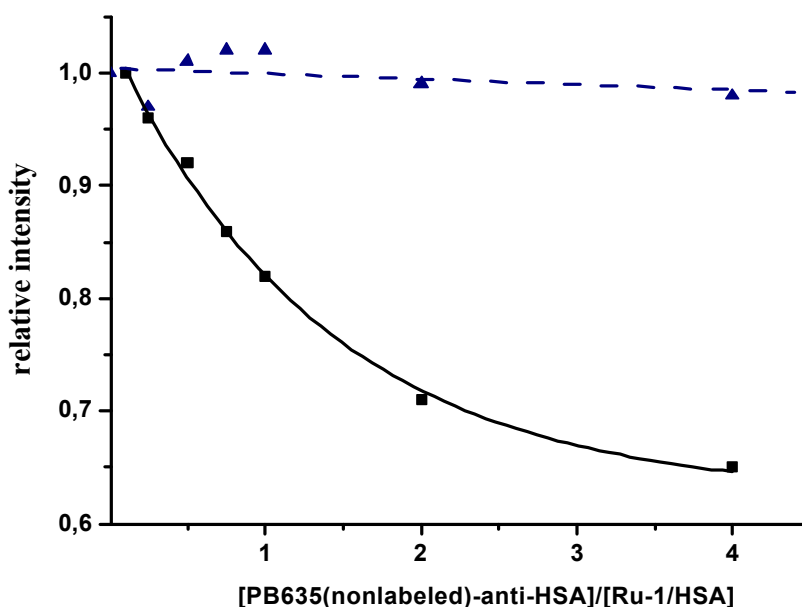
Fig. 5-12. *Changes in emission intensity of **Ru-1**/HSA in presence of increasing fractions of (a) **RB-631**/anti-HSA (−■−■−) and (b) non-labeled anti-HSA (--▲--▲--) concentration, respectively.*

Energy transfer studies based on measurement of luminescence decay time.

To further characterize the FRET in the antigen-antibody system, we investigated the decay times of **Ru-1**/HSA. In the absence of acceptor, the decay time was mono-exponential with a dominant component of 488 ns (see table 5-3). An investigation of the effect of oxygen on the decay time of the free and protein bound form was carried out as described before for the QYs. The decay times for **Ru-1** and **Ru-1**/HSA in air-equilibrated and argon-equilibrated buffer solutions were found at 375 ns (517 ns) and 488 ns (512 ns), respectively. The decay time measurements are in accordance with

the measurements of the QY. Therefore, measurements were carried out without further oxygen exclusion.

Table 5-3. Intensity decay analysis of **Ru1**/HSA at various concentrations of **RB-631**/anti-HSA and anti-HSA, respectively.

$\dfrac{anti - HSA}{\text{Ru -1}/HSA}$	**RB-631**/anti-HAS		
	t_i **(ns)**	f_i	c_R^2
0	0,488	0,98	4,1
	0,001	0,02	
0,25	0,434	0,82	4,2
	0,035	0,18	
0,5	0,412	0,72	3,9
	0,033	0,28	
0,75	0,396	0,61	4,1
	0,030	0,39	
1	0,379	0,55	5,3
	0,028	0,45	
2	0,359	0,51	2,3
	0,026	0,49	
4	0,348	0,42	3,4
	0,021	0,58	

In the presence of acceptor, a second (shorter) component appears, which is associated with the **RB-631**/anti-HSA complex. The effect of **RB-631** labeled anti-HSA and of anti-HSA on **Ru-1**/HSA are presented in figure 5-13. The decay time decreases with increasing **RB-631**/anti-HSA. At a molar ratio of **RB-631**/anti-HSA and **Ru-1**/HSA of 4:1 the decay time has decreased by 29%. The fact that the changes are similar in intensity (figure 5-12) and decay time support the assumption that the intensity changes are due to energy transfer and not due to dynamic quenching by protein after antigen - antibody interaction. The changes in the decay time of **Ru-1**/HSA following association with the HSA-antibody, demonstrate that **Ru-1** is a viable probe for decay time based immunoassay.

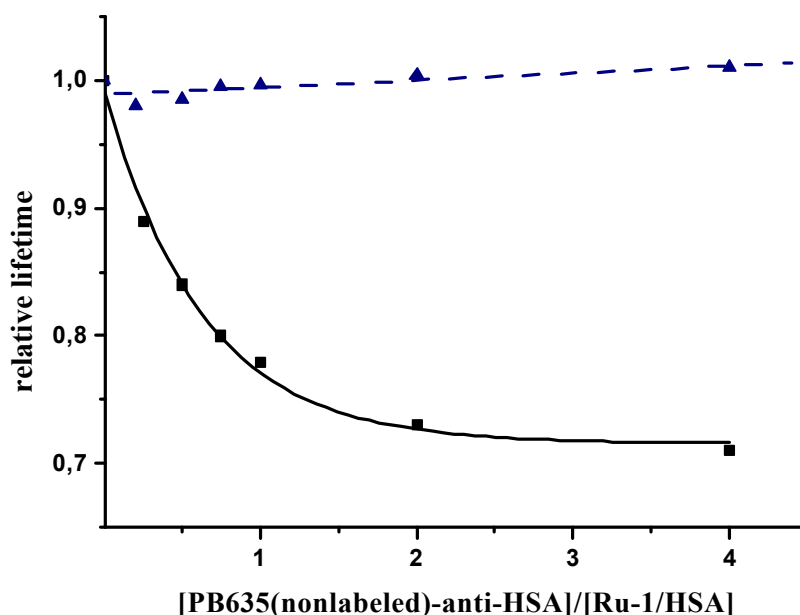**Fig. 5-13.** *Relative change in the decay time of **Ru-1**/HSA conjugate on addition of (a) **RB-631**/anti-HSA (−■−■−) and (b) non-labeled anti-HSA (--▲--▲--), respectively, normalized to unity (t = 488 nm). (Concentration of **Ru-1**/HSA: 3.2 μM).*

5.2.4. Conclusion

In this chapter, a resonance energy transfer immunosystem is introduced that undergoes changes in both emission intensity and decay time as a result of the formation of the Ag/Ab complex.

The fluorescent acceptor label used is water-soluble, displays a fairly large quantum yield (0.32) when covalently bound to proteins, a large molar absorbance (95,000 L/(mol·cm)). In the form of the reactive NHS ester it is a viable acceptor label for proteins, particularly for use in fluorescence energy transfer immunoassays. The spectral overlap of the absorption band of **RB-631** with the emission maximum of **Ru-1** at 639 nm makes the two dyes an efficient energy transfer pair.

The use of a ruthenium metal-ligand complex (MLC) as a donor in an energy transfer system enables immunoassays based on measurement of

decay times in the μs time regime. The close spatial proximity of donor and acceptor causes both the intensity and the decay time of the ruthenium donor to decrease. Decay time based assays using ruthenium MLCs are considered advantageous because of their long decay time and large Stokes' shifts. It is known that the autofluorescence of biological samples is the main limitation for high sensitivity immunoassays. Autofluorescence typically decays within several nanoseconds and thus does not interfere with detection of the slow ruthenium MLC emission.

5.2.5. References

[1]   Kessler M. A., Meinitzer A., Wolfbeis O. S., *Anal. Biochem.* **1997**, *248*, 180.

[2]   Kessler M. A. , Meinitzer A., Petek W., Wolfbeis O. S., *Clin. Chem.* **1997**, *43*, 996.

[3]   Hall M., Kazakova I., Yung.Mae Y., *Anal. Biochem.* **1999**, *272*, 165.

[4]   Ostermeyer A. G., Beckrich B. T., Komberly A. I., Grove K. E., Brown D. A., *J. Biol. Chem.* **1999**, *274 (48)*, 34459.

[5]   Hirsch-Lerner D., Barenholz Y., *Biochim. Biophys. Acta* **1999**, *1461*, 47.

[6]   Kaiser R. D., London E., *Biochemistry* **1998**, *37*, 8180.

[7]   Cheng K. H., Virtanen J., Somerharju P., *Biophys. J.* **1999**, *77*, 3108.

[8]   Ozinskas A. J. in Lakowicz J.R. (**1994**) *Topics in Fluorescence Spectroscopy*, Vol. 4, Probe Design and Chemical Sensing, Plenum, New York, pp. 449-496.

[9]   Szmacinski H., Terpetschnig E., Lakowicz J. R., *Biophys. Chem.* **1996**, *62*, 109.

[10]   Youn H. J., Terpetschnig E., Szmacinski H., Lakowicz J. R., *Anal. Biochem.* **1995**, *232*, 24.

[11]   Lakowicz J. R., **1999**, *Principles of Fluorescence Spectroscopy*, 2nd

Edition, Kluwer Academic Plenum Publishers, New York, 291-304.

[12] Terpetschnig E., Szmacinski H., Lakowicz J. R., *Methods in Enzymol.* **1997**, *278*, 295.

[13] Scorilas A., Bjartell A., Lija H., Moller C., Diamandis E.P., *Clin. Chem.* **2000**, *46*, 1450.

[14] Birmachu W., Voss J. C., Louis C. F., Thomas D. D., *Biochemistry* **1993**, *32*, 9445.

[15] Bartholdi M., Barrantes F. J., Jovin T. M., *Eur. J. Biochem.* **1981**, *120*, 389.

[16] Demas J. N, Harris E. W., McBride R. P., *J. Am. Soc.* **1997**, *99*, 3347.

[17] Li. L., Szmacinski H., Lakowicz J. R., *Biospectros.* **1997**, *3(2)*, 155.

[18] Waller K. V., Ward K. M., Wismatt D.K., *Clin. Chem.***1989**, *35*, 755.

[19] Szöllösi J., Damjanovich S., Matyus L., *Cytometry* **1998**, *34*, 159.

[20] Morrison L. E., *Anal. Biochem.* **1988**, *174*, 101.

[21] Khanna P. L., Ullmann E. F., *Anal. Biochem.* **1980**, *108*, 156.

[22] Kricka L. J., *Clin. Chem.* **1991**, *37(9),* 1472.

[23] Youn J.Y., Terpetschnig E., Szmacinski H., Lakowicz J. R.,. *Anal. Biochem.* **1995**, *232*, 24.

[24] Oswald B., Lehmann F., Simon L., Terpetschnig E., Wolfbeis O. S., *Anal. Biochem.* **2000**, *280*, 272.

[25] Selvin P. R., *Proc. Natl. Acad. Sci. USA* **1994**, *91*, 10024.

[26] Southwick P. L., Ernst L. A., Tauriello E. W., Parker S. R., Mujumdar R. B., Mujumdar R., Clever H. A., Waggoner A. S., *Cytometry* **1990**, *11*, 418.

[27] Oswald B., Patsenker L., Duschl J., Szmacinski H., Wolfbeis O. S., Terpetschnig E., *Bioconjug. Chem.* **1999**, *10*, 925.

[28] Li L., Szmacinski H., Lakowicz J. R., *Anal. Biochem.* **1997**, *244*, 80.

[29] Demas J. N., Crosby G. A., *J. Phys. Chem.* **1971**, *75*, 991.

[30]   Van Houten J., Watts R. J., *J. Am. Chem. Soc.* **1976**, *98*, 4853.

[31]   Amersham Life Science, FluoroLink Cy5, Monofunctional Dye 5-Pack.

[32]   Terpetschnig E., Szmacinski H. M., Lakowicz J.R., *Biophys*. J. **1995**, *68*, 342.

6. Hybridization systems

In this chapter the application of the ruthenium metal-ligand complex Ru-1 for the use in DNA analysis is demonstrated. Ru-1 was covalently linked to the 5' end of a 15mer oligonucleotide (A1). The properties of this labeled strand were investigated in terms of fluorescence intensity, lifetime and polarization. Furthermore, a hybridization study was performed. Therefore, the amino modiefied 3'- and 5'- end of the complementary strand of Ru-1/A1 were covalently attached to a squarine dye and the energy transfer was investigated occurring with hybridization. The efficiency of energy transfer was quantified with fluorescence intensity measurements.

6.1. Introduction

The evaluation of the human genetic code and the development of new gene diagnostics show the importance of DNA in human life during the last years [1-3]. The hybridization analysis is a major field of interest in medical health and clinical diagnostics. Two methods are widely used, the hybridization on solid supports and in solution. Several approaches have been reported to couple the high specific biochemical reaction of hybridization to a sensing surface [4]. Electrochemical determination makes use of double strand specific ligands, which are electrochemically active [5]. High sensitivity was obtained using gold electrodes [6]. Other approaches use the piezoelectric effect [7]. However, homogenous hybridization assays in solution are faster [8]. More and more fluorescent labels have been investigated for DNA analysis via fluorescence energy transfer systems in liquid [9-16].

An ideal label for a DNA probe should fulfill the criteria of [17]: (a) to be easily attached to DNA, (b) to be detectable at very low concentrations, (c) to produce a signal that is changed when the labeled DNA probe hybridizes to its complementary DNA sequence, and (d) to be stable at the elevated temperatures conditions used in hybridization studies.

In recent years, most FRET studies of nucleic acids have used fluorescein as the donor [18-20]. This fluorophore is easily excitable with a 488 nm Argon ion laser, but exhibit a small Stokes' shift of 25 nm, making separation of excitation and emission light very difficult.

In this chapter the ruthenium MLC **Ru-1** was used as the donor. This label has the advantage of a Stokes' shift of more than 100 nm, thereby overcoming the problem of separating the excitation and emission light. The near-infrared dye **RB-631** was used as acceptor for energy transfer. The optimal overlap of its excitation band at 631 nm with the emission band of **Ru-1**, the easy attachment to amino-modified oligonucleotides (oligos), in addition with the emission maxima in the optical window of blood makes this dye an optimal energy transfer partner for **Ru-1**.

6.2. Methods and Materials

The 15-mer oligos were purchased from Metabion GmbH (Munich, Germany) (see table 6-1).

Table 6-1. Properties of the oligos **A1**, **A2** and **A3**.

	Strand		MW	e (260 nm)	T_T / °C
A1	**5'-amino-**	**CCG GCA GCA AAA TGT–3'**	153540	4571	47
A2	**3'-**	**GGC CGT CGT TTT ACA–5'-amino**	135700	4544	47
A3	**3'-amino-**	**GGC CGT CGT TTT ACA–5'**	135700	4544	47

6. 2. 1. Dye labeling procedure

Donor-labeled and acceptor-labeled DNA strands were prepared by reaction of the 5'- and 3'-amino oligos (**A1**, **A2**, **A3**) with the succinimidyl esters of **Ru-1** (**A1**) and **RB-631** (**A2** and **A3**). A 30-50 fold molar excess of dye, diluted in 50 μL of DMF, was added to a 70 μg of oligonucleotide in 150 μL buffer (0.1 M NaHCO$_3$, pH 9). Reactions were performed for 12 h in the dark at room temperature. To this mixture, 1 mL of cold ethanol was added to precipitate the oligo. The solution was centrifuged three times and the ethanol was decanted to remove unreacted dye. The oligo was redissolved in 100 μL of 15 mM citrate buffer (150 mM NaCl, pH 7) and washed again with ethanol three times. The dried oligo was stored at -20 °C. Labeled oligos were quantified by their 260 nm absorbances. The dye to oligo ratio was also determined by absorbance measurements.

Fig. 6-1. *Ru-1*-labeled **A1** *(left)* and **RB-631**-labeled **A2** *(right) in the dry form.*

6.2.2. Hybridization procedure

For the hybridization step the strand **Ru-1/A1** was combined with strand **A2**. The same was performed with strand **RB-631/A2** and **RB-631/A3**, respectively. For each series, a constant concentration of **Ru-1/A1** (0.5 nM) was mixed with 0, 0.25, 0.5, 1.0, 2.5 and 5.0 nmol of the complementary strand and diluted to a constant volume of 600 μL with a 15 mM citrate buffer (150 mM NaCl, pH 7). These mixtures were heated to 65 °C for 2 h and cooled to 35 °C within 3 h. The following measurements were performed at 35 °C using a thermostated heating bath.

6.3. Results

6.3.1. The Ru-1 labeled oligonucleotide A1

First, the properties of **Ru-1/A1** were investigated in terms of fluorescence intensity, lifetime and polarization. Especially, the specific binding of **Ru-1** to oligos was examined. Therefore, the oligo **A1** was labeled on the one hand to the activated NHS ester of **Ru-1** (**Ru-1/A1**), and on the other hand to the non-activated carboxy form of **Ru-1** (**Ru-1°/A1**). The procedure for labeling was used as described in chapter 6.2.
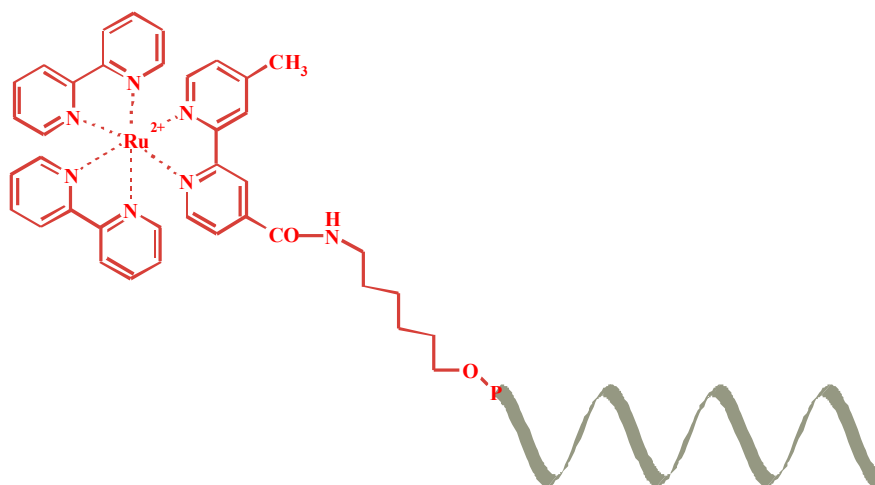

*Fig. 6-2. Schematic of the chemical structure of the **Ru-1**-labeled **A1**.*

Spectral characterization

The emission spectra of **Ru-1** dye in 15 mM citrate buffer (150 mM NaCl, pH 7) and **Ru-1** labeled **A1** are shown in figure 6-2. The emission maximum at 610 nm undergoes a small shift to higher wavelengths if the dye is covalently bound to an oligo.

Table 6-2. Spectroscopic properties of unlabeled **Ru-1°/A1** and the labeled
Ru-1/A1.

Dye	Abs.max. [nm]	Em. max. [nm]	Q.Y.	Dye/Oligo [mol/mol]	t [µs]	P (25 °C)
Ru-1°/A1[2]	456	610	0,051	—	0,35	0,024
Ru-1/A1[3]	456	645	0,055	0,98	1,03	0,135
$[Ru(bipy)_3]^{2+}$	456	610	0,042	—	—	—

The dye-to-oligo ratio was determined to be 0.98 at the absorption wavelengths of 260 nm and 456 nm for **A1** and **Ru-1**, respectively. The quantum yields were measured with reference to the known quantum yield of $[Ru(bipy)_3]^{2+}$ (0.042). Similar quantum yields were found for the labeled **Ru-1** and the carboxylic form of **Ru-1** (see table 6-2). In the following, the two mixtures **Ru-1/A1** and **Ru-1°/A1** were compared.
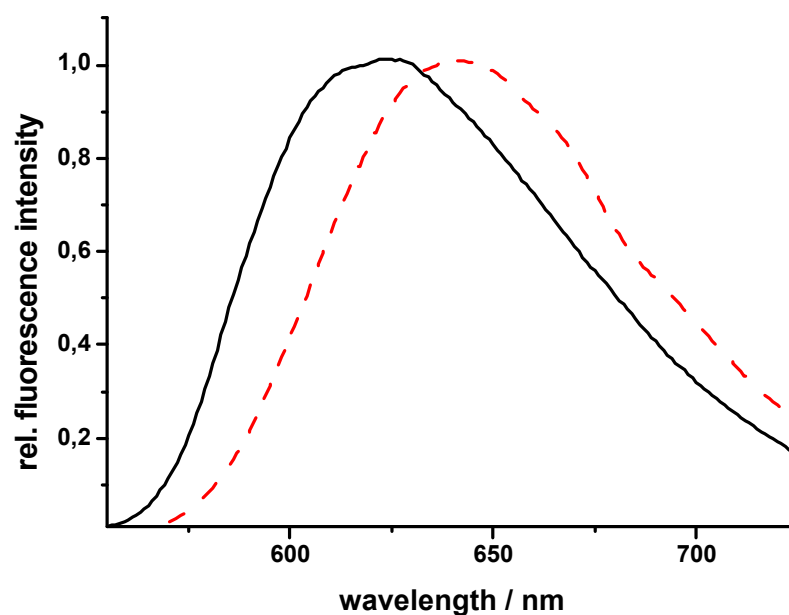
Fig. 6-3. *Emission spectra of free **Ru-1** (—) and **Ru-1** labeled to **A1** (-- --) in 15 mM citrate buffer (150 mM NaCl, pH 7).*

---

[2] **Ru-1** covalently attached to the strand **A1**
[3] the unreactive carboxy form of **Ru-1** and the strand **A1** in buffer solution

Lifetime and polarization measurements

The comparison of lifetime and polarization measurements of **Ru-1°/A1** (orange) and **Ru-1/A1** (yellow) are shown in figure 6-4. The respective data are presented in table-6-2. The decay time of **Ru-1°/A1** was double exponential with a main long delay of 360 ns (90%). The same was found for **Ru-1/A1**. However, it displays a three time longer decay time (1.1 μs, 75%) and a short component (280 ns). These differences in lifetime confirm in the first instance to a specific binding of the **Ru-1**-NHS ester to the amino group of the 15mer oligonucleotide **A1**.

The steady-state fluorescence polarization was investigated for both mixtures to verify the specific binding of **Ru-1** to **A1**. **Ru-1** exhibits in solution a small polarization, resulting from the high rotational freedom in solution. As expected, the polarization of **Ru-1°/A1** with a value of 0.024 is also in the range of the free dye in solution. The **Ru-1/A1** displays a five-fold increase in polarization, which confirms the specific binding of **Ru-1** to the oligo. The high polarization value combined with the lifetime results and the data obtained for **Ru-1°/A1** verify the covalent specific binding of **Ru-1** to **A1**.
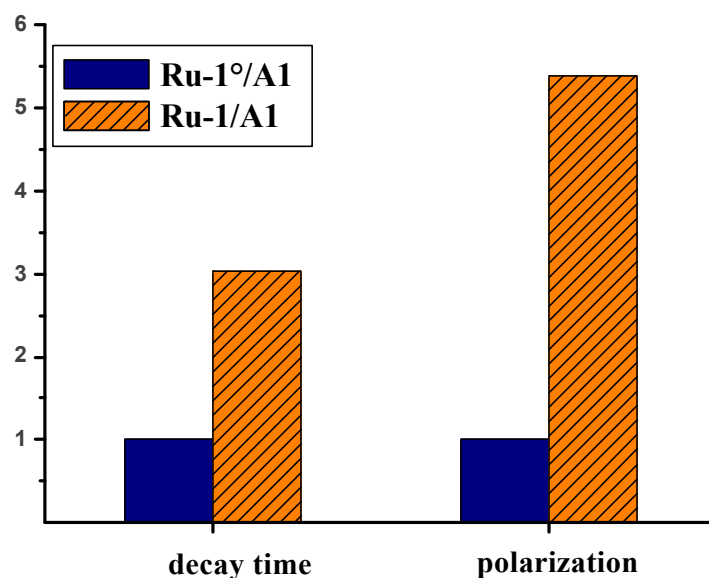

Fig. 6-4. *Comparison of the decay time and fluorescence polarization of **Ru-1°**/**A1** and **Ru-1**/**A1**.*

Hybridization study

Hybridization studies were carried out by titration of **Ru-1/A1** with the complementary strand of **A1** using the hybridization procedure described in chapter 6.3. For emission intensity and lifetime measurements no signal change can be observed when adding the complementary strand. For polarization measurement there was also no significant signal change to higher values (5%). As a result, the system is not suitable for hybridization studies.

6.3.2. Hybridization systems based on energy transfer

The issue of location of the dye labeled to the complementary strand was investigated for hybridization. A 15mer oligo was used for this purpose, reported to be sufficiently short for energy transfer [21]. The complementary strands to **A1** were amino-modified on the 3'-end (**A3**) and 5'-end (**A2**), respectively. The complementary strands **A2** and **A3** were labeled with the NHS activated squarine dye **RB-631** to perform the energy transfer studies (see chapter 3.1.2).

Spectral characterization of the complementary strands to A1

Several spectral data measured for the complementary strands **RB-631/A2** and **RB-631/A3** are listed in table 6-3. Absorption and emission maxima of **RB-631** exhibit a bathochromic shift when covalently bound to the oligonucleotides **A2** and **A3**. The quantum yields of the dyes labeled to the oligos were five times higher than the quantum yield of the unlabeled dye. The dye-to-oligo ratio was determined by absorbance measurement and was found to be 0.16 and 0.19 for the oligo **A2** and **A3**, respectively. The requirements for the dye in energy transfer studies were found to be similar to the energy transfer HSA immunosystem and were discussed in chapter 5.

Table 6-3. Characterization of the **RB-631** modified strands **A2** and **A3**.

Dye	Abs. max. [nm]	Em. max. [nm]	Q.Y.	Dye/Oligo [mol/mol]
RB-631	631	645	0.04	---
RB-631/A2	635	658	0.19	0.16
RB-631/A3	635	658	0.22	0.19
Cy5*	647	664	0.25	---

used as reference standard

Hybridization systems Ru-1/A1 – RB-631/A2 and Ru-1/A1 – RB-631/A3

Two titration experiments were carried out where fixed quantities of **Ru-1/A1** were titrated with increasing amounts of the complementary strand of **A1**. The complementary strands **A2** and **A3** were labeled on the 3'-end terminus and 5'- terminus with **RB-631**, respectively. The two hybridization systems are illustrated in figure 6-5. The hybridization was performed as described in chapter 6.3.

Figure 6-6 and figure 6-7 present the two titration experiments. In both titrations the **Ru-1** emission decreased with increased amounts of acceptor labeled oligomer until a ratio of acceptor labeled oligomer to **Ru-1**-oligomer close to 5 was reached. The emission intensity was constant at ratios of complementary oligomers larger than 5. The optimal energy transfer was expected at a complex with a 1:5 ratio, because the dye to oligo ratios of the labeled complementary strands were 0.16 and 0.19 for **A2** and **A3**, respectively. Therefore, approximately 80% unlabeled complementary strand were in hybridization solution and a five fold excess of the complementary strand was necessary to saturate the energy transfer system.
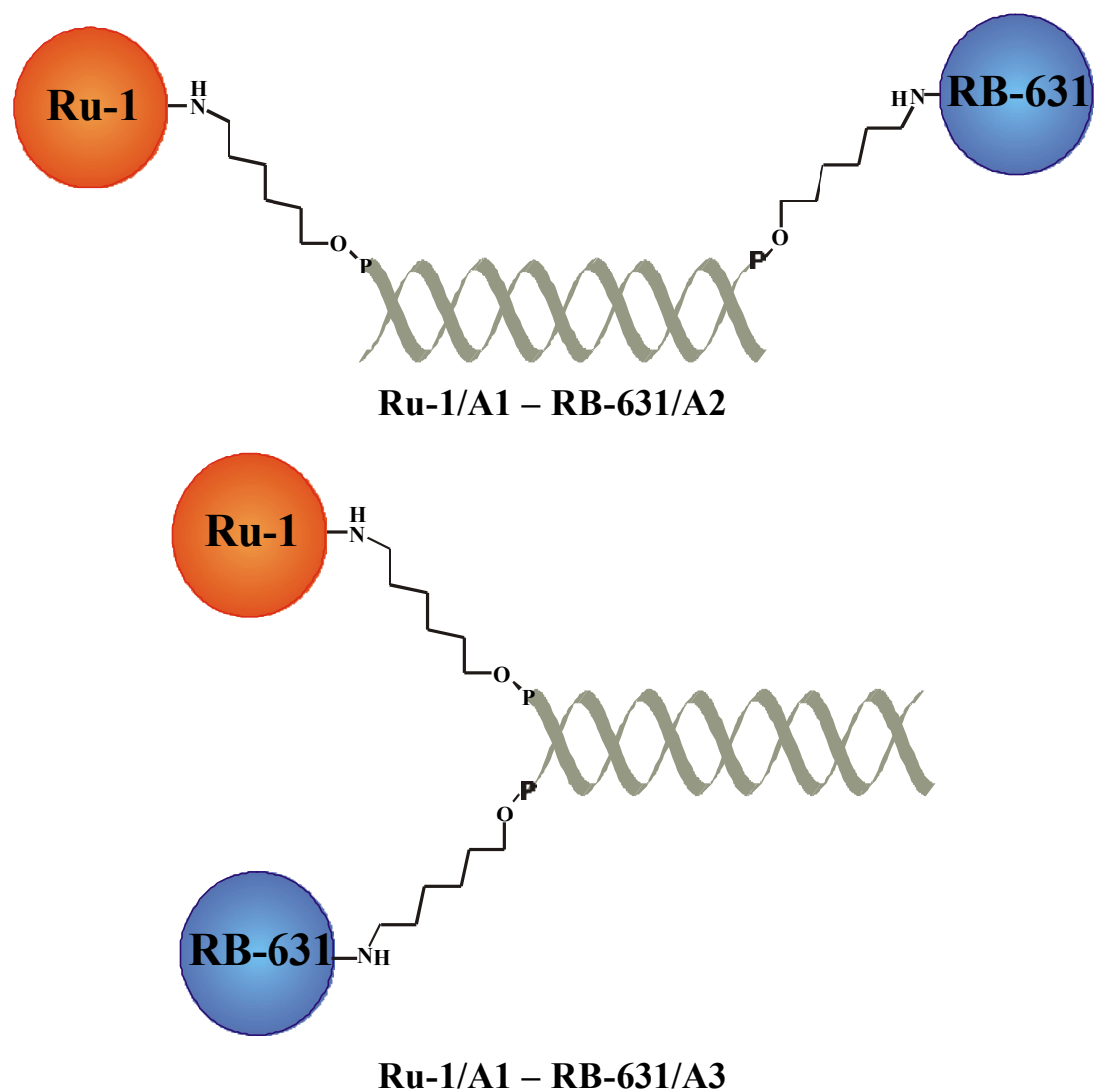
Ru-1/A1 – RB-631/A2

Ru-1/A1 – RB-631/A3

Fig. 6-5. *Schematic illustration of the energy transfer systems **Ru-1/A1 – RB-631/A2** and **Ru-1/A1 – RB-631/A3**.*
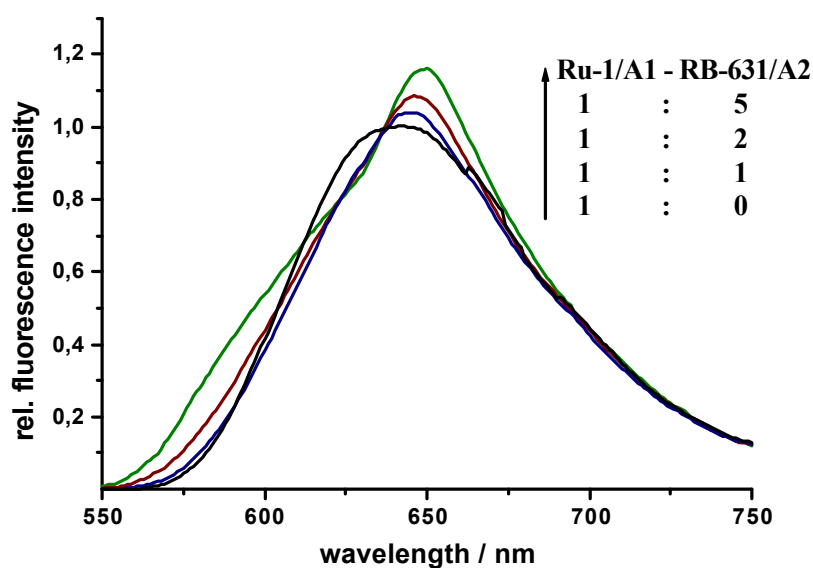
Fig. 6-6. *Luminescence energy transfer in the system A1⁄A2: The strand **Ru-1/A1** (dye⁄oligo = 0.98) of constant concentration (8.3 µM) was titrated with the strand **RB-631/A2** (dye⁄oligo = 0.16); (l_{ex}= 460 nm).*
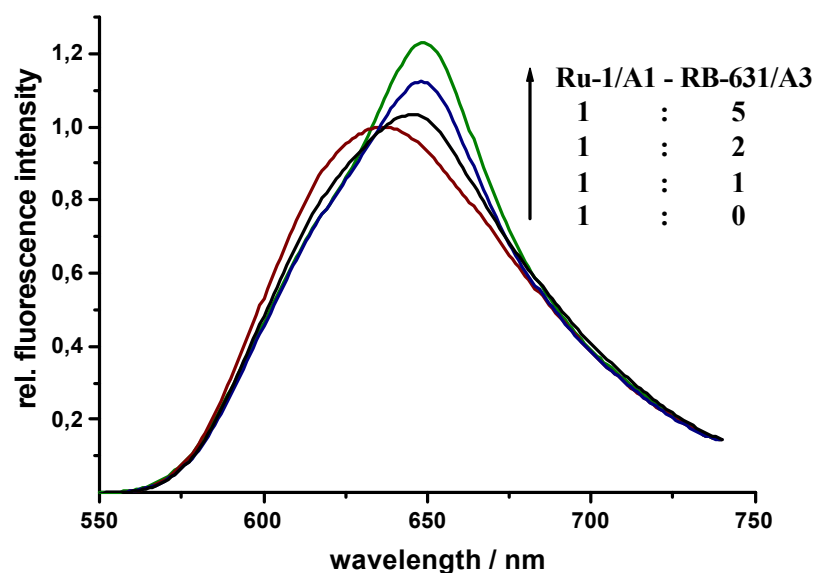

Fig. 6-6. *Luminescence energy transfer in the system A1⁄A2: The strand **Ru-1/A1** (dye⁄oligo = 0.98) of constant concentration (8.3 µM) was titrated with the strand **RB-631/A3** (dye⁄oligo = 0.19); (l_{ex}= 460 nm).*

To compare the two energy transfer systems, the fluorescence intensity was measured and the ratios of the two emission maxima at 639 nm (donor) and 651 nm (acceptor) were determined. In figure 6-8 the normalized ratios of the intensities are plotted against the ratio of **RB-631/A2** (**A3**) and **Ru-1/A1**. As can be seen, the energy transfer efficiency of the system with the complementary strand **A3** is more expressed than for the system with the **A2** strand. These results can be explained by the closer distance of the donor and acceptor dye by attaching the donor at the 5'-end of a 15mer oligo, and the acceptor at the 3'-end of the complementary strand. The linkage of the acceptor dye at the 5'-end of the complementary strand results in an energy transfer that differs in the efficiency.
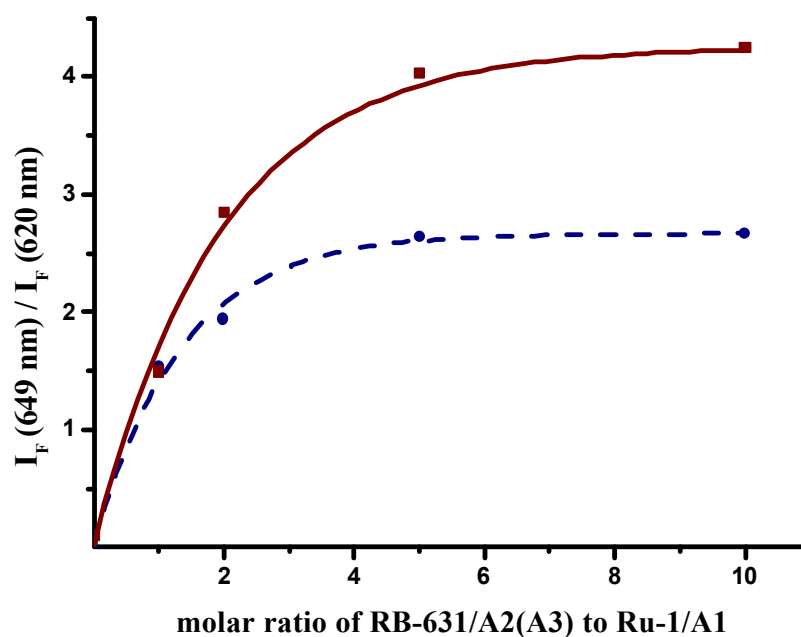

Fig. 6-7. *Comparison of the energy transfer efficiency of the hybridization systems **Ru-1/A1 RB-631/A2** (-------) and **Ru-1/A1 RB-631/A3** (———).*

6.4. Conclusion

In this chapter it is demonstrated that **Ru-1** can be coupled to 5'-NH$_2$-modified oligos. Due to the linkage to the oligonucleotide, the fluorescence decay time and the steady-state fluorescence polarization of the complexes increased. The hybridization with the unlabeled complementary strand did not change the **Ru-1** intensity.

Ru-1 as donor label in combination with the near-infrared acceptor label **RB-631** turned out to be a very useful donor-acceptor pair for performing hybridization studies by non-radiative fluorescence energy transfer. The attachment of **RB-631** to the 5' and 3' ends of the complementary strands of the **Ru-1**-modified oligo were carried out when coupling the NHS ester of **RB-631** to the amino-modified complementary strands. Upon hybridization of the complementary strand (**A2**, **A3**) modified with **RB-631** at the 5'- and 3'-end with the **Ru-1** modified oligo, a decrease in **Ru-1** emission intensity and an enhancement in **RB-631** emission was observed. In conclusion, the energy transfer occurs in both systems, but the attachment of the donor at the 5'-end and the acceptor at the 3' end of the complementary strands is more efficient. This is interpreted in terms of a closer distance of both dyes after hybridization.

The use of **Ru-1** for primers can also be taken in consideration, because of the excitation that is possible at 488 nm, which is often used for standard primer dyes like fluorescein and rhodamine. The emission intensity of **Ru-1** at 610 nm makes this dye an additional opportunity for multiplex analysis. Another possibility is to introduce **Ru-1** modified oligos in flow cytometry, using an argon ion laser routinely.

6.5. References

[1]   Ewin B., Green P., *Nature Genet.* **2000**, *25*, 232.

[2]   Liang F., Holt I., Pertea G., Karamycheva S., Salzberg S.L., Quackenbush J. *Nature Genet.* **2000**, *25*, 239.

[3]   Hattori M. et.al., *Nature* **2000**, *402*, 311.

[4]   Kleinjung F., Bier F. F., Warinke A., Scheller F. W., *Anal. Chim. Acta* **1997**, *350,* 71.

[5]   Millan K. M., Saraoullo A., Mikkelsen S. R., *Anal. Chem.* **1993**, *65*, 2317.

[6]   Steel A. B., Herne T. M., Tarlov M. J., *Anal. Chem.* **1998**, *70*, 4670.

[7]   Su H., Kallury K. M. R., Thompson M., Roach A., *Anal. Chem.* **1994**, *66*, 769.

[8]   Ishiguro T., Saitoh J., Yawata H., Otsuka M., Inoue T., Sugiura Y., *Nucleic Acids Res.* **1996**, *24*, 4992.

[9]   Norman D. G., Graininger R. J., Uhrin D., Lilley D. M. J., *Biochemistry* **2000**, *39,* 5317.

[10]   Hu X., Gregory D. S., Sykora M., Lee S. J., Grinstaff M. W., *Inorg. Chem.* **2000**, *39,* 2500.

[11]   Mergny J. L., *Biochemistry* **1999**, *38*, 1573.

[12]   Stühmeier F., Welch J. B., Murchie A. I. H., Liley D. M. J., Clegg R. M., *Biochemistry* **1997**, *36*, 13530.

[13]   Clegg R. M., Murchie A. I. H., Zechel A., Carlberg C., Diekmann S., Lilley D. M. J., *Biochemistry* **1992**, *31*, 4846.

[14]   Kelley S. O., Barton J. K., *Science* **1999**, *283*, 375.

[15]   Yang M., Ren L.-Q., Huang M., Kong R. Y. C., Fong F. W., *Anal. Biochem.* **1998**, *259*, 272.

[16]   Grinstaff M. W., *Angew. Chem., Int. Ed. Engl.* **1999**, *38*, 3629.

[17]   Matthews J. A., Kricka L. J., *Anal. Biochem.* **1988**, *169*, 1.

[18]   Parkhurst K. M., Parkhurst L. J., *Biochemistry* **1995**, *34*, 293.

[19]   Morrison H. E., Halder T. C., Stols L. M., *Anal. Biochem.* **1989**, *183*, 231.

[20]   Yang M., Millar D. P., *Biochemistry* **1996**, *35*, 7959.

[21]   Ju J., Kheterpal I., Scherer J. R., Ruan C., Fuller C. W., Glazer A. N., Mathies R. A., *Anal. Biochem.* **1995**, *231*, 131.

7. Experimental Part

7.1. General Remarks

7.1.1 Chemicals, Proteins and Buffers

All chemicals and solvents used were obtained from Merck (Darmstadt, Germany), Aldrich (Steinhein, Germany) and Fluka (Buchs, Switzerland). All chemicals were analytical grade and were used as received. Cy5 was obtained from Amersham Life Science (Pittsburgh, USA). DPPC, PE, HSA and anti-HSA were obtained from Sigma (Germany). **Ru-(phen)$_2$-(C$_{16}$)$_2$** was synthesized by Roche (Penzberg, Germany). Fluorescein-NHS was a gift from Roche (Penzberg, Germany). Anhydrous diethylether and anhydrous DMF were prepared, according to a standard procedures published in [1]. Ethylenediamine was freshly distilled. Water was double distilled.

Phosphate buffer of pH 7.2, 0.1 M: 3.17 g of NaH$_2$PO$_4\cdot$ H$_2$O and 13.7 g of Na$_2$HPO$_4\cdot$ 2 H$_2$O were dissolved in 1 L of double distilled water. Bicarbonate buffer of pH 9.0, 0.05 M: 2.1 g of NaHCO$_3$ were dissolved in 500 mL of double distilled water. The buffers were adjusted to the corresponding pH value with 0.1 N HCl and 0.1 N NaOH, respectively.

7.1.2 Chromatography

For analytical thin-layer chromatography (TLC), RP-18 F$_{254}$ aluminium sheets (thickness 0.2 mm) for polar solvents, and silica gel 60 F$_{254}$ aluminium sheets (thickness 0.2 mm) for non-polar solvents were used. They all were purchased from Merck (Darmstadt, Germany).

Medium pressure liquid chromatography (MPLC) was carried out on a Büchi 681 MLC apparatus. The column length was 26 cm with a diameter of 2 cm, the pre-column was 13 cm long with a diameter of 2 cm. For non-polar substances, both, pre-column and column were filled with Europrep 60-20, 60 Å, 15-25 µm (irregular) from Knauer. For polar substances, the pre-column was filled with Europrep 60-60-C18 and the main column was filled with Europrep 60-20-C18 from Knauer.

Gel permeation chromatography was carried out using Sephadex G25 (coarse) from Pharmacia (Uppsala, Sweden) as the stationary phase (0.5 x 20 cm column) and a 22 mM phosphate buffer solution (pH 7.2) as the eluent.

7.1.3 Analysis and Spectroscopy

Melting points were measured with an apparatus SMP-20 from Büchi and were not corrected. pH values were measured at room temperature with a pH meter WTW 538 (Weilheim, Germany). UV spectra were recorded with a U-3000 spectrophotometer from Hitachi. Emission spectra were acquired with a luminescence spectrometer Aminco (Series 2) from SLM with a standard 150 W xenon lamp as the excitation source and with a multi frequency fluorimeter K2 from ISS with a argon ion laser (488 nm) or a standard 300 W xenon lamp as the excitation sources. Fluorescence lifetimes and polarization measurements were measured with a multi frequency fluorimeter K2 from ISS with a argon ion laser (488 nm) and standard 300 W xenon lamp as the excitation source, respectively.

^{1}H-NMR spectra were recorded with a 250 MHz PFT-NMR spectrometer (AC 250 from Bruker). The internal standard used was TMS. The chemical shifts are given in ppm. The following abbreviations were used to describe the signals: s = singlet, d = doublet, dd = double of doubletts, t = triplet, q = quartett, m = multiplet, br = broad peak. Mass spectra were recorded with a Finnigan MAT 95 (fast-atom bombardment, FAB and chemical

ionization, CI) and a Finnigan MAT 311 A (electron impact EI) at the University of Regensburg.

7.1.4 Determination of the Molar Absorbance

The dyes (~0.55 mg) were dissolved in 100 mL of doubly distilled water. From this stock solution, three dilutions (1:20, 1:50, 1:100) were made and the molar absorbance was measured. The extinction coefficients were calculated according to Lambert-Beer's law ($E = \varepsilon \cdot c \cdot d$).

7.1.5 Determination of Quantum Yields [2]

The quantum yields of the dyes and the dye-protein conjugates were measured in phosphate buffer (22 mM, pH 7.2) relative to a reference fluorophor with a known quantum yield. These references were Cy5 (Amersham) for **RB-631** and with a quantum yield of 0.28 in PBS [3] and $Ru(bipy)_3^{2+}$ for the ruthenium MLCs with a quantum yield of 0.042 [4] in ethanol. The following formula is used to determine the quantum yields:

$$\varphi_S = \varphi_{Ref} \cdot (E_{Ref}/E_S) \cdot (A_S/A_{Ref}) \cdot (n^2_S/n^2_{Ref}), \qquad (7\text{-}1)$$

where

$\boldsymbol{\varphi}_S$ is the quantum yield of the substance to determine,

$\boldsymbol{\varphi}_{Ref}$ is the quantum yield of the reference,

$\mathbf{E}$ is the absorbance at the excitation wavelength of the substance to determine,

$\mathbf{E_{Ref}}$ is the absorbance at the excitation wavelength of the reference,

$\mathbf{A}$ is the integrated area of the fluorescence spectrum of the substance to determine,

$\mathbf{A_{Ref}}$ is the integrated area of the fluorescence spectrum of the reference,

$\mathbf{n^2_S}$ is the refractive index of the solvent for the substance to determine,

$\mathbf{n^2_{Ref}}$ is the refractive index of the solvent for the reference.

The quantum yield was determined as follows:

(1) The absorbance spectra of sample and reference are measured (the extinction of the solutions must be lower than 0.1 to avoid the inner filter effect).

(2) The emission spectra of sample and reference are measured (excitation of sample and reference must be at the same wavelength).

(3) Integration of the areas of the emission spectra.

(4) The quantum yield was then determined via the formula above

7.2. Syntheses and Purification of the Dyes

7.2.1. Ruthenium metal-ligand complexes

7.2.1.1. Synthesis of the Ru-(bipy)$_2$-mcbpy (Ru-1)

➢ *4´-Methyl-2,2´-bipyridine-4-carboxaldehyde [5]*
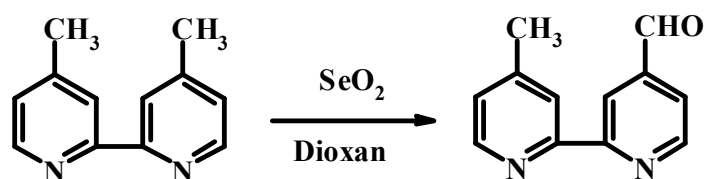
SeO$_2$ (1.74 g, 15.7 mmol) was added to a solution of 4,4´-dimethyl-2,2´-bipyridine (2.64 g, 14.3 mmol) in 75 mL dioxane and refluxed for 24 h. The solution was then filtered hot, and the dioxane was removed by rotary evaporation. Next the residue was dissolved in ethyl acetate and filtered to remove additional solid material. The ethyl acetate layer was subsequently extracted with 1 M Na$_2$CO$_3$ (2 x 100 mL) to remove additional carboxylic acid and 0.3 M Na$_2$S$_2$O$_5$ (3 x 100 mL) to form the aldehyde bisulfite. The combined aqueous extracts were adjusted to pH 10 with Na$_2$CO$_3$ and extracted with CH$_2$Cl$_2$ (4 x 100 mL). The organic phases were collected and evaporated.

Yield: 1.75 g (62%), white powder, C$_{12}$H$_{10}$N$_2$O (198.22 g/mol).

m.p.: 131°C.

^{1}H-NMR (CDCl$_3$, TMS external, 250 MHz): δ 2.45 (s, 3 H); 7.15-8.8 (m, 6 H); 10.1 (s, 1 H).

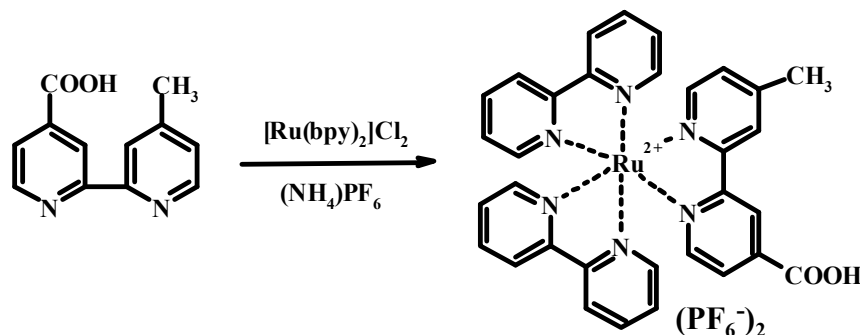> *4´-Methyl-2,2´-bipyridine-4-carboxylic acid [6]*
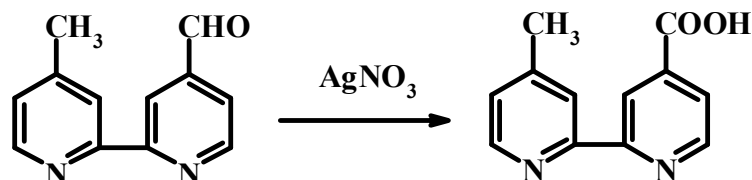
A solution of AgNO$_3$ (1.57 g, 9.24 mmol) in 16 mL water was added to a suspension of 4´-Methyl-2,2´-bipyridine-4-carboxaldehyde (1.75 g, 8.83 mmol) in 75 mL 95% ethanol. The suspension was stirred rapidly, and 40 mL 1 M NaOH was added dropwise over 20 min to form Ag$_2$O. The dark black solution was stirred for an additional 15 h. Finally, the ethanol was removed by rotary evaporation, and the remaining water solution was filtered to remove Ag$_2$O. The residue was washed with 1.3 M NaOH (2 x 20 mL) and 20 mL H$_2$O. The combined filtrates were extracted with CH$_2$Cl$_2$ to remove unreacted aldehyde and adjusted to pH 3.5 with 1:1 (v/v) 4 N HCl:AcOH to afford a white compound. The product precipitated overnight at -10 °C, and the compound was collected.

Yield: 1.26 g (67%), white powder, C$_{12}$H$_{10}$N$_2$O$_2$ (214.22 g/mol).

m.p.: 280°C.

^{1}H-NMR (CDCl$_3$, TMS external, 250 MHz): δ 2.5 (s, 3 H); 7.15-9 (m, 6 H).

➢ *Ruthenium-bis(2,2´-bipyridine)-(4´-methyl-2,2´-bipyridine-4-carboxylic acid)-*

*bis(hexafluorophosphate) (**Ru-1**) [6]*

Ru-(bipy)$_2$Cl$_2$ (0.3 g, 0.57 mmol) was added to a solution of 4´-methyl-2,2´-bipyridine-4-carboxylic acid (0.15 g, 0.58 mmol) in 25 mL 70% ethanol/H$_2$O and refluxed for 10 h. Next, the reaction mixture was cooled and ethanol was removed in vacuum. After standing for 4 h at room temperature, the solution was filtered and the solid compound washed with cold water. A saturated aqueous solution of NH$_4$PF$_6$ was added until no further precipitate was observed. The mixture was kept at room temperature for an additional 2 h and then finally filtered washed with cold water and ether, and dried overnight.

Yield: 0.42 g (81%), orange pwoder, C$_{32}$H$_{26}$F$_{12}$N$_6$O$_2$P$_2$Ru (917.6 g/mol).

m.p.: > 250°C.

R$_f$ (RP-C18, methanol:water 2:1 v/v): 0.55.

FAB-MS: m/e (M - 2H$^+$, dianion) for C$_{32}$H$_{26}$N$_6$O$_2$Ru calcd. 738.9, found 738.6.

7.2.1.2. Synthesis of the Ru-(bipy)$_2$dcbpy (Ru-2)

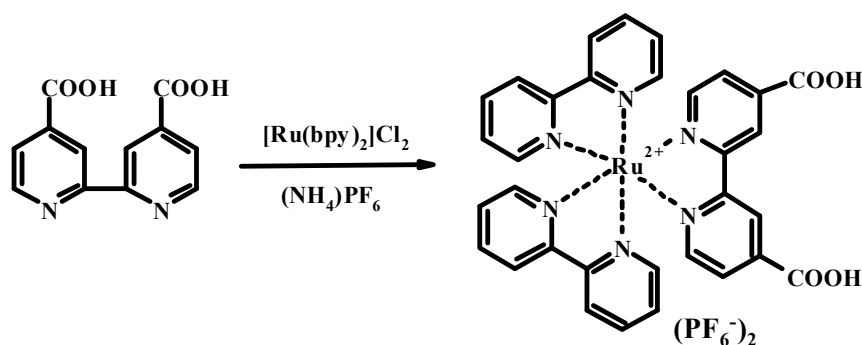➢ *2,2´- bipyridine-4,4´-dicarboxylic acid [7-9]*
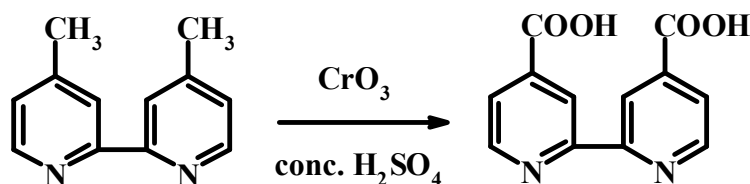
1.0 g (5.2 mmol) of 4,4´-dimethylbipyridyl is solved in 200 mL conc. H_2SO_4 and cooled to 0 °C. Then 3.3 g (33 mmol) CrO_3 is added in four portions. The solution is then stiffed for 4 h at 75 °C, and then 12 h at room temperature. The reaction mixture is added to 2 L ice water. The formed precipitate was centrifugated and washed three times with water. The white precipitate is solved in KOH and then precipitated with conc. HCl. The precipitate was collected by filtration and washed with water, methanol and diethyl ether.

Yield: 1.0 g (75%), white powder, $C_{12}H_8N_2O_4$ (244.21 g/mol).

m.p.: > 250°C.

FAB-MS: m/e (M - H^+, dianion) for $C_{12}H_8N_2O_4$ calcd. 243.2, found 242.9.

➢ *Ruthenium-bis(2,2´-bipyridine)-(2,2´- bipyridine-4,4´-dicarboxylic acid)-bis(hexafluorophosphate)* (**Ru-2**)

0.1 g (0.21 mmol) Ru(bpy)$_2$Cl$_2$, 0.1 g NaHCO$_3$ and 0.08 g (0.3 mmol) 2,2´-bipyridine-4,4´dicarboxylic acid are heated in MeOH: H_2O (v/v) 4:1 for 10 h. The solution is cooled in an ice bath for 2 h, and the pH is adjusted with concentrated H_2SO_4 to 4. The formed precipitate is filtered and washed with MeOH. The filtrate is treated with 5 g NaPF$_6$ in 25 mL H_2O, then cooled in an ice bath, and the precipitate is collected by filtration.

Yield: 0.13 g (67%), violett crystals, $C_{32}H_{24}F_{12}N_6O_4P_2Ru$ (948.22 g/mol).

m.p.: > 250°C.

R_f (RP-C18, methanol:water 1:1 v/v): 0.6.

FAB-MS: m/e (M - H^+, dianion) for $C_{32}H_{24}N_6O_4Ru$ calcd. 947.2, found 946.8.

7.2.1.3. Synthesis of the Ru-(bipy)₂-mcbpy membrane probes (Ru-1-R)
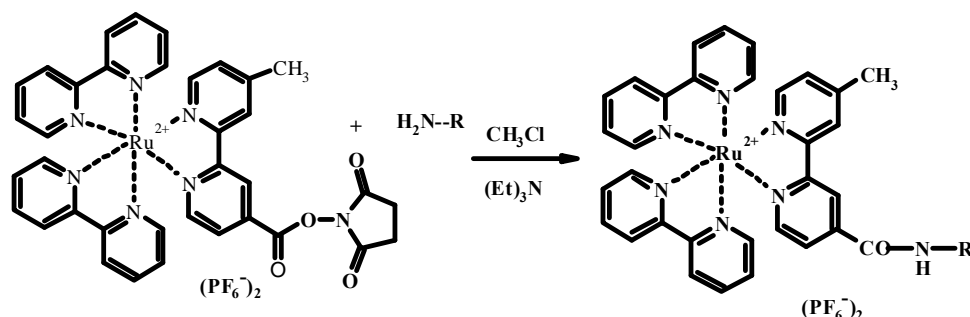
➢ *Ru-1-NHS*
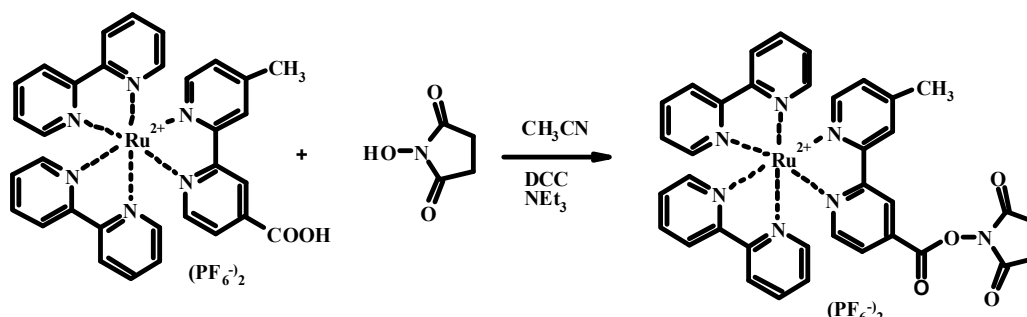
Ru-1 (50 mg, 55 μmol) and 10 mg (86 μmol) of N-hydroxysuccinimide (NHS) were dissolved in 1 mL of acetonitrile at room temperature. N,N'-dicyclohexylcarbodiimide (DCC, 17 mg, 83 μmol) was then added. The mixture was sealed and stirred for 5 h. The formed precipitate was removed by filtration through a syringe filter and the filtrate was added to a stirring solution of 2-propanol. The mixture was kept at -4 °C for 1 h. The precipitate, **Ru-1**-NHS was collected by filtration and washed with dry ether (3 x 5.5 mL).

Yield: 44 mg (30%), blue crystals, $C_{38}H_{46}N_2O_{10}S_2$ (740.88 g/mol).

m.p.: > 250°C.

R_f (RP-C18, methanol:water 2:1 v/v): 0.55.

FAB-MS: m/e (M - 2H⁺, dianion) for $C_{37}H_{42}N_2O_{10}S_2$ calcd. 738.9, found 738.6.

➢ *Ru-1-R*

Ru-1-NHS (50 mg, 49 μmol) and the lipid (80 μmol) were dissolved in 1.5 mL dry chloroform under nitrogen atmosphere. Then 10μL of NEt$_3$ was added. The mixture was stirred for 20 h in the dark. The solvent was evaporated in vacuum and the residue purified by medium pressure liquid chromatography on a column of silica gel-60 (230-400 mesh), with a mixture of chloroform-methanol-water as the eluent.

> *Ru-1-PE*

Yield: 15 mg (20%), orange crystals, C$_{69}$H$_{96}$F$_{12}$N$_7$O$_9$P$_3$Ru (1591.6 g/mol).

m.p.: > 250°C.

R$_f$ (silica gel, chloroform:methanol:water 65:25:4 v/v): 0.55.

^{1}H-NMR (CDCl$_3$, TMS external, 250 MHz): δ = 0.87 (m, 6 H); 1.24 (s, 48 H); 1.39 – 1.57 (m, 4 H); 2.25 – 2.31 (m, 4 H); 2.6 (m, 2 H); 3.57 (m, 2 H); 4.1 – 4.21 (m, 5 H); 4.4 (dd, J$_1$= 3.1, J$_2$=11.5, 2 H); 5.23 – 5.25 (m, 1 H); 7.41 – 7.52, 7.64 – 7.72, 8.0 – 8.1, 8.4 – 8.7 (m, 22 H).

^{31}P-NMR (CDCl$_3$): δ = 2.7; -143 ppm.

FAB-MS: m/e (M^{2+}) for C$_{69}$H$_{96}$N$_7$O$_9$Ru calcd. 1301.4, found 1300.4

> ➤ **Ru-1-C₁₆H₃₃**
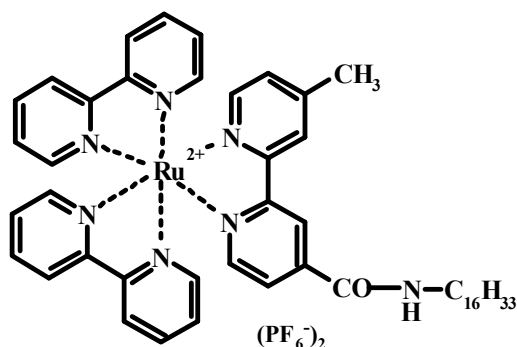
Yield: 4.5 mg (9%), orange crystals, $C_{48}H_{59}F_{12}N_7OP_2Ru$ (1141.6 g/mol).
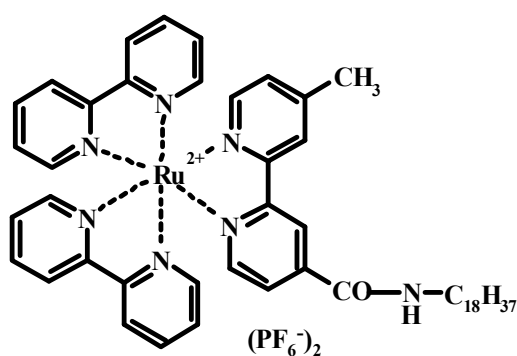
m.p.: > 250°C.

R_f (silicagel, chloroform:methanol 3:1 v/v): 0.75.

^{1}H-NMR (CDCl$_3$, TMS external, 250 MHz): δ 0.87 (t, J = 6.83, 3 H); 1.23 (s, 28 H); 1.61 – 1.83 (m, 3 H); 3,42 (m, 2 H); 7.42 – 7.47, 7.65 – 8.05, 8.40 – 8.43 (m, 22 H).

^{31}P-NMR (CDCl$_3$): δ = -143 ppm.

FAB-MS: m/e (M^{2+}) for $C_{48}H_{59}N_7ORu$ calcd. 851.2, found 851.4.

> ➤ **Ru-1-C₁₈H₃₇**

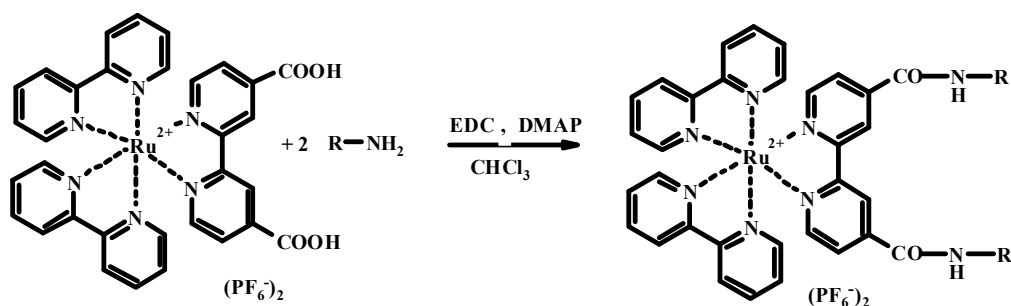Yield: 9 mg (17%), orange crystals, $C_{50}H_{63}F_{12}N_7OP_2Ru$ (1169.6 g/mol).

m.p.: > 250°C.

R_f (silicagel, chloroform:methanol 3:1 v/v): 0.75.

^{1}H-NMR (CDCl$_3$, TMS external, 250 MHz): δ 0.87 (t, J = 6.62, 3 H); 1.23 (s, 32 H); 1.61 – 1.83 (m, 3 H); 3,42 (m, 2 H); 7.42 – 7.47, 7.65 – 8.05, 8.40 – 8.43 (m, 22 H).

^{31}P-NMR (CDCl$_3$): δ = -143 ppm.

FAB-MS: m/e (M^{2+}) for C$_{50}$H$_{63}$N$_7$ORu calcd. 879.2, found 878.5.

7.2.1.3. Synthesis of the Ru-(bipy)$_2$-dcbpy membrane probes (Ru-2-R$_2$)

Ru-2 (19 mg; 20 μmol), lipid (50 μmol) and 4-(dimethylamino)pyridine (2.4 mg; 20 μmol) were suspended in 3 mL of CHCl$_3$ and stirred in an ice bath. Then, 1-ethyl-3-(3-(di-methylamino)propyl) carbodiimide hydrochloride (9 mg; 58 μmol) was added, and the reaction mixture kept at 0 °C for 2 h and afterwards for two days at room temperature. The solvent was evaporated in vacuum and the residue purified by medium pressure liquid chromatography on a column of silica gel-60 (230-400 mesh), with a mixture of chloroform-methanol-water as the eluent.

➢ **_Ru-2-PE₂_**
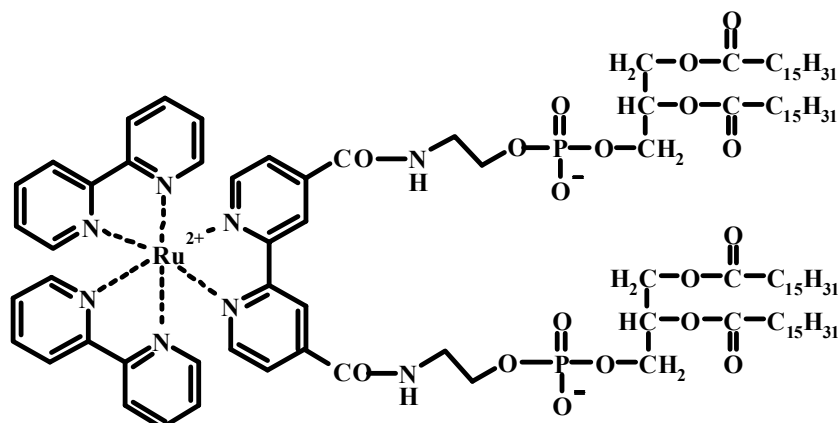
Yield: 11 mg (22%), orange crystals, $C_{106}H_{166}F_{12}N_8O_{18}P_4Ru$ (2298 g/mol).
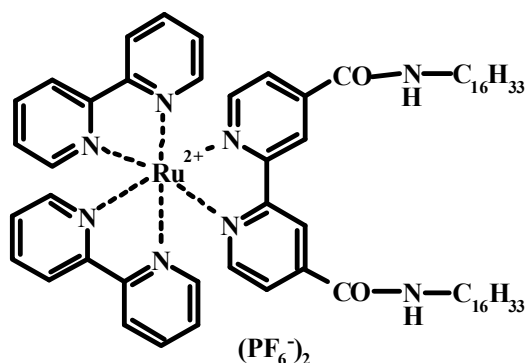
m.p.: > 250°C.

R_f (silica gel, chloroform:methanol:water 65:25:4 v/v): 0.7.

^{1}H-NMR (CDCl$_3$, TMS external, 250 MHz): δ = 0.83 (t, J = 6.28, 12 H); 1.23 (s, 96 H); 1.48 – 1.65 (m, 8 H); 2.15 – 2.31 (m, 8 H); 3.1 (t, J = 4.28, 4 H); 3.94 – 4.23 (m, 10 H); 4.36 (dd, J$_1$= 2.89, J$_2$=12,01, 2 H); 5.12 – 5.24 (m, 2 H); 7.35 – 7.5, 7.6 – 7.8, 7.9 – 8.2, 8.45 – 8.6 (m, 22 H).

^{31}P-NMR (CDCl3): δ = 0.23; -143.

FAB-MS: m/e (M^{2+}) calcd. for $C_{106}H_{166}N_8O_{18}P_2Ru$: 2003.2, found 2003.5.

➢ **_Ru-2-(C₁₆H₃₃)₂_**

Yield: 9 mg (30%), orange crystals, $C_{64}H_{90}F_{12}N_8O_2P_2Ru$ (1395.2 g/mol).
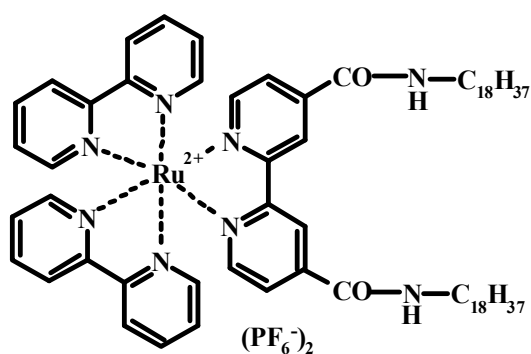
m.p.: > 250°C.

R_f (silica gel, chloroform:methanol:water 65:25:4 v/v): 0.8.

^{1}H-NMR (CDCl$_3$, TMS external, 250 MHz): δ 0.88 (t, J = 6.85, 6 H); 1.24 (s, 52 H); 1.61 – 1.83 (m, 4 H); 3.21 (q, J_1= 7.01, J_2=12,91, 4 H); 7.42 – 7.47, 7.65 – 8.05, 8.40 – 8.43 (m, 22 H).

^{31}P-NMR (CDCl$_3$): δ = -143 ppm.

FAB-MS: m/e (M2+) for C$_{64}$H$_{90}$N$_8$O$_2$Ru calcd. 1104.3, found 1104.5.

➤ **Ru-2-(C$_{18}$H$_{37}$)$_2$**

Yield: 11 mg (33%), blue crystals, C$_{68}$H$_{98}$F$_{12}$N$_8$O$_2$ P$_2$Ru (1450.32 g/mol).
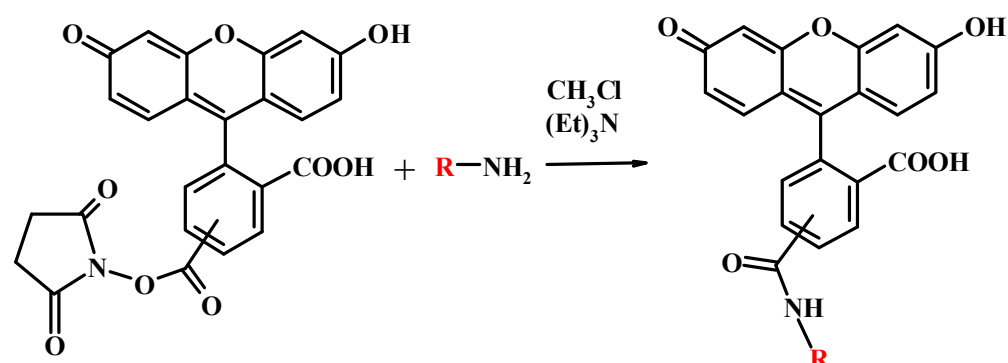
m.p.: > 250°C.

R_f (silica gel, chloroform:methanol:water 65:25:4 v/v): 0.8.

^{1}H-NMR (CDCl$_3$, TMS external, 250 MHz): δ 0.89 (t, J = 6.85, 6 H); 1.22 (s, 68 H); 1.63 – 1.81 (m, 4 H); 3.21 (q, J_1= 6.95, J_2=12,52, 4 H); 7.43 – 7.47, 7.66 – 8.01, 8.38 – 8.41 (m, 22 H).

^{31}P-NMR (CDCl$_3$): δ = -143 ppm.

FAB-MS: m/e (M^{2+}) for C$_{68}$H$_{98}$N$_8$O$_2$Ru calcd. 1159.2, found 1160.6.

7.2.2. Fluorescein membrane probes Fl-R

Fluorecein-NHS (10 mg, 21 μmol) and the lipid (27 μmol) were dissolved in 1.5 mL dry chloroform under nitrogen atmosphere. Then 10μL of NEt$_3$ was added. The mixture was stirred for 20 h in the dark. The solvent was evaporated in vacuum and the residue purified by medium pressure liquid chromatography on a column of silica gel-60 (230-400 mesh), with a mixture of chloroform-methanol as the eluent.

> **Fl-PE**
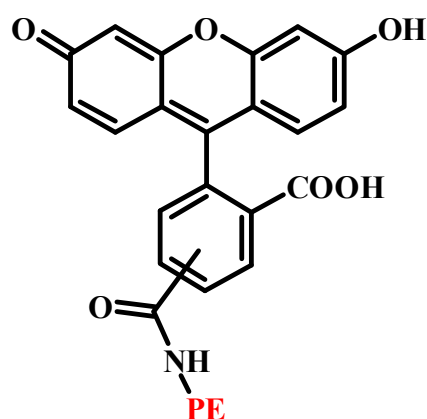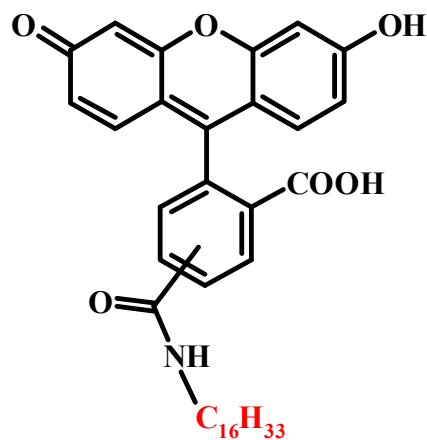

Yield: 6 mg (52%), orange crystals, C$_{58}$H$_{84}$NO$_{14}$P (1050.1 g/mol).

m.p.: > 250°C.

R$_f$ (silica gel, chloroform:methanol:water 65:25:4 v/v): 0.8.

FAB-MS: m/e (M-H$^+$) for C$_{58}$H$_{84}$NO$_{14}$P calcd. 1049.1, found 1048.8.

➢ **Fl-C$_{16}$H$_{33}$**

Yield: 8 mg (60%), orange crystals, C$_{37}$H$_{45}$NO$_6$ (599.01 g/mol).

m.p.: > 250°C.

R$_f$ (silica gel, chloroform:methanol:water 65:25:4 v/v): 0.65.

FAB-MS: m/e (M-H$^+$) for C$_{37}$H$_{45}$NO$_6$ calcd. 598.0, found 598.5.

➢ **Fl-C$_{18}$H$_{37}$**
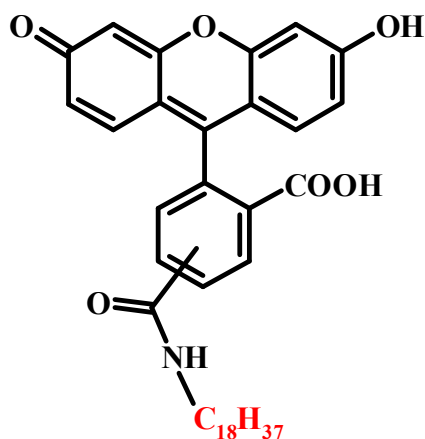
Yield: 6 mg (52%), orange crystals, C$_{39}$H$_{49}$NO$_6$ (628.9 g/mol).

m.p.: > 250°C.

R$_f$ (silica gel, chloroform:methanol:water 65:25:4 v/v): 0.65.

FAB-MS: m/e (M-H$^+$) for C$_{37}$H$_{45}$NO$_6$ calcd. 627.9, found 628.5.

7.2.3. Squarylium dye RB-631

7.2.3.1. 1-Ethyl-2,3,3-tetramethylindoleninium-5-sulfonate [10]
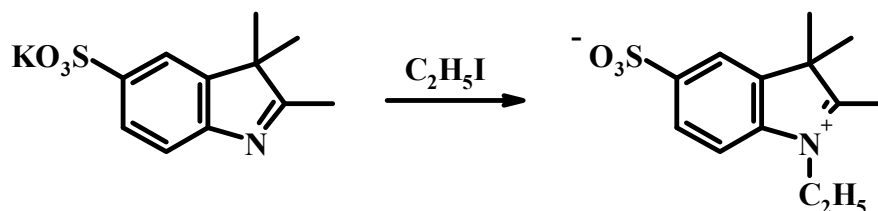
1.1 g (4.0 mmol) of potassium 2,3,3-trimethylindolenine-5-sulfonate are suspended in 30 mL of ethyl iodide. The reaction mixture is heated to boiling for 25 h in a sealed tube. After cooling, excess ethyl iodide is decanted and the residue is suspended in 50 mL of acetone and stirred at room temperature for 20 min. The solution is filtered, the residue is washed with acetone and ether and dried in a desiccator over $CaCl_2$.
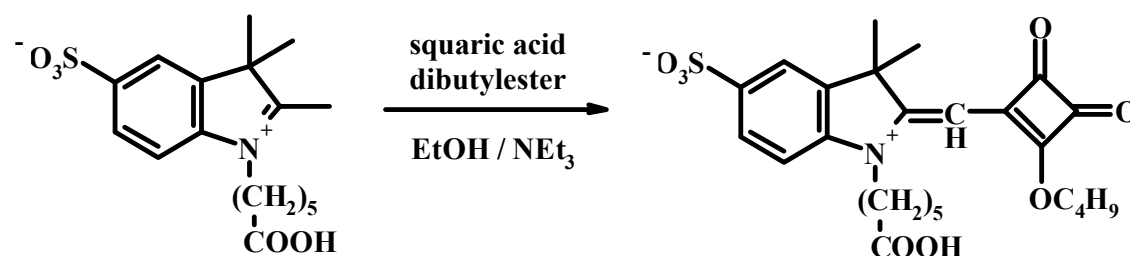
Yield: 912 mg (90%), light pink powder, $C_{13}H_{17}NO_3S$ (267.31 g/mol).

m.p.: 215-217°C

R_f (silica gel; 2-propanol:water:ammonia 9:1:1 v/v): 0.30.

^{1}H-NMR (d_6-DMSO, TMS external, 250 MHz): δ 8.05 (s, 1H), 7.65 (d, 1H), 7.45 (d, 1H), 3.95 (s, 3H) 2.75 (s, 3H), 1.55 (s, 6H).

7.2.3.2. 1-[1-[5-Carboxypentyl]-3,3-dimethyl-5-sulfo-2-indolinylidene methyl]-2-butoxycyclobutene-3,4-dione [11]

0.5 g (1.4 mmol) of 1-(5-carboxypentyl)-2,3,3-trimethylindoleninium-5-sulfonate are dissolved in 20 mL of ethanol containing 1 mL of triethylamine. Then 325 μL (1.5 mmol) of squaric acid dibutyl ester are added slowly. The

mixture is warmed to 60 °C and stirred for 6 h. Then another 50 μL of squaric acid dibutyl ester are added and the mixture is refluxed for 2 h. After cooling to room temperature, the solvent is removed under reduced pressure. The yellow residue is dissolved in 20 mL of water and extracted three times with 20 mL of chloroform. The aqueous phase is collected and the water is removed on a rotary evaporator. The yellow amorphous residue is triturated with ether and stirred over night at room temperature until the product crystallizes. The raw product is recrystalized from 2-butanol.

Yield: 355 mg (50%), orange powder, $C_{25}H_{31}NO_8S$ (505.58 g/mol).
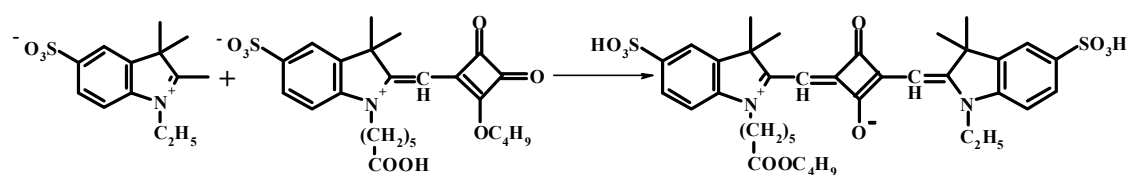
m.p.: 105°C (decomp.).

R_f (RP-18, methanol:water 2:1 v/v): 0.50.

^{1}H-NMR (D_2O, TMS external, 250 MHz): δ 7.65 (m, 2H), 7.05 (d, 1H), 5.35 (s, 1H), 4.60 (t, 2H), 3.75 (t, 2H), 2.2 (m, 2H), 1.65-1.15 (m, 10H), 1.40 (s, 6H), 1.15 (t, 3H).

FAB-MS: m/e (M + H$^+$, cation) for $C_{25}H_{32}NO_8S$, calcd. 506.6, found 506.3.

UV: λ (H_2O) = 432 nm.

7.2.3.3. RB-631-butylester [11]

100 mg (0.20 mmol) of 1-[1-[5-carboxypentyl]-3,3-dimethyl-5-sulfonic acid-2-indolinylidenemethyl]-2-butoxycyclobutene-3,4-dione and 50 mg (0.20 mmol) of 1-ethyl-2,3,3-tetramethylindoleninium-5-sulfonate are dissolved in 50 mL of a 1-butanol/toluene mixture (1:1 v/v) and are refluxed for 10 h using a Dean-Stark trap. After cooling, the solvents are removed under reduced pressure. The product is purified by MPLC using Europrep 60-20-C18 as the stationary phase and a methanol:water mixture (60:40 v/v) as the eluent.

Yield: 44 mg (30%), blue crystals, $C_{38}H_{46}N_2O_{10}S_2$ (740.88 g/mol).

R_f (RP-C18, methanol:water 2:1 v/v): 0.55.

FAB-MS: m/e (M - 2H$^+$, dianion) for $C_{37}H_{42}N_2O_{10}S_2$ calcd. 738.9, found 738.6.

7.2.3.4. RB-631 [12]
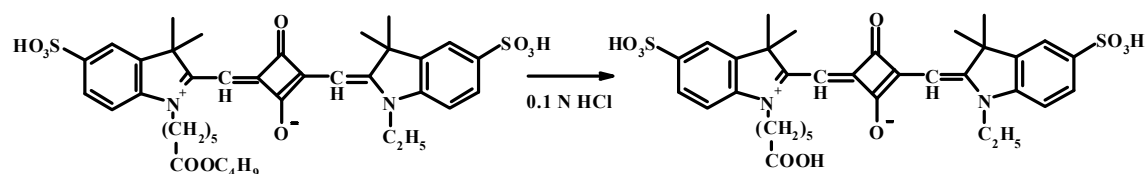
16 mg (21 μmol) of RB-631-butylester are dissolved in 1 mL of water, and 10 mL of 0.1 N HCl are added. The mixture is refluxed for 1.5 h. At the end of the reaction, 5 mL of 1 N HCl are added. After cooling, the solvent is removed, the product is washed with ether, and dried in the vacuum of an oil pump.

Yield: 40 mg (98%), blue crystals, $C_{33}H_{36}N_2O_{10}S_2$ (684.77 g/mol).

m.p.: > 250°C.

R_f (RP-C18, methanol:water 2:1 v/v): 0.70.

^{1}H-NMR (D$_2$O, TMS external, 250 MHz): δ 7.70-7.55 (m, 4H), 7.20-7.00 (m, 2H), 5.50 (s, 1H), 5.40 (s, 1H), 4.45 (t, 2H, J=6.5 Hz), 4.00 (s, 3H), 2.05-2.30 (m, 2H), 1.50-1.25 (m, 6H), 1.20 (t, 12H).

FAB-MS: m/e (M - 2H$^+$, dianion) for $C_{34}H_{36}N_2O_{10}S_2$ calcd. 682.8, found 682.7.

7.2.3.5. RB-631-NHS-ester [13]
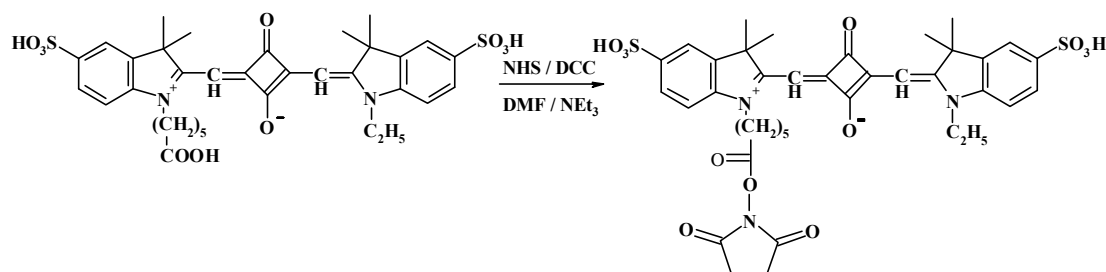
10 mg (14.6 μmol) of RB-631, 4.5 mg (22 μmol) of dicyclohexylcarbodiimide and 2.5 mg (22 μmol) of N-hydroxysuccinimide are dissolved in 0.5 mL of dry

DMF and $10\,\mu$L of triethylamine. The solution is stirred for 16 h at room temperature. Then, the reaction mixture is filtered over a filter syringe and washed with anhydrous DMF. The solvent is removed in vacuum and the product is tritrated with anhydrous ether until it crystallizes. The solvent is decanted and the blue crystals are dried in a desiccator over $CaCl_2$.

Yield: 8 mg (70%), blue powder, $C_{38}H_{41}N_3O_{12}S_2$ (781.84 g/mol).

m.p.: > 250°C.

R_f (RP-18, methanol:water 2:1 v/v): 0.65.

FAB-MS: m/e (M - $2H^+$, dianion) for $C_{37}H_{37}N_3O_{12}S_2$, calcd. 781.8, found 781.9.

7.3. References

[1]   Organikum, 19. Aufl., *Dt. Verl. der Wiss., Leipzig*, **1993**.

[2]   Demas J. N., Crosby G. A*., J. Phys. Chem.* **1971**, *75*, 991.

[3]   Fluoro Link Cy5, Product Description, Cat. No. PA25001, Amershan Life Science, Inc. (IL, USA).

[4]   Van Houten J., Watts R. J., *J. Am. Chem. Soc.* **1976**, *98*, 4853.

[5]   Kus P., Czuchajowski L., *J. Heterocyclic Chem.* **1990**, *27*, 1161.

[6]   Peck B. M., Ross G. T., Edwards S. W., Meyer G. I., Meyer T. J., Erickson B. W., *Int. J. Peptide Protein Res.* **1991**, *38*, 113.

[7]   Cooper C. H., Rickard R. L., *Synthesis* **1971**, 31.

[8]   Garelli N., Vierling D., *J. Org. Chem.* **1992**, *57*, 3046.

[9]   Kocia O., Mortimer R. J., *Tetrahedron Lett.* **1990**, *31*, 5068.

[10]   Mujumdar R. B., Ermst L. A., Mujumdar S. R., Lewis C. J., Waggoner A. S., *Bioconj. Chem.* **1993**, *4*, 105.

[11]   Terpetschnig E., Lakowicz J. R., *Dyes and Pigments* **1993**, *21*, 227.

[12]   Oswald B., Patsenker L., Duschl J., Szmacinski H., Wolfbeis O. S., Terptschnig E., *Bioconj. Chem.* **1999**, *10*, 925.

Summary

This thesis describes the synthesis and spectral characterization of novel dyes for HSA labeling, DNA labeling and MLC membrane probes. The dyes were especially quantified in case of suitability as labels and probes in biological systems.

Chapter 1 gives a short overview of the importance of fluorescent markers in life science. Chapter 2 introduces the measurement background of lifetime, fluorescence RET and steady-state polarization.

In chapter 3 the syntheses and spectral characterization of the dyes are described. Two classes of dyes were synthesized.

The first class of dyes were labels for the use as suitable markers in bioassays. A ruthenium ligand complex and a squarine dye are synthesized for steady-state polarization and energy transfer studies. These two labels were converted into reactive NHS esters by the standard NHS/DCC procedure to make them amino-reactive for covalent coupling to protein or oligonucleotides.

The second class of dyes were probes for the use in membrane characterization. A set of new fluorescein and ruthenium ligand complex membrane probes were synthesized and purified by chromatic methods, mainly by MPLC. The properties of the amphiphilic membrane probes were varied by attaching different phospholipid and lipid anchors to the respective fluorophore. The dyes were characterized by their absorption and emission spectra and their decay times. All dyes show an absorption maximum in the range of 480 nm, and are therefore compatible with a 488 nm argon ion laser used in clinical routine.

In chapter 4 the synthesized dyes were evaluated for the use as a membrane probe by temperature dependent polarization (a) in glycerin, (b) when the dye is embedded in DPPC liposomes and (c) when the membrane probe is embedded in DPPC liposomes with different cholesterol concentrations. The results show that the ruthenium ligand complex

membrane probes are well suited as replacement of the common membrane probes of DPH derivatives for measuring membrane dynamics.

In chapter 5 the ruthenium ligand complex and squarine label were tested in the HSA/anti-HSA system using steady-state polarization and fluorescence resonance energy transfer for evaluation. A competitive homogenous immunoassay was developed for the system HSA/anti-HSA by labeling HSA with the MLC label. Additionally, an energy transfer system was evaluated, using a ruthenium complex as donor and the squarine label as acceptor. The results show that the dyes are well suited for such studies, since energy transfer could be detected in the system examined.

In chapter 6, the influence of the ruthenium label attached to an amino functionalized oligonucleotide was investigated in terms of steady-state polarization and decay time. To this system the complementary strand labeled with the synthesized squarine label was established for energy transfer hybridization studies. The location of the dye at the complementary strand was investigated to optimize energy transfer.

Zusammenfassung

Diese Arbeit beschreibt zum einen die Synthese bzw. die spektrale Charakterisierung von neuen Farbstoffen als Label für HSA und DNA und zum anderen die Entwicklung von Ruthenium MLC Membranproben. Die Farbstoffe wurden für den Einsatz als Label oder Probe in biologischen Systemen evaluiert.

Kapitel 1 gibt einen kurzen Überblick über die Wichtigkeit von fluoreszenten Marker im Lifesciencebereich. Kapitel 2 beschreibt die Methodik der Lebenszeitmessung, des Fluoreszenzresonanzenergietransfers und der Polarisation.

In Kapitel 3 wird auf die Synthese und spektrale Charakterisierung der Farbstoffe eingegangen. Zwei Klassen von Farbstoffen wurden synthetisiert.

Die erste Klasse von Farbstoffen sind Marker für den Einsatz in Bioassays. Ein Ruthenium MLC und ein Squarinefarbstoff wurden für Polarisation- und Energietransferstudien synthetisiert. Beide Label konnten durch die NHS/DCC Methode in NHS-Ester umgewandelt werden, um sie reaktiv für Aminogruppen für ein kovalente Kopplung an Proteine oder Olignucleotide zu machen.

Die zweite Klasse von Farbstoffen sind Proben zur Charakterisierung von Membranen. Eine Reihe von neuen Fluoreszein- und Ruthenium MLC-Proben wurden synthetisiert und durch chromatographische Methoden, hauptsächlich mittels MPLC, gereinigt. Die Eigenschaften der amphiphilen Membranproben erhielt man durch Variation unterschiedlicher Phopholipid- und Lipidanker an dem jeweiligen Fluorophor. Die Farbstoffe wurden mittels ihrer Absorptions- und Emissionsspektren und ihrer Lebenszeit charakterisiert. Alle Farbstoffe zeigten ein breites Absorptionsmaximum nahe 460 nm und sind deshalb kompatibel mit einem 488 nm Argonionenlaser, der in der klinischen Laborroutine verwendet wird.

In Kapitel 4 wurden die synthetisierten Farbstoffe für den Einsatz als Membranprobe durch temperaturabhängige Polarisationsmessungen (a) in Glycerin, (b) eingebaut in DPPC Liposomen und (c) eingebaut in DPPC Liposomen mit verschiedenen Cholesteringehalten, evaluiert. Die Ergebnisse zeigten, dass die Ruthenium MLC Membranproben als Ersatz der gewöhnlichen DPH-Derivate für die Messung von Membraneigenschaften geeignet sind.

In Kapitel 5 wurden die Effekte der Ruthenium MLC- und Squarinelabel im System HSA/anti-HSA mittels Polarisation und FRET getestet. Zur Entwicklung eines kompetitiven homogenen Immunoassays für das System HSA/anti-HSA kam ein mit HSA markierter MLC-Label zum Einsatz. Zusätzlich wurde ein Energietransfersystem mit dem MLC Label als Donor und dem Squarinelabel als Akzeptor evaluiert. Die Ergebnisse zeigten, dass die Farbstoffkombination für die Proteindetektion geeignet ist, da in dem System der Effekt des Energietransfers beobachtet werden kann.

Kapitel 6 beschreibt den Einfluß des Rutheniumlabels gebunden an ein aminomodifiziertes Oligonucleotid mittels Polarisation und Lebenszeit. Für eine Hybridisierungsuntersuchung mittels Energietransfer wurde der squaringelabelte Gegenstrang zu diesem System gegeben. Die Variation des Abstandes der Farbstoffe und den komplementären Strängen diente der Ermittlung des optimalen Energietransfers.

Curriculum Vitae

Persönliche Daten

	Christine Augustin geboren am 23.02.1969 in Burglengenfeld / Oberpfalz ledig

Schulbildung

09.1975 – 07.1979	Grundschule Burglengenfeld
09.1979 – 07.1981	Gymnasium Burglengenfeld
09.1981 – 07.1985	Realschule Burglengenfeld
09.1988 – 07.1990	Berufsoberschule Regensburg

Ausbildung

09.1985 – 07.1988	Ausbildung zur Chemielaborantin an der Brautechn. Prüf- und Versuchsanstalt, Freising

Studium

11.1990 – 10.1997	Studium der Chemie an der Universität Regensburg Abschluß: Dipl. Chem. Diplomarbeit am Institut für Organische Chemie (Prof. Daub) der Universität Regensburg Thema: *Kohlenhydratmodifizierte Bor-Pyrromethen-Komplexe*
09.1995 – 10.1996	MSc-Kurs in Analytischer Chemie an der Universität Aberdeen, Schottland Abschluß: Master of Science (MSc, postgraduate) MSc-Arbeit an der Technischen Universität München Thema: *Behavior of the chelating agents EDTA and NTA during waste water treatment*
03.1998 – 05.2001	Promotionsarbeit am Institut für Analytische Chemie, Chemo- und Biosensorik, Universität Regensburg, Thema: *Ruthenium-ligand complexes as bioanalytical luminescent probes for polarization and energy transfer systems*
10.1997 –	Studium der Betriebswirtschaftslehre an der Fernuniversität Hagen Vordiplom März 2001